NASA/TM-20220013310 CD–2021–182

Dynamic Radioisotope Power System (DRPS) Design Reference Mission (DRM) Lunar Rover

Steven Oleson and Elizabeth Turnbull
Glenn Research Center, Cleveland, Ohio

Paul Schmitz
Power Computing Solutions, Avon, Ohio

Kirby Runyon
Johns Hopkins University, Applied Physics Laboratory, Laurel, Maryland

Tony Colozza, Tom Packard, and John Gyekenyesi
HX5, LLC, Brook Park, Ohio

Brandon Klefman, Brent Faller, Natalie Weckesser,
Onoufrious Theofylaktos, Christine Schmid, and Chris Heldman
Glenn Research Center, Cleveland, Ohio

James Fittje
SAIC, Brook Park, Ohio

Ben Bussey and Paul Ostdiek
Johns Hopkins University, Applied Physics Laboratory, Laurel, Maryland

Tom Parkey and Cassandra Chang
Glenn Research Center, Cleveland, Ohio

October 2022

NASA STI Program . . . in Profile

Since its founding, NASA has been dedicated to the advancement of aeronautics and space science. The NASA Scientific and Technical Information (STI) Program plays a key part in helping NASA maintain this important role.

The NASA STI Program operates under the auspices of the Agency Chief Information Officer. It collects, organizes, provides for archiving, and disseminates NASA's STI. The NASA STI Program provides access to the NASA Technical Report Server—Registered (NTRS Reg) and NASA Technical Report Server—Public (NTRS) thus providing one of the largest collections of aeronautical and space science STI in the world. Results are published in both non-NASA channels and by NASA in the NASA STI Report Series, which includes the following report types:

- TECHNICAL PUBLICATION. Reports of completed research or a major significant phase of research that present the results of NASA programs and include extensive data or theoretical analysis. Includes compilations of significant scientific and technical data and information deemed to be of continuing reference value. NASA counter-part of peer-reviewed formal professional papers, but has less stringent limitations on manuscript length and extent of graphic presentations.

- TECHNICAL MEMORANDUM. Scientific and technical findings that are preliminary or of specialized interest, e.g., "quick-release" reports, working papers, and bibliographies that contain minimal annotation. Does not contain extensive analysis.

- CONTRACTOR REPORT. Scientific and technical findings by NASA-sponsored contractors and grantees.

- CONFERENCE PUBLICATION. Collected papers from scientific and technical conferences, symposia, seminars, or other meetings sponsored or co-sponsored by NASA.

- SPECIAL PUBLICATION. Scientific, technical, or historical information from NASA programs, projects, and missions, often concerned with subjects having substantial public interest.

- TECHNICAL TRANSLATION. English-language translations of foreign scientific and technical material pertinent to NASA's mission.

For more information about the NASA STI program, see the following:

- Access the NASA STI program home page at http://www.sti.nasa.gov

- E-mail your question to help@sti.nasa.gov

- Fax your question to the NASA STI Information Desk at 757-864-6500

- Telephone the NASA STI Information Desk at 757-864-9658

- Write to:
  NASA STI Program
  Mail Stop 148
  NASA Langley Research Center
  Hampton, VA 23681-2199

NASA/TM-20220013310 CD–2021–182

Dynamic Radioisotope Power System (DRPS) Design Reference Mission (DRM) Lunar Rover

Steven Oleson and Elizabeth Turnbull
Glenn Research Center, Cleveland, Ohio

Paul Schmitz
Power Computing Solutions, Avon, Ohio

Kirby Runyon
Johns Hopkins University, Applied Physics Laboratory, Laurel, Maryland

Tony Colozza, Tom Packard, and John Gyekenyesi
HX5, LLC, Brook Park, Ohio

Brandon Klefman, Brent Faller, Natalie Weckesser,
Onoufrious Theofylaktos, Christine Schmid, and Chris Heldman
Glenn Research Center, Cleveland, Ohio

James Fittje
SAIC, Brook Park, Ohio

Ben Bussey and Paul Ostdiek
Johns Hopkins University, Applied Physics Laboratory, Laurel, Maryland

Tom Parkey and Cassandra Chang
Glenn Research Center, Cleveland, Ohio

National Aeronautics and
Space Administration

Glenn Research Center
Cleveland, Ohio 44135

October 2022

Acknowledgments

This work was sponsored by the NASA Radioisotope Power Systems Program.
The authors wish to thank them for their support and guidance during this study.

This report contains preliminary findings,
subject to revision as analysis proceeds.

Level of Review: This material has been technically reviewed by technical management.

This report is available in electronic form at http://www.sti.nasa.gov/ and http://ntrs.nasa.gov/

Contents

Dynamic Radioisotope Power System (DRPS) Design Reference Mission (DRM) Lunar Rover

Steven Oleson and Elizabeth Turnbull
National Aeronautics and Space Administration
Glenn Research Center
Cleveland, Ohio 44135

Paul Schmitz
Power Computing Solutions
Avon, Ohio 44011

Kirby Runyon
Johns Hopkins University
Applied Physics Laboratory
Laurel, Maryland 20723

Tony Colozza, Tom Packard, and John Gyekenyesi
HX5, LLC
Brookpark, Ohio 44142

Brandon Klefman, Brent Faller, Natalie Weckesser,
Onoufrious Theofylaktos, Christine Schmid, and Chris Heldman
National Aeronautics and Space Administration
Glenn Research Center
Cleveland, Ohio 44135

James Fittje
SAIC
Brookpark, Ohio 44142

Ben Bussey and Paul Ostdiek
Johns Hopkins University
Applied Physics Laboratory
Laurel, Maryland 20723

Tom Parkey and Cassandra Chang
National Aeronautics and Space Administration
Glenn Research Center
Cleveland, Ohio 44135

1.0 Executive Summary

The Radioisotope Power Systems (RPS) Program tasked the Compass Team to evaluate use of Dynamic Radioisotope Power Systems (DRPS) for lunar science rovers. The object was to identify their advantages and challenges as well as to influence the technology developments with flight-type requirements. This was easily done by using the promising Volatiles Investigating Polar Exploration Rover (VIPER) (Ref. 1) solar-powered rover mission as a platform to ‘swap in’ a DRPS.

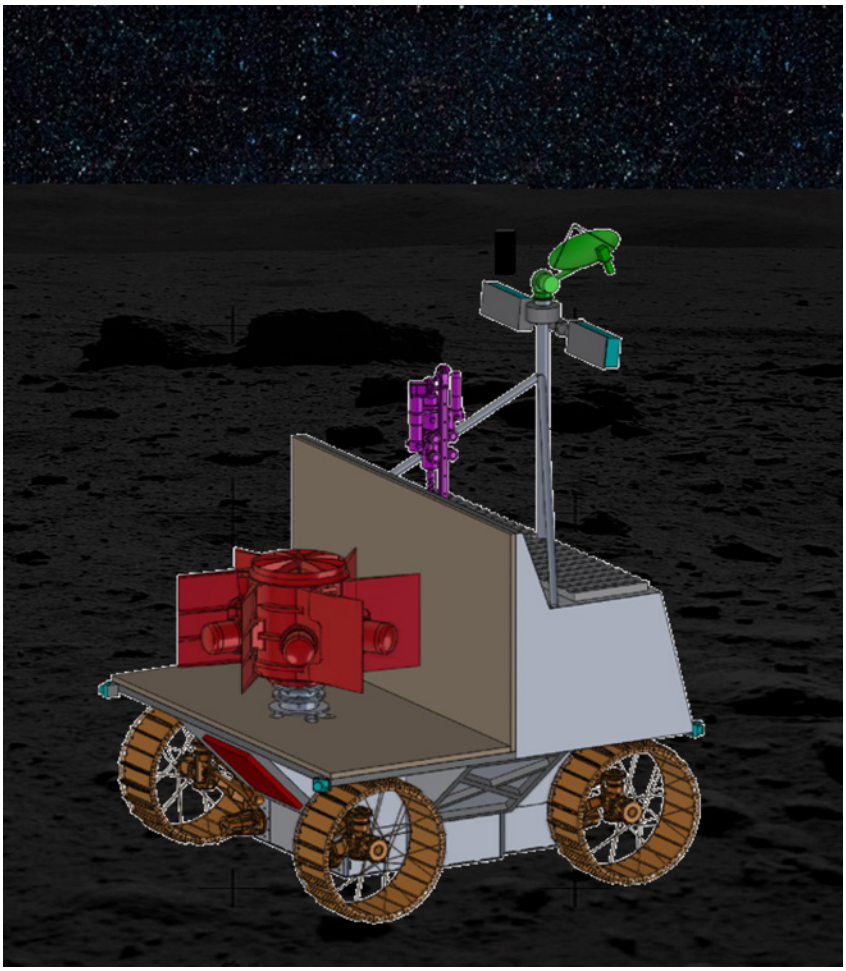

Figure 1.1.—A representative DRPS integrated to a VIPER Class Lunar Rover shown in a Permanently Shadowed Region.

The resulting design is shown in Figure 1.1. The ‘pickup truck bed’ approach allowed both simplified installation and operation of the DRPS while keeping the forward lunar surface ‘blocked’ from the DRPS waste heat which could sublimate the icy surface. It was found that with the Stirling DRPS option the mass is within the planned VIPER lander capability and is very close to VIPER (Ref. 1) mass and size (the DRPS replaces large battery pack/solar arrays). The Stirling DRPS option produced ~300 We using six general purpose heat source (GPHS) bricks and eight Stirling convertors. Replacing the solar/battery power with radioisotope power allows a continuous presence (instead of 6 h) in a permanently shadowed region (PSR) and over 18 months of operations with minimal science impact (rearward surface heating). It was also found that use of a dynamic system (instead of a thermoelectric system) reduces the heat impact on the science environment two-to-three times. The DRPS, along with a relay link (like Gateway), can provide continuous access to PSRs. The system was also found to be capable of roving for 8 h/day with a range of over 500 km in 18 months. Preliminary costs estimates fit into a Class D mission but only assuming VIPER heritage and launch, lander, operations, nuclear specific costs [National Environmental Policy Act (NEPA), fueling, transport, Launch Services Program (LSP), etc.] and DRPS are not included.

2.0 Introduction

Permanently shadowed regions on the Moon hold out the promise of almost unlimited water ice resources but present severe power and thermal challenges for even prospecting for the resource, much less mining and processing it(Ref. 2). The VIPER rover, utilizing only solar/battery power, will explore these PSRs, but only for a few hours at a time (Ref. 1). A more capable power/thermal source based on a radioisotope heat source would alleviate these challenges. Combined with an almost continuous relay spacecraft (like the Gateway System (Ref. 3)), such a system could provide continuous access to prospect these areas for many years. This conceptual design study was commissioned to do just that: investigate what a VIPER-type rover that uses a radioisotope power/heat source (in this case a DRPS) might look like.

3.0 Study Background and Assumptions

The study's objective was twofold: to investigate the impacts of using a DRPS on a prospecting rover and to gather requirements that can influence the technology developments of a DRPS. The study assumed as much of the VIPER architecture as possible including the science suite, lander, and landing site. Due to the use of a DRPS and the assumption of a nearly continuous relay link, the concept of operations (CONOPS, Section 3.3.1) was changed from those of VIPER, especially the inside of PSR duration (increased from 6 h to unlimited) as well as its range and lifetime.

3.1 Assumptions and Approach

The main purpose of this design study was to put a demonstration version of a DRPS on a 'copy' of VIPER to perform science in a PSR for a cost between $150M and $250M [Class D, without launch and lander, DRPS as government furnished equipment (GFE), and protoflight.]

Requirements included:

- Launch date: 2029-2030
- Duration: ~ 18 months (initial)
- Location (PSR or lunar poles)
- Cost: Class D (~$150-250M launch/lander/DRPS/operations not included)
- Risk: Class D risk – but single fault tolerance for DRPS

3.1.1 Ground Rules and Assumptions Summary

The primary goals of the lunar demonstration of the DRPS design were as follows:

- Full power electrical output for at least 18 months (ability to supply some power for up to 10 years)
- Demonstrate operation under launch, landing, roving loads
- Determine degradation rates in the PSR environment
- Demonstrate survival in lunar environments (Sun, shadowed, and PSR)

Secondary DRPS Demonstration Goals included:

- Assess the impacts to a DRPS exposed to environment (dust, heat sink, sunlight)

- Assess exposure of lunar surface and science environment to heating and sublimation from the DRPS heat source
- Assess the impact of the DRPS low level radiation to the science instruments

3.1.2 Figures of Merit (FOM)

The Figures of Merit which drove the design included: simplicity of DRPS operation, science gathered (number of drillings, distance traveled/surface mapped), and cost.

3.1.3 Redundancy

Redundancy was assumed as single fault tolerant except for the science and mobility systems. The expectation was for an 18-month mission.

3.1.4 Science Goals

The Science goals for the DRPS system replicate those of VIPER's high priority goals but at many more locations, including terrain that VIPER cannot sample. Those goals include the following tasks, abilities, and expectations:

- Travel further into permanently shadowed regions
- Travel over 100 km during an 18-month mission
- The VIPER science suite: (3 spectrometers and a 1 m drill), plus room for an additional instruments
- Investigate the Volatile Distribution (concentration, including lateral and vertical extent and variability)
- Investigate the Volatile Physical State (H_2, OH, H_2O, CO_2, ice vs. bound, etc.).
- Provide Context and Correlation, including:
  - Accessibility/Overburden: How much and which types of material needing to be removed to get to ore
  - Environment: Sun/Shadow fraction, soil mechanics, trafficability, temperatures
  - Distribution and Form versus Environment
- Extrapolate small scale distributions to global data sets, critical for developing "mineral/resource models"
- Provide information to help plan In-Situ Resource Utilization (ISRU) operations

Due to the capabilities provided by the DRPS, there were the following additional science benefits:

- Deposition rate of volatiles in shadowed craters
- Understanding of volatile transport and sequestration
- Mapping of surface frost
- Information on traceability and geotechnical properties of permanently shadowed regolith
- Opportunistic examination of geology in PSRs
- ISRU demonstrations of components and mapping of mining operations

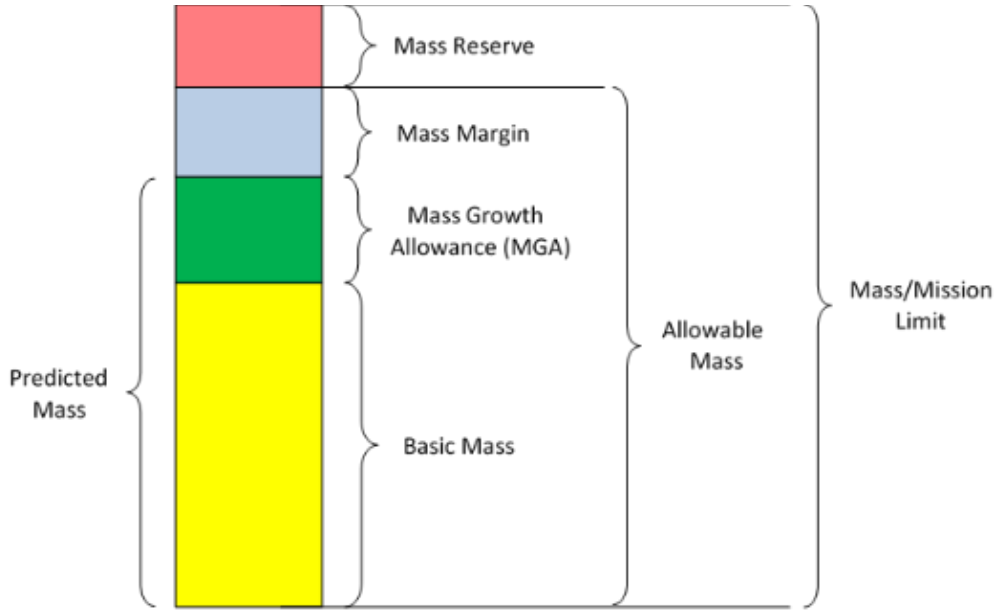

Figure 3.1.—Graphic of General Mass Definitions.

3.2 Growth, Contingency, and Margin Policy

The mass growth, contingency, and mass margin policy used by the Compass Team is congruent with the standards described in AIAA S–120A–2015(Ref. 4). This methodology starts with the basic mass of the components and adds the mass growth allowance (MGA). This subtotal is defined as the predicted mass. Mass margin is then added to the predicted mass to calculate the allowable mass (see Figure 3.1). The aerospace community typically refers to the mass margin as system level growth.

3.2.1 Terms and Definitions Regarding Mass

Mass *The measure of the quantity of matter in a body.*

Basic Mass (aka CBE Mass) *Mass data based on the most recent baseline design. This is the bottoms-up estimate of component mass, as determined by the subsystem leads.*

Note 1: This design assessment includes the estimated, calculated, or measured (actual) mass, and includes an estimate for undefined design details like cables, multi-layer insulation, and adhesives.

Note 2: The mass growth allowances (MGA), and uncertainties are not included in the basic mass.

Note 3: Compass has referred to this as current best estimate (CBE) in past mission designs.

*Note 4: During the design study, the Compass Team carries the propellant as line items in the propulsion system in the Master Equipment List (MEL). Therefore, propellant is carried in the basic mass listing, but MGA is **not** applied to the propellant. Margins on propellant are handled differently than they are on dry masses.*

CBE Mass	*See Basic Mass.*
Dry Mass	*The dry mass is the total mass of the system or S/C when no propellant or pressurants are added.*
Wet Mass	*The wet mass is the total mass of the system, including the dry mass and all the pressurants and propellants (used, predicted boil-off, residuals, reserves, etc.*
Inert Mass	*In simplest terms, the inert mass is what the trajectory analyst plugs into the rocket equation to size the amount of propellant necessary to perform the mission delta-Velocities (ΔVs). Inert mass is the sum of the dry mass, along with any non-used, and therefore trapped, wet materials, such as residuals and pressurants. When the propellant being modeled has a time variation along the trajectory, such as is the case with a boil-off rate, the inert mass can be a variable function with respect to time.*
Basic Dry Mass	*This is basic mass (aka CBE mass) minus the propellant, or wet portion of the S/C mass. Mass data is based on the most recent baseline design. This is the bottoms-up estimate of component mass, as determined by the subsystem leads. This does not include the wet mass (e.g., propellant, pressurant, cryo-fluids boil-off, etc.).*
CBE Dry Mass	*See Basic Dry Mass.*
MGA	*MGA is defined as the predicted change to the basic mass of an item based on an assessment of its design maturity, fabrication status, and any in-scope design changes that may still occur.*
Predicted Mass	*This is the basic mass plus the mass growth allowance for to each line item, as defined by the subsystem engineers.* *Note: When creating the MEL, the Compass Team uses Predicted Mass as a column header and includes the propellant mass as a line item of this section. Again, propellant is carried in the basic mass listing, but MGA is not applied to the propellant. Margins on propellant are handled differently than they are handled on dry masses. Therefore, the predicted mass as listed in the MEL is a wet mass, with no growth applied on the propellant line items.*
Predicted Dry Mass	*This is the predicted mass minus the propellant or wet portion of the mass. The predicted mass is the basic dry mass plus the mass growth allowance as the subsystem engineers apply it to each line item. This does not include the wet mass (e.g., propellant, pressurant, cryo-fluids boil-off, etc.).*
Mass Reserve (aka Margin)	*This is the difference between the allowable mass for the space system and its total mass. Compass does not set a mass reserve, it is arrived at by subtracting the total mass of the design from the design requirement established at the start of the design study, such as an allowable mass. The goal is to have a mass reserve greater than or equal to zero to arrive at a feasible design case. A negative mass reserve would indicate that the*

	design has not yet been closed and cannot be considered feasible. More work would need to be completed.
Mass Margin	*The extra allowance carried at the system level needed to reach the AIAA recommended "green" mass risk assessment level, which is currently set at greater than 15 percent for the Authorization to Proceed program milestone. This value is defined as the difference between allowable mass and predicted mass, with the percentage being with respect to basic mass:* *Percent Mass Margin = (Allowable Mass - Predicted Mass)/Basic Mass*100* *For the current Compass design process, a mass margin of 15 percent is applied with respect to the basic mass and added to the predicted mass. The resulting total mass is compared to the allowable mass as the design progresses. If the total mass is less than the allowable mass, then the mass margin is greater than 15 percent and the design closes while maintaining a "green" mass risk assessment level.* *If total mass is greater than or equal to the allowable mass, then the design does not close with the required 15 percent mass margin, and either the total mass needs to be reduced, or the mass risk posture reevaluated, and the mass margin reduced. However, depending on the numerical difference, the design may not close even if the mass margin is set to 0 percent.*
System-Level Growth	*See Mass Margin*
Total Mass	*The summation of basic mass, applied MGA, and the mass margin (aka system-level growth).*
Allowable Mass	*The limits against which margins are calculated.* *Note: Derived from or given as a requirement early in the design, the allowable mass is intended to remain constant for its duration.*

Table 3.1 expands definitions for the MEL column titles to provide information on the way masses are tracked through the MEL used in the Compass design sessions. These definitions are consistent with those in Figure 3.1 and in the terms and definitions. This table is an alternate way to present the same information to provide more clarity.

For the conceptual level studies conducted by the Compass Team, a mass margin of 15 percent based on basic dry mass is used, which is recommended in the AIAA standard for a grade of "green" at the authorization to proceed milestone, as is shown in Table 3.2. It is worth noting that we assume 30 percent MGA + Mass Margin is suitable for a green rating, providing that there is more allowable mass that would fit to push the percentage slightly above 30 percent. For this study, a "green" rating was achieved across the board.

3.2.2 Mass Growth

The Compass Team normally uses the in AIAA standard S–120A–2015 (Ref. 4), "Mass Properties Control for Space Systems," as the guideline for its mass growth calculations. Table 3.3 on the following page shows the percent mass growth of a piece of equipment based on both its level of design maturity and its functional subsystem.

3.2.3 Power Growth

The Compass Team typically uses a 30 percent growth on the bottoms-up power requirements of the bus subsystems when modeling the amount of required power. There is an exception, however, for the mobility subsystem. Only 5 percent growth is applied to the power requirements needed for the mobility system. No additional margin is carried on top of this power growth.

TABLE 3.1.—DEFINITION OF MASSES TRACKED IN MEL

Item	Definition
Basic Mass	Mass data based on the most recent baseline design (includes propellants and pressurants)
	Basic Dry Mass + Propellants + Pressurants + Residuals
MGA (Growth)	Predicted change to the basic dry mass of an item phrased as a percentage of basic dry mass
	MGA percentage * Basic Dry Mass = Growth
Predicted Mass	The basic mass plus the mass growth allowance (MGA)
	Basic Dry Mass + Propellant + Growth

TABLE 3.2.— MASS RISK ASSESSMENT

Program Milestone	Recommended MGA (%)	Recommended Mass Margin (%)	MGA + Mass Margin (%)	Grade
Authorization to Proceed	> 15	> 15	> 30	Green
	9 < MGA ≤ 15	10 < Mass Margin ≤ 15	19 < MGA + Mass Margin ≤ 30	Yellow
	≤ 9	≤ 10	≤ 19	Red

TABLE 3.3.—AIAA MASS GROWTH ALLOWANCE GUIDELINES FROM AIAA S–120A–2015 (REF. 4)

Maturity Code		Design Maturity (Basis for Mass Determination)	Percentage Mass Growth Allowance												
			Electrical/Electronic Components			Primary Structure	Secondary Structure	Mechanisms	Propulsion, Fluid Systems Hardware	Batteries	Wire Harnesses	Solar Array	ECLSS, Crew Systems	Thermal Control	Instrumentation
			0-5 kg	5-15 kg	>15 kg										
E	1	Estimated	20-35	15-25	10-20	18-25	20-35	18-25	15-25	20-25	50-100	20-35	20-30	30-50	25-75
	2	Layout	15-30	10-20	5-15	10-20	10-25	10-20	10-20	10-20	15-45	10-20	10-20	15-30	20-30
C	3	Preliminary Design	5-20	3-15	3-12	4-15	8-15	5-15	5-15	5-15	10-25	5-15	5-15	8-15	10-25
	4	Released Design	5-10	2-10	2-10	2-6	3-8	3-4	2-7	3-7	3-10	3-5	3-8	3-8	3-5
A	5	Existing Hardware	1-5	1-3	1-3	1-3	1-5	1-3	1-3	1-3	1-5	1-3	1-4	1-3	1-3
	6	Actual Mass	Measured mass of specific flight hardware; no MGA; use appropriate measurement uncertainty.												
S	7	CFE or Specification Value	Typically, an NTE value is provided, and no MGA is applied.												
Expanded Definitions of Maturity Categories															
E1		Estimated	a. An approximation based on rough sketches, parametric analysis, or incomplete requirements.												
			b. A guess based on experience.												
			c. A value with unknown basis or pedigree.												
E2		Layout	a. A calculation or approximation based on conceptual designs (layout drawings or models) prior to initial sizing.												
			b. Major modifications to existing hardware.												
C3		Preliminary Design	a. Calculations based on new design after initial sizing but prior to final structural, thermal, or manufacturing analysis.												
			b. Minor modification of existing hardware.												
C4		Released Design	a. Calculations based on a design after final signoff and release for procurement or production.												
			b. Very minor modification of existing hardware.												
A5		Existing Hardware	a. Measured mass from another program, assuming that hardware will satisfy program requirements with no changes.												
			b. Values substituted based on empirical production variation of same or similar hardware or qualification hardware.												
			c. Catalog values.												

Note: The MGA percentage ranges in the above table are applied to the basic mass to arrive at the predicted mass.

3.3 Mission Description

By targeting a mass and size similar to that of VIPER (the DRPS was found to have similar mass to that of the solar/battery power system of VIPER), it was found the DRPS VIPER should fit on the same launcher and lander as VIPER. Additional accommodations will need to be made for loading the DRPS system through the fairing. These are described below in the CONOPS section .

3.3.1 Concept of Operations (CONOPS) – Case 1

3.3.1.1 Launch and Delivery

The DRPS is loaded into the lander on the pad. The system is then launched on Vulcan/Falcon 9-class launch vehicle. The team assumed that nuclear material will be cleared to launch on these vehicles. While on the pad, a built-in shunt radiator and cooling fans are used. There is a 4-day trip to the Moon, during which time the rover is assumed to be self-powered using the DRPS. The system lands near Spudis Ridge, providing access to PSR, in sunlight on an Astrobotic Griffin Lander (Ref. 5) (used as representative due to its selection to deliver VIPER).

3.3.1.2 Deployment and Exploration

The Compass Team chose the same baseline landing site for the DRPS rover as the planned VIPER to provide both commonality for landing and deployment as well as to utilize the VIPER mission's findings of terrain and science. This would allow for more in depth investigations of the promising VIPER sites.

A notional journey for the DRPS rover is shown in Figure 3.2. It shows a landing on Spudis Ridge with a journey next to various PSR and even a deep dive into De Gerlache crater and its PSR regions.

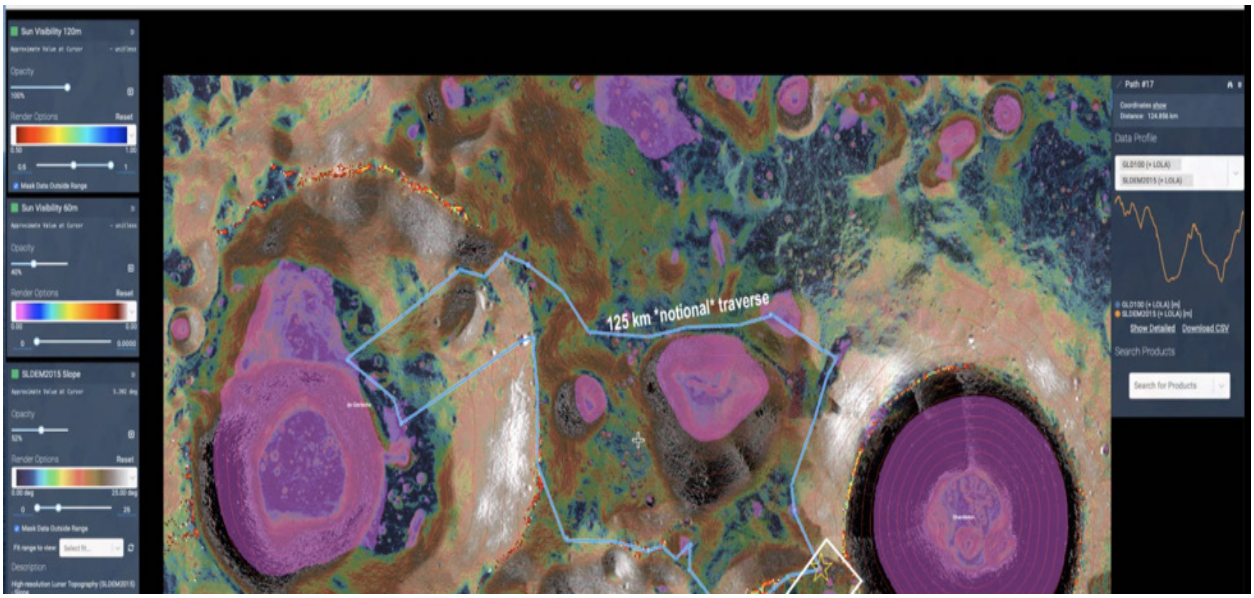

Figure 3.2.—DRPS VIPER Notional Journey.

3.3.1.3 Primary Mission

The lander deploys ramps, releases the rover, safes the lander and then shuts down over the course of 10 h. Following this, rover checkout occurs over the course of 1 day. Communications link is made through the Lunar Gateway for the duration of the mission with an option for direct to Earth (DTE) (~250 kbps). After checkout, the rover descends one of the ramps and performs the minimum science (drilling) and evaluation over the course of 1 week.

There is an option for real time driving by astronauts on Gateway (less than 1 s delay), but nominally main operations will be accomplished using waypoint driving and science support from Earth (6 s round trip delay). The rover will then begin exploration of various craters on Spudis Ridge at 20 cm/s (10 cm/s for H_2 imaging). More than 100 km of transit distance is expected over 18 months, assuming a slope capability of approximately 15° and 4 h of driving time, 4 h of drilling and stationary science time, and 16 h of charge time per day.

The science package consists of a drill, cameras, and three spectrometers from VIPER (Ref. 2). A 10.5 kg of additional instrument mass and 10 W of additional power was included on top of the VIPER system to allow for the addition of more science instruments. Science investigations are limited to forward of the rover, underneath the rover and below the surface due to the waste heat from the DRPS.

3.3.1.4 Extended Mission Possibilities

Due to the potential of DRPS power for longer than the 18-month nominal mission, several ‘extended mission’ options were suggested. The rover could be used to identify easy paths for future in-situ resource utilization (ISRU) rovers, to explore the circumference of many PSR and ‘dip’ in to conduct science, to explore the floor of large craters (e.g., Shackleton or De Gerlache), or to serve as a relay or navigation asset for future missions. Alternatively, it could capture the deposition rate of volatiles inside PSR over time from lunar atmosphere or lunar impacts. The rover could conduct a test of DRPS convertor failure and recovery. Finally, there are potentials to remove and reuse the DRPS for another lunar mission, use inductive charging to provide power to other surface assets, or provide heat to other assets to survive the night.

4.0 Baseline Design

The DRPS rover demonstration targets a mass and size similar to that of VIPER so that it fit on the same launcher and lander as VIPER.

4.1 Top-Level Design Details

The rover consists of a single element with all electronics and science instruments in the bottom and front, shielded from the DRPS on a truck-like bed in the rear. The thermal shielding also prevents the DRPS from exposing the science area to waste heat.

4.1.1 Master Equipment List (MEL)

Table 4.1 provides the DRPS DRM Rover MEL. This MEL is a top-level summary of all the subsystem masses. Each subsystem section provides details for these values. The masses include basic mass and subsystem margin as applied by each subsystem lead, but do not show the additional 15 percent mass margin added at the vehicle level.

The team also ran an additional case, substituting a Brayton power conversion system in for the Stirling system. This was not a full design and should not be considered as such, but a top level MEL was estimated and is shown in Table 4.2.

TABLE 4.1.—CASE 1, STIRLING OPTION MEL

Description Case 1_DRPS_DRM_Rover CD-2021-182	Basic Mass	Growth	Growth	Total Mass
	(kg)	(%)	(kg)	(kg)
DRPS DRM Rover	327	16%	54	381
Rover	327	16%	54	381
Radioisotope Power System	96.4	15%	14.5	110.8
Attitude Determination and Control	4.7	12%	0.6	5.3
Command & Data Handling	18.4	42%	7.7	26.1
Communications and Tracking	10.7	10%	1.1	11.8
Electrical Power Subsystem	13.4	35%	4.6	18.0
Thermal Control (Non-Propellant)	34.8	18%	6.3	41.0
Science	40.0	3%	1.2	41.2
Mobility	67.0	15%	10.1	77.1
Structures and Mechanisms	42.1	18%	7.6	49.6

TABLE 4.2.—CASE 2, BRAYTON OPTION MEL

Description Case 2_Brayton_DRPS_DRM_Rover CD-2021-182	Basic Mass	Growth	Growth	Total Mass
	(kg)	(%)	(kg)	(kg)
DRPS DRM Rover	390	16%	64	454
Rover	390	16%	64	454
Radioisotope Power System	151.0	15%	22.6	173.6
Attitude Determination and Control	4.7	12%	0.6	5.3
Command & Data Handling	18.4	42%	7.7	26.1
Communications and Tracking	10.7	10%	1.1	11.8
Electrical Power Subsystem	17.0	35%	5.9	22.9
Thermal Control (Non-Propellant)	36.2	18%	6.5	42.7
Science	40.0	3%	1.2	41.2
Mobility	67.0	15%	10.1	77.1
Structures and Mechanisms	45.6	18%	8.2	53.8

4.1.2 Architecture Details – Launch Vehicle Payload Assumptions

Astrobotic's Griffin Lander (Ref. 5) was assumed to be representative in this case because, as of the date of this report, it is contracted to carry the VIPER rover. An estimated payload capacity of 475 kg delivered to the lunar surface was assumed. This lander includes two ramps on opposite sides from which the rover can exit. Table 4.3 shows that the rover mass, including MGA and margin fits within the assumed lander capability for the primary design case (the Stirling option).

4.1.3 Spacecraft Total Mass Summary

The MEL in Table 4.4 captures the bottoms-up current best estimate (CBE) and growth percentage on the Rover that was calculated for each subsystem by the subsystem team leads. Mass details per subsystem are provided in Section 5.0 Subsystem Breakdown of this document.

To meet the AIAA MGA and margin recommendations, an allocation is necessary for margin on basic dry mass at the system-level, in addition to the growth calculated on each individual subsystem. This additional margin is shown in the line "Recommended Mass Margin (Additional System Level Growth)."

TABLE 4.3.—LANDER CAPABILITY

LV Summary: Case 1_DRPS_DRM_Rover CD-2021-182	Single Launch
Architecture Details	**Rover**
Representative Lander	Griffin Lander
Performance (pre-margin)	475
Margin (%)	0%
Total Wet Mass w/15% Growth	**430**
Available LV Margin	**45**
Available LV Margin (%)	**9%**

TABLE 4.4.—SUMMARY OF SYSTEM LEVEL MASS

MEL Summary: Case 1_DRPS_DRM_Rover CD-2021-182	Rover
Main Subsystems	**Basic Mass (kg)**
Radioisotope Power	96.4
Attitude Determination and Control	4.7
Command & Data Handling	18.4
Communications and Tracking	10.7
Electrical Power Subsystem	13.4
Thermal Control (Non-Propellant)	34.8
Science	40.0
Mobility	67.0
Structures and Mechanisms	42.1
Element Total	***327.3***
Element Dry Mass (no prop,consum)	327.3
Element Propellant	0.0
Element Mass Growth Allowance (Aggregate)	53.5
MGA as a %'age	16%
Predicted Mass (Basic + MGA)	380.9
Recommended Mass Margin (Additional System Level Growth) 15%	49.1
Margin as a %'age	15%
Element Dry Mass (Basic+MGA+Margin)	430.0
Element Inert Mass (Basic+MGA+Margin)	430.0
Total Wet Mass (Allowable Mass)	***430.0***

4.1.4 Power Equipment List (PEL)

Table 4.5 provides definitions of the power system power modes. These power modes are used by the subsystem leads to identify the power requirements for each subsystem in each mode.

Table 4.6 is the power equipment list (PEL) top-level summary from the bottoms-up analysis on the Rover. The power summary represents the sum of all power requirements estimated by individual subsystem team leads and include growth allowances assumed in the study. The difference between power modes 5 and 8 is accounted for by turning off MSolo when driving in the PSR. Further discussion of the power and energy requirements of this design can be found in Section 5.1, Electrical Power Subsystem.

TABLE 4.5.—POWER MODE TITLES AND DESCRIPTIONS

Power Mode Title	Power Mode Duration	Power Mode Description
DRPS Loading on Pad/Launch	30 days	System will have requirement to be able to accommodate 30 days on the pad
Lunar Transit and Descent	4 days	Self-powered by DRPS, land near a PSR
Rover Checkout	1 day	Stationary- communication through Gateway for duration of PSR mission, no science- limited checkout to get rover on the surface
Peak Roving	30 min	Peak power requirement for roving on difficult terrain
Roving Science- Sunlit	8 h	Nominal roving plus cameras, Near-Infrared Volatiles Spectrometer System (NIRVSS), Msolo, and Neutron Spectrometer System (NSS)
Drilling Science- Sunlit	1 h	All science (NSS, NIRVSS, cameras, Msolo, placeholder science), can drill 100 cm in less than 1 h per VIPER info (Ref. 1)
Standby Phase	15 h	Battery charge phase
Roving Science- Shadowed	8 h	Nominal roving plus cameras, NIRVSS, and NSS
Drilling Science- Shadowed	1 h	All science (NSS, NIRVSS, cameras, Msolo, placeholder science) , can drill 100 cm in less than 1 h per VIPER info

TABLE 4.6.—POWER EQUIPMENT LIST

Description	Power Mode 1	Power Mode 2	Power Mode 3	Power Mode 4	Power Mode 5	Power Mode 6	Power Mode 7	Power Mode 8	Power Mode 9
Case 1_DRPS_DRM_Rover CD-2021-182	DRPS Loading on Pad/ Launch	Lunar Transit and Descent	Rover Checkout	Peak Roving	Roving Science-Sunlit	Drilling Science-Sunlit	Standby Phase (if necessary)	Roving Science-Shadowed	Drilling Science-Shadowed
	30 days	4 days	1 day	30 mins	8 hours	1 hour	16 hrs	8 hours	1 hour
	(W)	(W)	(W)	(W)	(W)	(W)	(W)	(W)	(W)
DRPS DRM Rover	85.5	128.0	254.3	564.0	363.8	430.1	174.5	333.8	430.1
Rover	85.5	128.0	254.3	564.0	363.8	430.1	174.5	333.8	430.1
Radioisotope Power System	39.0	39.0	39.0	39.0	39.0	39.0	39.0	39.0	39.0
Attitude Determination and Control	0.0	0.0	54.7	54.7	54.7	11.0	7.0	54.7	11.0
Command & Data Handling	28.0	28.0	28.0	47.6	49.3	49.3	20.4	49.3	49.3
Communications and Tracking	0.0	42.5	42.5	42.5	42.5	42.5	42.5	42.5	42.5
Electrical Power Subsystem	10.1	10.1	10.1	30.3	30.3	30.3	15.6	30.3	30.3
Thermal Control (Non-Propellant)	6.8	6.8	6.8	6.8	6.8	6.8	6.8	6.8	6.8
Science	1.6	1.6	73.2	43.2	81.2	251.2	43.2	51.2	251.2
Mobility	0.0	0.0	0.0	300.0	60.0	0.0	0.0	60.0	0.0
Structures and Mechanisms	0.0	0.0	0.0	0.0	0.0	0.0	0.0	0.0	0.0
Bus Power, System Total	86	128	254	264	304	430	174	274	430
30% growth	26	38	76	79	91	129	52	82	129
Total Bus Power Requirement	111	166	331	343	395	559	227	356	559
EP System power, System total	0	0	0	300	60	0	0	60	0
5% growth	0	0	0	15	3	0	0	3	0
EP System total Requirement	0	0	0	315	63	0	0	63	0
Total System power with growth	111	166	331	658	458	559	227	419	559

4.2 Concept Drawing and Description

The primary goal of the DRPS lunar Rover design was to develop a strong Class D mission that demonstrates how the use of a DRPS could provide additional science output when compared to solar power on a rover located in or around a PSR near the Lunar south pole. NASA's VIPER was used as the starting point for integrating the DRPS into the Lunar Rover design to leverage its established mass, cost, and science capabilities.

The Compass Team decided to utilize the mobility system from an earlier iteration of the VIPER design, along with the structural portion of the chassis. The mobility system was integrated with the chassis to reduce the overall cost because the mobility system will have been proven on the Lunar surface near the south pole during the VIPER mission. This will also allow the same lander to be used since the interface points to the lander will remain the same along with the width and spacing of the deployment ramps. Similarly, the suite of science instruments is also taken from the same iteration of the VIPER design, not only to reduce costs, but to allow for easier comparison of the science output between the solar powered VIPER (6 h in PSR before solar charging of batteries is required) and the DRPS Lunar Rover (time in PSR is not limited by the need for solar charging of the battery). Figure 4.1 shows the portion of the VIPER mobility system, chassis, and the suite of science instruments that were used to build the configuration for the DRPS Lunar Rover design. More details on these components can be found in their respective subsystem sections later in this document.

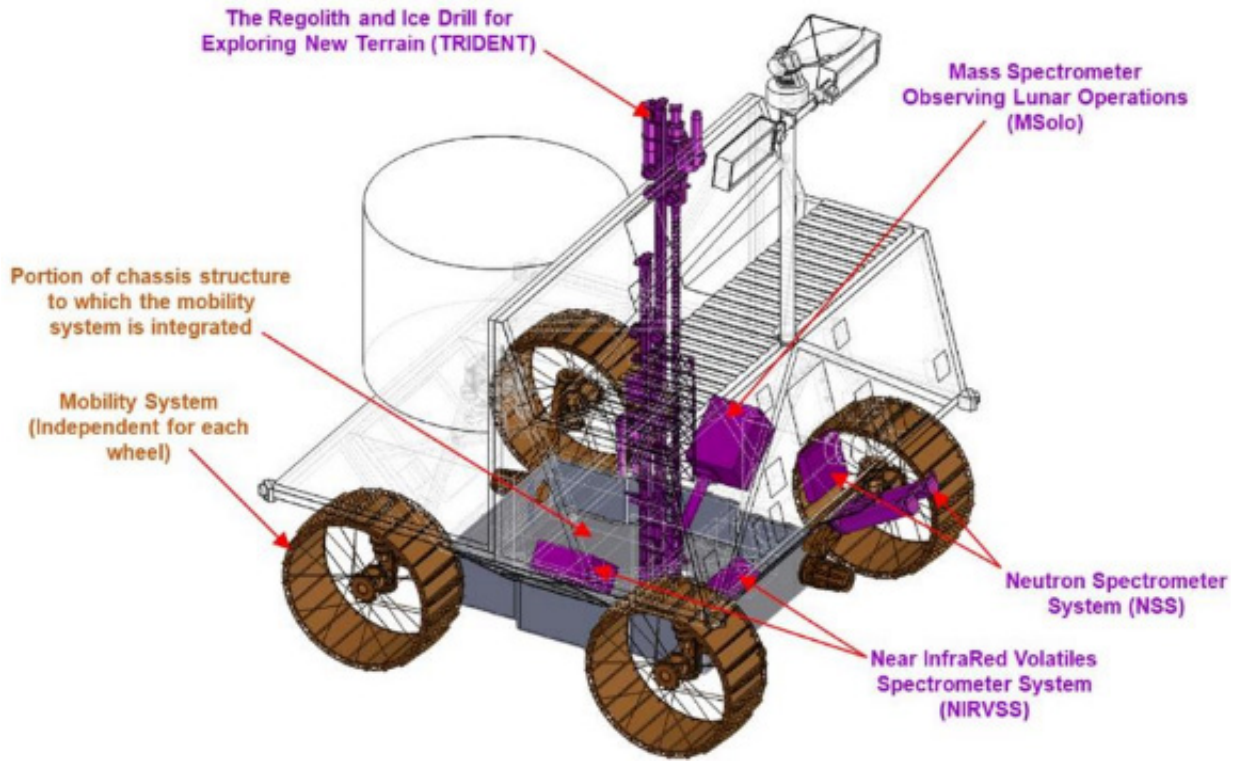

Figure 4.1.—Elements of the DRPS Lunar Rover that were taken from the VIPER design.

All remaining structures are designed specifically for the DRPS Lunar Rover and are driven by the integration of the DRPS as well as maintaining the same volume within the wheel wells to allow the mobility system to fully articulate the wheels as designed. The remainder of the chassis is composed of a space frame integrated to the portion of the structure taken from VIPER and close out sheet panels that enclose the bus to provide a thermally controlled environment and define the volume of the wheel wells. A majority of the close out panels are mounted to the outside of the space frame, while three are mounted to the inside of the space frame to allow easy mounting of some of the internal science instruments and electronics. In addition to the spaceframe and close out panels, a structural mast with mechanisms to allow the Navigation Cameras (navcams) and lights to both rotate and tilt, two mast reinforcement struts, and a strut system and mounting interface for the DRPS complete the structures for the DRPS Lunar Rover. By utilizing a strut system to integrate the DRPS, heat flow from the DRPS to the interior of the bus, and potentially to the surface below the rover, is minimized. Figure 4.2 shows the structural elements designed specifically for the DRPS Lunar Rover. Additional details on the structures can be found in Section 5.3, Structures in this document.

While maintaining the same mobility system and lowest portion of the chassis design from VIPER allows the same ramp width and spacing, as well as the same tie down structure and location to be used on the lander, maintaining similar overall dimensions as VIPER also ensures that the DRPS Lunar Rover will fit on the deck of the lander without the potential need to relocate any of the other components contained on the lander deck. Similarly, maintaining approximately same mass as VIPER will allow the same lander to be used for the DRPS Lunar Rover, thus minimizing costs. Figure 4.3 shows the overall dimensions of the DRPS Lunar Rover design. It should be noted that the wheels shown in all the figures within this section are in the highest position as they would be while stowed and integrated to the lander deck.

Figure 4.2.—Structures specific to the DRPS Lunar Rover design.

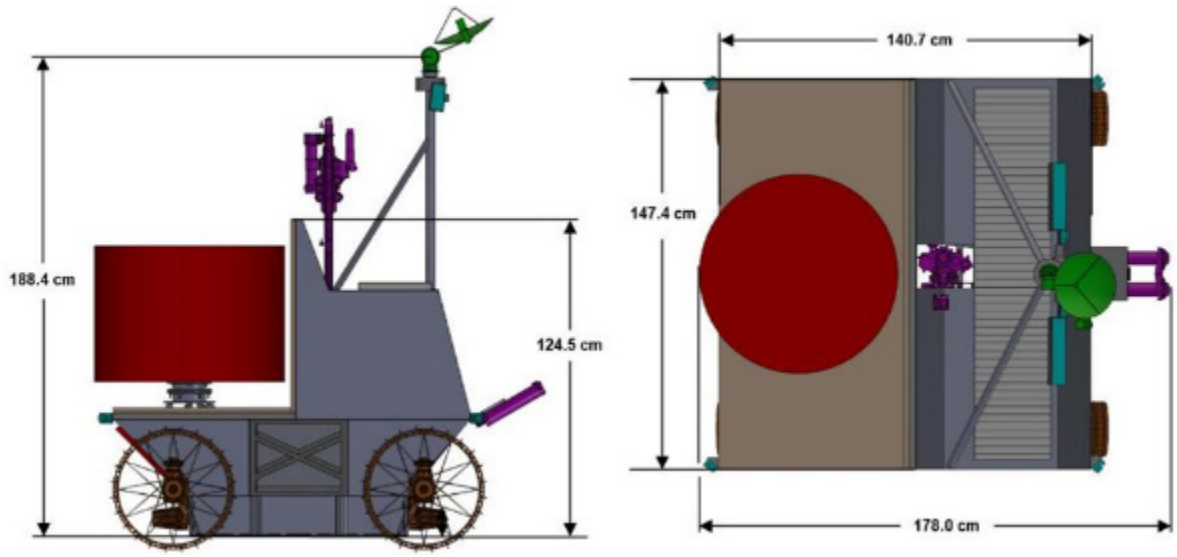

Figure 4.3.—Overall dimensions of the DRPS Lunar Rover.

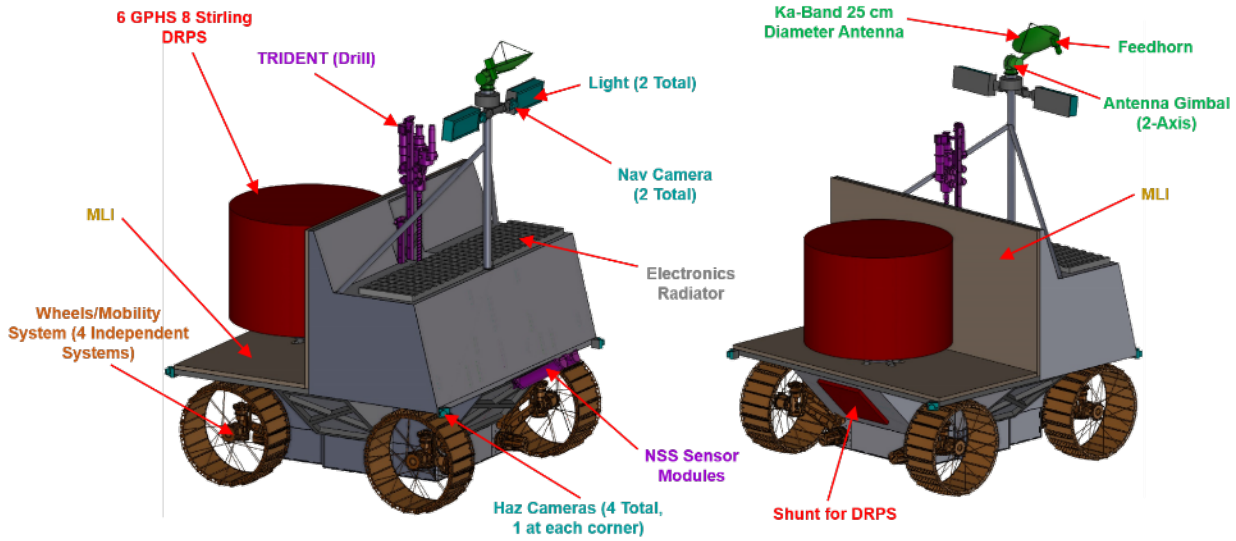

Figure 4.4.—External components on the DRPS Lunar Rover.

Those components other than the mobility system that are located externally on the DRPS Lunar Rover include: the DRPS and shunt of the RPS; the multi-layer insulation (MLI) and radiator of the thermal control system; the four hazard avoidance cameras (hazcams), two navigation cameras (navcams), and two lights of the attitude determination and control (AD&C) system; the parabolic dish antenna, feedhorn, and 2-axis gimbal of the communications system; and the neutron spectrometer system (NSS) sensor module and The Regolith and Ice Drill for Exploring New Terrains (TRIDENT) of the science system. Figure 4.4 shows these externally located components.

It should be noted that the DRPS shown in the DRPS Lunar Rover model is a simple cylinder that represents the maximum envelope dimensions for the central cylinder containing the six GPHS generator, Stirling converters, and the fins utilized for heat rejection. The DRPS is located near the rear of the rover between and just above the two rear wheel wells. Integration is done through a flange adaptor attached to the bottom of the DRPS. This flange adaptor allows the DRPS to be bolted to another flange adaptor that

is supported by six struts that extend downward to six points located on the space frame structure of the rover. As mentioned earlier, the six struts are utilized to minimize the heat flow from the DRPS to the rover structure, and thus to the other components on the rover, as well as the surrounding lunar surface. The shunt for the RPS is mounted to the closeout panel located between the two rear wheels of the rover. More details on the RPS can be found in its respective section later in this document.

To minimize the waste heat of the DRPS radiating to the surface and the other system electronics located in the front section of the rover, two adiabatic walls of MLI are included in the design. The horizontal wall below the DRPS minimizes the flow to the lunar surface below the rover while the vertical wall minimized the heat flow to the system components contained inside the front of the rover as well as the lunar surface in front of the rover. This is to prevent increasing the temperature of the lunar surface, which would negatively impact science by altering surface conditions from their original state prior to the arrival of the rover. Adiabatic walls on the sides and aft of the DRPS were deemed not necessary as science operations are done forward of the DRPS. While omitting these walls limits science operations to a 180°swath in front of the rover, it reduces the rover mass and allows the DRPS to reject its waste heat more efficiently through the fins. Further work needs to be done to examine how the two adiabatic walls will impact the heat rejection from the fins of the DRPS.

Rounding out the thermal control system is the electronics radiator panel. This panel is located on top of the bus structure between the drill and mast and radiates the waste heat of the electronics contained inside the rover structure upwards and away from the lunar surface. More details on the thermal control system can be found in Section 5.2 of this document.

Located at the four corners of the rover are the four hazcams. Each is angled 45° from the two sides that meet to form the corner at which they are located. This allows the four hazcams to provide a full 360° view around the rover to locate potential hazards to avoid while roving on the lunar surface. The two navcams and two lights are located near the top of the mast and can simultaneously rotate around the mast, providing a full 360° view around the rover, as well as simultaneously tilt up and down. This ensures that both the lights and navcams are pointed in the same direction at the same time. More details on the AD&C components can be found Section 5.7, Navigation System.

Located at the top of the mast are the Ka-band parabolic dish antenna, feedhorn, and two-axis gimbal. The gimbal is attached directly to the top of the mast allowing it to rotate about the mast and tilt up and down within the position to which it is rotated. Attached directly to the gimbal is the parabolic dish antenna, with the feedhorn attached directly to the parabolic dish antenna. This allows both the antenna and feedhorn to be pointed in the same direction by the gimbal. This configuration allows full hemispherical coverage around and above the rover. More details on the communication subsystem components can be found in Section 5.8.2, Communications System Assumptions.

Lastly are the NSS sensor and TRIDENT of the Science System. The NSS sensor is located at the front of the rover just above and in the middle of the two front wheels. This location ensures that the sensor will obtain readings from the surface that have not been impacted by the rover, whether it be from the wheels stirring up the surface or from the heat rejected from the DRPS. As for TRIDENT, much of the drill is located within the bus structure, the top portion of the drill extends out of the top of the bus structure. When drilling into the surface, the drill will extend out through a cutout in the bottom structure of the bus. TRIDENT was located as close to the center of the rover as possible to ensure a relatively even mass distribution of the rover around the drill, providing more stability when drilling into the lunar surface. More details on these science instruments can be found in Section 5.4, Science Subsystem.

Those components enclosed inside the rover include: the Stirling controller of the RPS; the 28-V power electronics box and Li-ion battery of the electrical power system (EPS); the avionics enclosure of the command and data handling (C&DH) system; the inertial measurement unit (IMU), hazcam and

navcam electronics, and the digital video recorder (DVR) for the cameras of the AD&C system; the electronics boxes for the communications system; and the MSolo, Near-Infrared Volatiles Spectrometer System (NIRVSS) sensor head and electronics box, and the NSS electronics box of the science system. Figure 4.5 and Figure 4.6 shows two different views of those components that are contained inside the structure of the DRPS Lunar Rover.

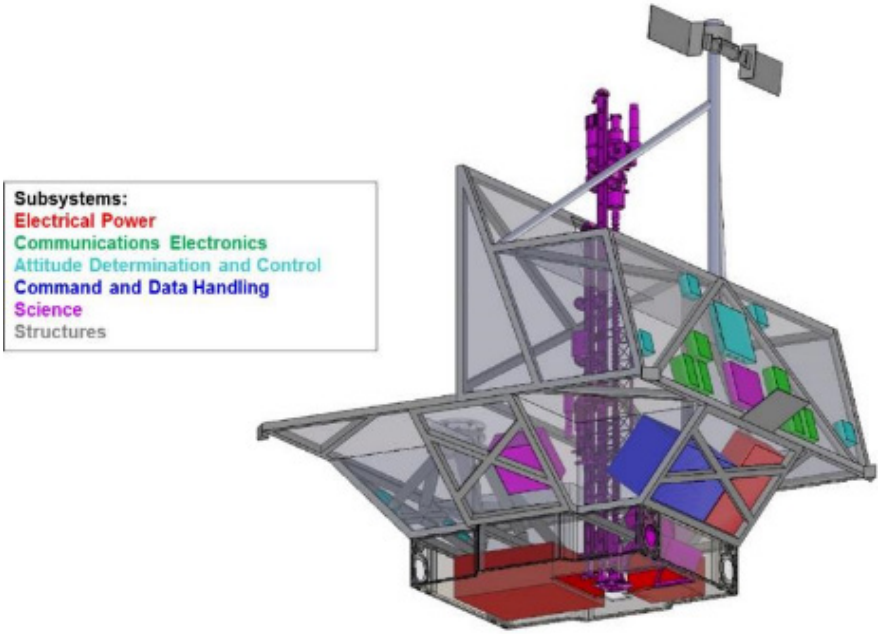

Figure 4.5.—Internal components on the DRPS Lunar Rover.

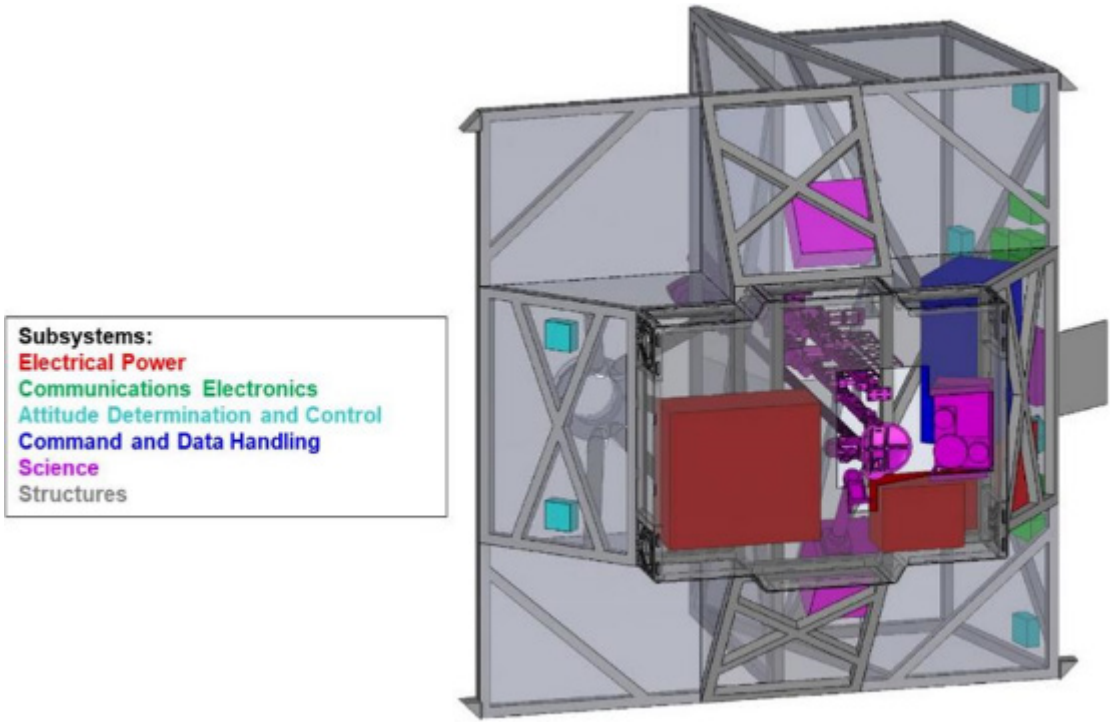

Figure 4.6.—Additional view of the internal components on the DRPS Lunar Rover.

The Stirling controller is mounted almost directly below the DRPS to the bottom panel of the rover chassis structure to which the mobility system is integrated. This location not only provided the area to interface the controller to the structure but helps to counteract the Center of Gravity (CG) impact of the relatively high location of the DRPS and lower the overall CG point for the rover. By being almost directly below the DRPS, cable lengths running between the controller and DRPS are shortened and thus are lighter in mass. More details on the Stirling controller of the RPS can be found in Section 5.1, Electrical Power Subsystem.

The 28-V power electronics box is mounted to the same panel of the chassis as the Stirling controller, though up near front of this panel. This location again helps to counteract the CG of the relatively high DRPS by lowering the CG point of the rover, as well as moving the CG point closer to the front of the rover, counteracting the CG of the DRPS located at the rear of the rover. The Li-ion battery is mounted to the face sheet that closes out the bus structure between the front wheels, thus helping to move the CG point imposed by the DRPS located in the rear of the rover towards the front of the rover. More details on these components of the EPS can be found in Section 5.1, Electrical Power Subsystem.

The avionics enclosure is mounted just next to the battery on the close out panel between the two front wheels. Again, this pushes the CG point of the entire rover more towards the front to counteract the DRPS located at the rear of the rover. More details on the Command and Data Handling System can be found in Section 5.6 of this document.

The IMU, DVR and four of the six camera controllers are mounted to the inside of the front closeout panel on the rover bus structure. This location also helps to push the CG point of the entire rover forward to counteract the DRPS located at the rear of the rover. The rear closeout panel between the two rear wheels is used to mount the electronics boxes for the two rear hazcams. This location minimizes the cable lengths between the cameras and their respective electronics boxes.

Mounted to that same front closeout panel as the IMU, DVR, and four camera electronics boxes are all the electronics boxes for the Communications System. Though these components are light in mass, this forward-most location helps to push the CG of the overall rover forward to counteract the impact of the DRPS located in the rear.

Lastly are those science components that are located inside the rover. The MSolo is mounted to the closeout panel located between the front and rear wheel on the left side of the rover. As this portion of the bus is angled, it allows the sensor head of the MSolo to be close to and get a good view of the material being extracted by the drill. The view of the MSolo to the extracted material is provided by the same cutout in the bottom structure that allows the drill access to the surface. The NIRVSS sensor head is mounted directly to the bottom panel of the chassis structure, also having a view of the material extracted by the drill through the same cutout used by the drill and MSolo. While it is necessary to have this cutout to allow TRIDENT, MSolo, and NIRVSS access to the surface below the rover, further analysis is needed to determine the thermal impacts between the lunar surface and the interior of the rover, and potentially the need for a cover or door to close that cutout when not collecting science data. Mounted to the closeout panel located between the front and rear wheels on the left side of the rover is the electronics box for NIRVSS. Finally, the electronics box for the NSS is mounted to the inside of the front closeout panel with the Communications electronics, IMU, DVR, and four of the camera electronics boxes. This allows shorter cable runs between the NSS sensor head and electronics box as the sensor head is located just on the outside of this panel. More details on the components in the Science Subsystem can be found in its respective section in this document.

Transparent views of the bottom and front of the DRPS Lunar Rover showing the internal components can be seen in Figure 4.7, while a transparent side view is shown in Figure 4.8. Two additional transparent views of the DRPS Lunar Rover are shown in Figure 4.9.

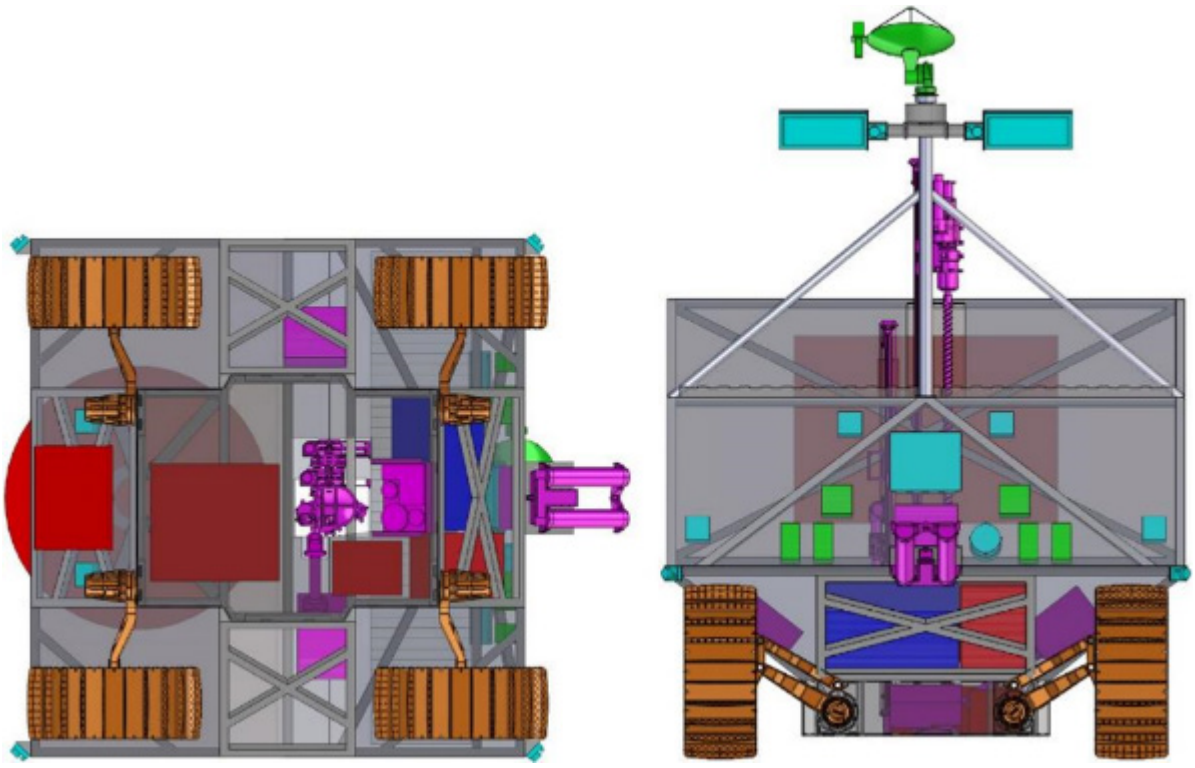

Figure 4.7.—Transparent bottom and front views of the DRPS Lunar Rover.

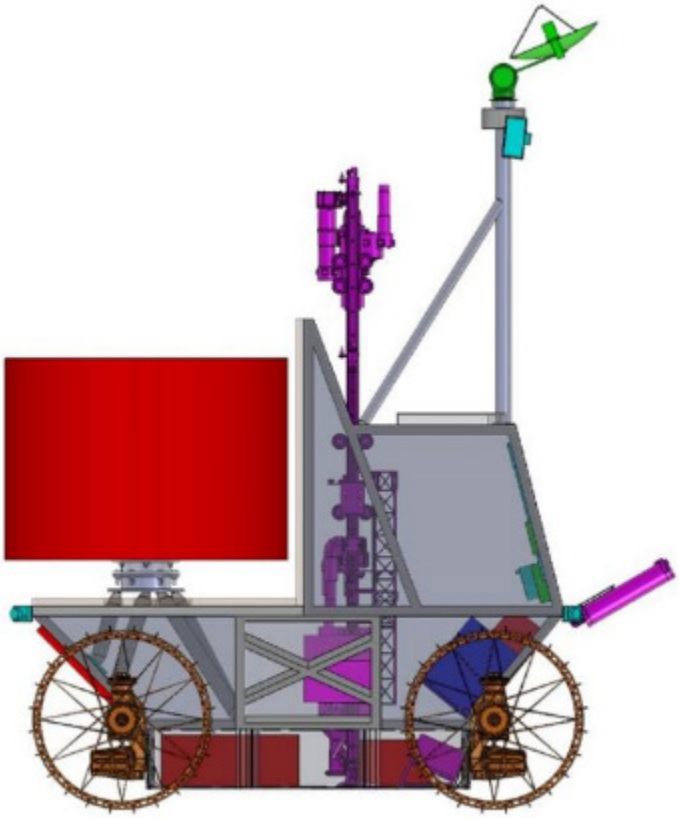

Figure 4.8.—Transparent side view of the DRPS Lunar Rover.

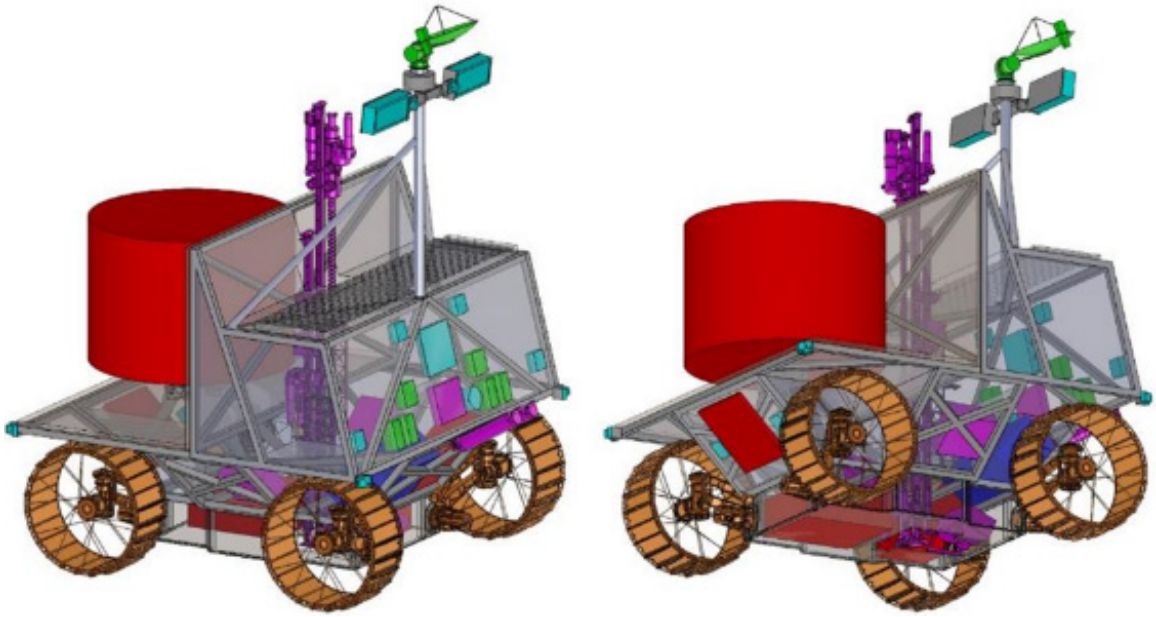

Figure 4.9.—Additional transparent views of the DRPS Lunar Rover.

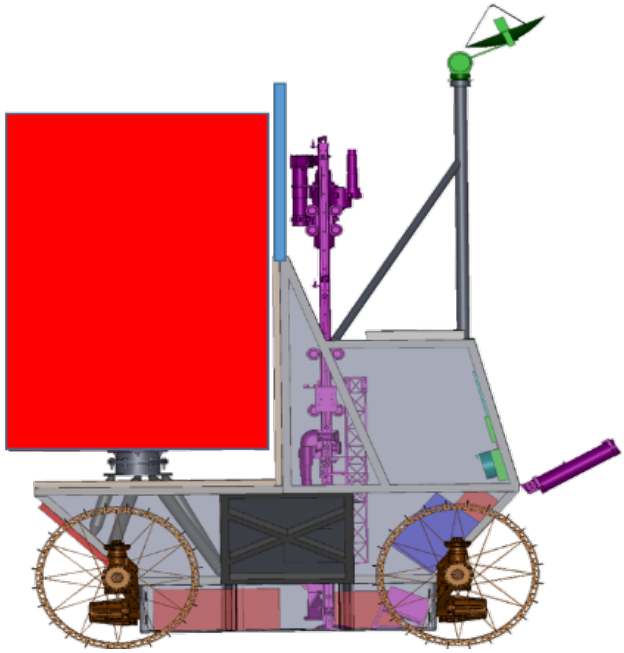

Figure 4.10.—Basic visualization of Brayton option.

4.3 Trades

A quick trade to integrate a Brayton based (instead of Stirling based) DRPS was made, shown roughly in Figure 4.10. While the power was sufficient given additional charge time, it was found that the Brayton system was both quite large and its mass made the DRPS Brayton rover too large for the lander. Table 4.7 shows the top-level MEL for the Bryton case.

TABLE 4.7.—TOP LEVEL MEL FOR BRAYTON CASE

MEL Summary: Case 2_Brayton_DRPS_DRM_Rover CD-2021-182	Rover
Main Subsystems	**Basic Mass (kg)**
Radioisotope Power	151.0
Attitude Determination and Control	4.7
Command & Data Handling	18.4
Communications and Tracking	10.7
Electrical Power Subsystem	17.0
Thermal Control (Non-Propellant)	36.2
Science	40.0
Mobility	67.0
Structures and Mechanisms	45.6
Element Total	***390.5***
Element Dry Mass (no prop,consum)	390.5
Element Propellant	0.0
Element Mass Growth Allowance (Aggregate)	63.9
MGA as a %'age	16%
Predicted Mass (Basic + MGA)	454.3
Recommended Mass Margin (Additional System Level Growth) 15%	58.6
Margin as a %'age	15%
Element Dry Mass (Basic+MGA+Margin)	512.9
Element Inert Mass (Basic+MGA+Margin)	512.9
Total Wet Mass (Allowable Mass)	***512.9***

5.0 Subsystem Breakdown

This section provides a detailed description of each major vehicle subsystem. In addition to the descriptions and diagrams, each subsection includes a subsystem MEL, which rolls up into the overall system level MEL and mass summary for each case.

5.1 Electrical Power Subsystem

The Electrical Power Subsystem is responsible for generating, storing, and distributing electrical power to the various loads around the spacecraft. Power generation is provided by a DRPS. The DRPS has six GPHS coupled to eight Stirling convertors. The DRPS takes the heat generated from the GPHS and converts the heat into alternating current electrical power. A controller monitors and converts the AC power output to 28 Vdc. The DRPS generates enough power to meet the load demand during standby operations but cannot support roving operations alone, so an energy storage device is used to provide the peaking load demand. The energy storage consists of a Li-ion battery which is discharged during roving and drilling (science) operations which can last up to 9 h continuously per day. The rover will then spend the remainder of the day (15 h) recharging the battery for the next set of operations. Note that the 9 h of continuous operations is expected to bound the energy storage sizing and may not reflect the real-world operations of the rover. Power from the DRPS and Li-ion battery is distributed to the various system loads using a 28 Vdc architecture with commercial off-the-shelf (COTS) power management and distribution (PMAD) cards. These cards provide battery charge/discharge regulation and fault protection to the various spacecraft loads.

5.1.1 System Requirements

While there were no set requirements for power production a six GPHS/eight Stirling convertors generator was assumed. The mission life is 18 months plus an assumed 3-year storage (total 4.5 years) of life. While this was the mission life requirement the generator was required to be designed to operate for 17 years (three storage plus 14 mission). Additionally, the generator must be single fault tolerant. This was accomplished by allowing a pair of convertors to fail while still providing the full power output from the generator. Additionally, the DRPS must fit within the existing department of energy (DOE) shipping container which transports the fueled generator from the Idaho National Lab to the Kennedy Space Center.

The energy storage sizing is driven by the total energy demand in each of the mission phases which is a function of the peaking load demand (above the DRPS capability) and the total, continuous time spent in each of the mission phases. A nominal workday of 8 h of roving operations plus 1 h of drilling operations is assumed to size the energy storage. Using the PEL, the total rover load demand can be used to calculate the required battery energy consumption for each mission phase. This is shown in Table 5.1.

End-of-life (EOL) DRPS power generation and worst-case load estimates are assumed when calculating the energy consumed. Thirty percent growth is applied to the expected load demand except for mobility power which assumes 5 percent growth. These growth factors are intended to capture any increases in the estimated power consumption of the components as the design matures. Based on these results, after 8 h of continuous roving operations plus 1 h of drilling, the energy storage must provide at least 818.5 Wh of energy.

TABLE 5.1.—ENERGY STORAGE REQUIREMENTS

Power Modes	DRPS Loading on Pad/ Launch	Lunar Transit and Descent	Rover Checkout	Peak Roving	Roving Science-Sunlit	Drilling Science-Sunlit	Standby Phase	Roving Science-Shadowed	Drilling Science-Shadowed	Standby Phase-In Shadow
Duration (h)	720	96	24	0.5	8	1	15	8	1	15
Bus Power with Growth (W)	47.3	102.6	266.7	568.1	367.8	469.0	155.8	328.9	469.0	100.4
EPS Parasitic Power (W)	10.1	10.1	10.1	10.1	10.1	10.1	10.1	10.1	10.1	10.1
EPS Dissipation (W)	0.0	0.0	0.0	16.8	16.8	16.8	7.9	16.8	16.8	7.9
Total Power (W)	57.4	112.7	276.8	595.0	394.7	495.9	173.8	355.8	495.9	118.4
DRPS Power (W)	315.0	315.0	315.0	315.0	315.0	315.0	315.0	315.0	315.0	315.0
Energy Storage Power (W)	–257.6	–202.3	–38.2	280.0	79.7	180.9	–141.2	40.8	180.9	–196.6
Energy Consumed (Wh)	0.0	0.0	0.0	140.0	637.6	180.9	0.0	326.0	180.9	0.0

5.1.2 System Assumptions

The following assumptions are made regarding the design of the EPS components.

- DRPS
  - Single fault tolerant Stirling based DRPS
  - Stirling able to operate at reduced power because of thermal barrier between DRPS and front of rover
- Energy Storage
  - The energy storage uses a rechargeable Li-ion battery technology.
  - The battery consists of COTS LG M36T (Ref. 6) battery cells.
  - The battery provides a nominal voltage of 28 Vdc to the power bus.
  - One spare parallel battery string is included for redundancy.
  - The maximum depth of discharge (DoD) of the battery is assumed to be 80 percent. This provides margin for contingency scenarios and accounts for expected battery degradation through the mission.
- PMAD
  - Load switching and fault protection is handled by the Terma Equipment Power Distribution Module (Ref. 7).
  - Battery charge and discharge regulation is handled by the Terma Battery charge/discharge (C/D) Regulation Module (Ref. 8).
  - Each PMAD function includes an additional card for redundancy.
  - The mass of the harnessing between the various EPS components is assumed to be 25 percent of the base EPS mass.

5.1.3 System Trades

Dynamic power conversion systems are being considered for future RPS. The advantage of DRPS are higher power conversion efficiencies which reduce the consumption of scarce ^{238}Pu. The Radioisotope Program Office (RPO) is developing three power conversion devices which may be used in future DRPS. Two of the power convertors are based upon the Stirling cycle and the third is based upon the Brayton cycle (Ref. 9). SunPower® and American Superconductor Corporation (AMSC) are developing the Stirling convertors while Creare® LLC is developing the Brayton system. During the development of these convertors, some work was performed as to how these power convertors might be integrated into a generator. Based upon the contractor's work, estimates were made as to the mass and power output of a six-GPHS, eight-Stirling convertor system. Additionally, a six-GPHS dual parallel loop Brayton system was also developed. Both Stirling generators produced relatively similar mass and power output and a blended performance estimate between the two was made for this study. The Brayton system was relatively heavier and had lower performance, so it was decided to perform a "one-off" study to assess the impacts of the performance difference at the end of the primary Compass run.

Using the Brayton converter for the RPS system reduces the conversion efficiency and thus the amount of power generated by the EPS from 315 W down to 299 W. The estimated load demand in the system remains unchanged, so this requires additional battery energy for the same planned operations. The estimated battery energy required increases from 818.5 to 1100 Wh. With the additional energy required, the battery will increase by 2.9 kg. However, instead of sizing for the same continuous 8 h of roving plus 1 h of drilling operations, the same battery can be used if the roving operations are limited to only 6 h plus the same 1 h of drilling operations. The PMAD design remains unchanged for this case.

TABLE 5.2.—EPS ENERGY BALANCE

Operational Phases	Duration (h)	Total Power (W)	RPS Power (W)	Battery Power Demand (W)	Starting SOC (%)	Energy Consumed (Wh)	Final SOC (%)
Roving Phase	8	394.7	315.0	79.7	100.0	637.6	46.9
Drilling Phase	1	495.9	315.0	180.9	46.9	180.9	31.8
Standby Phase	6	173.8	315.0	–141.2	31.8	–818.5	100.0

5.1.4 Analytical Methods

With an energy storage device, it is important to ensure positive energy balance is maintained during the nominal operations of the mission. Positive energy balance ensures the energy storage device is fully recharged before the next discharge event. For this design, the nominal daily operation includes roving operations for up to 8 h continuously, with 1 h of drilling operations. After these events, the rover must be placed into standby mode to ensure the energy storage device can fully recharge before the next day's events. For nominal daily operation, the rover will be placed into standby mode for up to 15 h/day. Thus, the energy storage has 15 h to fully recharge before the next day. The energy balance analysis is shown in Table 5.2.

This energy balance analysis shows that, as designed, the battery can support the nominal 8 h of roving plus 1 h of drilling operations each day. The maximum battery DoD is 68.2 percent which does not exceed the limit of 80 percent. Additionally, the standby phase requires 6 h to fully recharge the battery which is less than the 15 h of available recharge time each day. It should be noted that this analysis uses the worst-case conditions including the maximum expected load demand with growth and EOL DRPS power generation, so earlier in the mission, there will be considerable energy margin in the battery.

5.1.5 Risk Inputs

Any new generator design carries its own unique set of risks in addition to those found in the previously developed Advanced Stirling Radioisotope Generator (ASRG). Specifically, the requirement for single fault tolerance for this new generator will create challenges that were not present in the ASRG. A generator that is designed to share heat from a centralized GPHS heat source and connect to multiple Stirlings must be able to tolerate the failure of any of the Stirling convertors within the generator. Defining what constitutes a fault and the mitigation steps for each fault are required. Examples of mitigation steps may include:

1. Shutting down a working convertor if it is paired with a second Stirling convertor to reduce shaking forces exported to the generator
2. Switching to a new electronic Stirling controller if a controller failed
3. Changing the heat input into the working convertors to increase their electrical power output to compensate for the lost convertor
4. Changing heat input into the working convertors to reduce Stirling hot side temperature due to the failure of convertors
5. Activation of a dampener react to shaking forces within the generator.

In addition to these steps greater sensor information than a zero-fault tolerant generator may be required. Temperature and shaking force measurements may be required for control of the generator to react to faults and the rapidity of these reactions may be too fast to have a human in the loop to react to the changes caused by faults and thus increase the complexity of the control system.

TABLE 5.3.—STEP 2 GPHS DIMENSIONS

Height (cm)	Width (cm)	Length (cm)
5.82	9.32	9.96

5.1.6 System Design

The GPHS has been the core element of modern RPS used for many deep space missions when there is a lack of adequate solar illumination to power solar cells. It is a Department of Energy (DOE) standardized thermal source that produces approximately 250 W of thermal power at the beginning of life (BOL). Dimensions of a GPHS module are shown in Table 5.3.

PuO_2 is the ceramic form of Pu-238 that is used as the fuel for the GPHS. PuO_2 is placed in four iridium capsules and surrounded by a graphite shell to form each GPHS module. ^{238}Pu was chosen because most of its radioactive decay energy comes from an alpha emission, and it has a long half-life (87.7 years). Relatively low amounts of neutron emission come from both spontaneous fission and (α, n) reactions, which result from the interactions of the high-energy alpha particles with materials of low atomic mass. Specifically, the Ir capsule prevents the alpha particles from leaving the fuel pellet (and interacting with the surrounding graphite), but interactions with both O_{16} and O_{17} in the PuO_2 mixture does produce some neutron flux as well as spontaneous fissions of the ^{238}Pu. Production of ^{238}Pu is commonly done by neutron irradiation of ^{237}Np in a high-flux reactor. The product of this irradiation is ^{237}Np that decays (2.117 day half-life) via beta emission into ^{238}Pu.

The RPS design used for this mission relies on Stirling converters. Stirling convertors have a history of very long-life operation. At NASA Glenn Research Center (GRC), gas bearing convertors similar to those under development by SunPower® for this DRPS contract have over 10 years of operation without a failure. Flexure based Stirling convertors similar to the AMSC convertors have operated for over 14 years without failure. Both convertors continue to operate on their respective test stands today.

5.1.6.1 Case 1 – Six-GPHS Dynamic RPS

Case 1 utilizes a dynamic RPS consisting of six general purpose heat source (GPHS) modules and eight Stirling convertors that convert thermal power into electrical power. The eight Stirling converters are operated as balanced pairs to create four strings in the generator. Each pair of Stirling convertors has a controller card which monitors the health of both convertors, provides an AC source to control both stroke and frequency of the pair and converts the AC power output from the Stirlings to 28 Vdc. Figure 5.1 illustrates the block diagram of the DRPS and Figure 5.2 shows examples of Stirling DRPS

Normally, the DRPS would be designed to operate in a 4 K deep space environment. However, the primary purpose of this rover is to assess the water content of both the surface and subsurface lunar regolith. Therefore, a heat shield was created to prevent sublimation in front of and below the DRPS. The heat shield keeps the waste heat generated during the power conversion process from disturbing any water ice content in front of or below the rover. The heat shield reduces the effective radiator area by approximately one-third.

The heat shield also reduces the power output of the generator. In a deep space environment, the DRPS should produce about 353 Wdc. However, with the heat shield, the DRPS produces a maximum of 335 Wdc of electrical power, which decays to 315 W at end of mission (EOM) (4.5 years after fueling). While the mission life for this rover concept is only 4.5 years, the DRPS are designed for 17 years of life (3 years storage plus 14-year missions). The DRPS envelope is 0.8 m in diameter and 0.5 m tall with a total heat rejection of 1127 W at BOL. The system has a specific power of 3.8 W/kg, a mass of 95.3 kg. Table 5.4 shows a mass summary.

TABLE 5.4.—MAJOR COMPONENTS
OF THE DRPS SYSTEM

Category	Mass (kg)
Convertors	33.7
GPHS	9.6
Housing	19.7
Fins	4.6
Insulation	10.0
Misc.	3.7
Controller	13.9
Totals	95.3

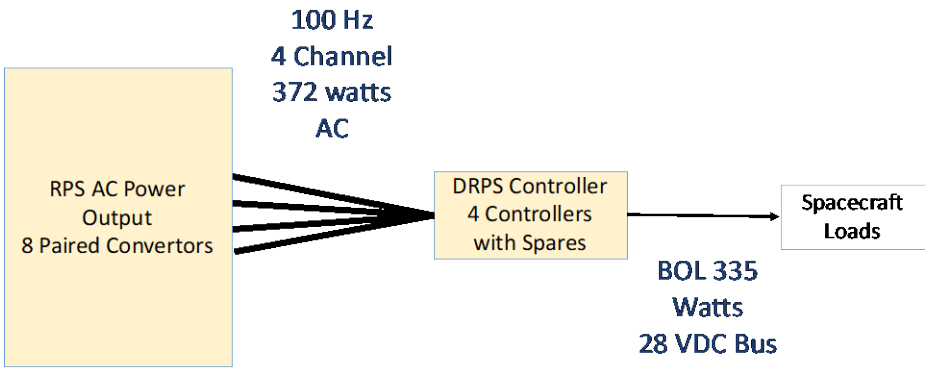

Figure 5.1.—Case 1 RPS Schematic.

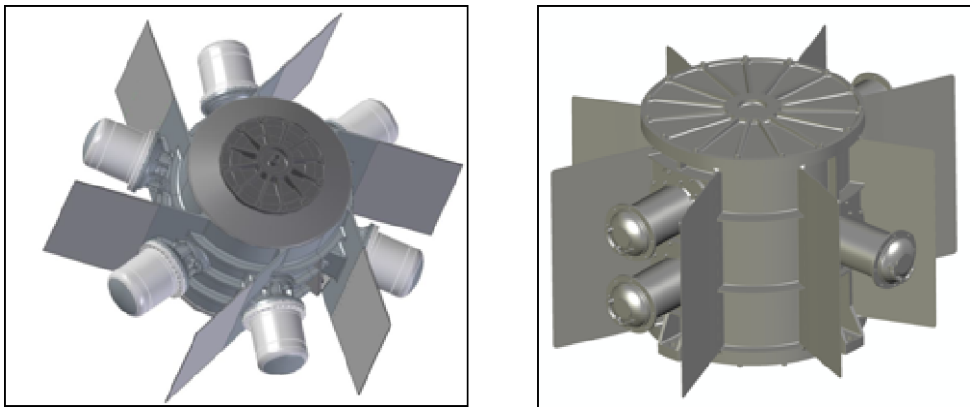

Figure 5.2.—AMSC and SunPower® SRG.

5.1.6.2 Case 2 – Creare® Brayton System

For Case 2, the Compass Team substituted the Creare® Brayton system (shown in Figure 5.3) into the MEL to see if we could still land the rover on the lunar surface. Mass for the Brayton system was 138 kg not including margin and the system is approximately 50 cm taller than either Stirling system. Unfortunately for this case we were over our allotted mass for the rover and the system did not close. Figure 5.4 shows a mass break down of the major components of the DRPS system.

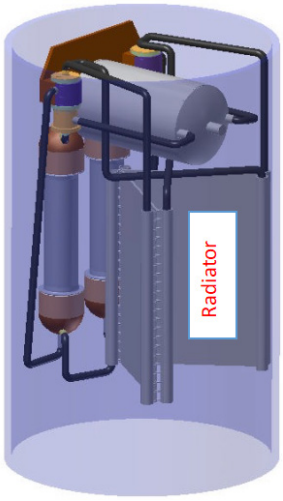

Figure 5.3.—Creare's® Brayton Cycle DRPS.

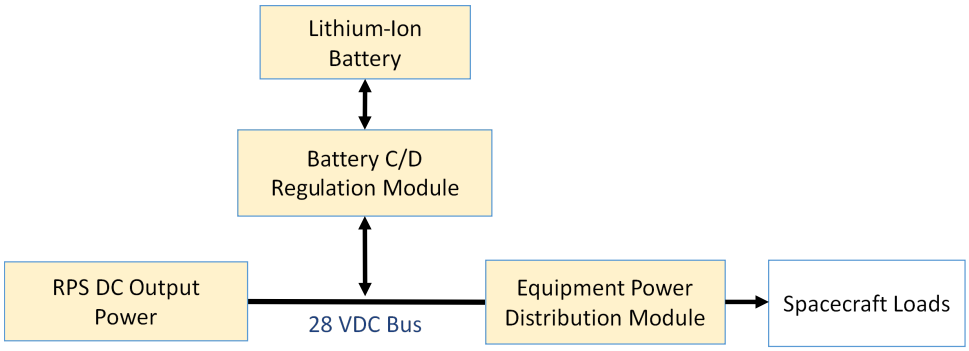

Figure 5.4.—EPS Block Diagram.

Power out of the DRPS is converted into 28 Vdc to feed the main power bus. This power is fed to the loads using two Equipment Power Distribution Modules. Each Equipment Power Distribution Module can support up to 16 individual loads, each with a maximum output of 5 A (Ref. 7). The outputs can be wired in parallel to support loads with current demand greater than 5 A. Power from the DRPS is also used to recharge the Li-ion battery. The Battery C/D Regulation Module regulates the charge power to the battery, preventing over-charge. In addition, the module provides discharge regulation for the battery, limiting the maximum current draw to protect the battery. This power is fed to the main power bus when the loads exceed the capability of the DRPS. The efficiency of the module is 96.0 percent when charging and 94.0 percent when discharging (Ref. 8). The Li-ion battery design includes an 8S-12P configuration. Eight battery cells in series provides the nominal 28 Vdc battery voltage, while the 12 parallel strings provide the total battery energy required. With a maximum depth of discharge (DOD) of 80 percent, the battery as designed has a total of 1200 Wh of energy with a specific energy of 173 Wh/kg. A block diagram of the EPS is shown in Figure 5.4.

For this design, the battery and PMAD components have a high technology readiness level (TRL) as many off-the-shelf components were utilized. The Li-ion battery uses COTS battery cells combined in a new battery configuration, so it is considered TRL 6. The PMAD components have flight heritage, so the Terma(T) Equipment power distribution module and Battery C/D regulation module are both considered TRL 9. The EPS harnessing is considered TRL 8 as the layout will be unique for this rover design, but the materials have flight heritage.

5.1.7 Master Equipment List

Table 5.5 to Table 5.8 show the DRPS and EPS MELs for the two cases.

TABLE 5.5.—RPS MEL CASE 1

Description Case 1_DRPS_DRM_Rover CD-2021-182	QTY	Unit Mass	Basic Mass	Growth	Growth	Total Mass
Radioisotope Power System			**96.4**	**15%**	**14.5**	**110.8**
RPS System			**96.4**	**15%**	**14.5**	**110.8**
6 GPHS, 8 Stirling DRPS	1	81.0	81.0	15%	12.2	93.2
Controller	1	14.0	14.0	15%	2.1	16.1
shunt	1	1.4	1.4	15%	0.2	1.6

TABLE 5.6.—RPS MEL CASE 2

Description Case 2_Brayton_DRPS_DRM_Rover CD-2021-182	QTY	Unit Mass	Basic Mass	Growth	Growth	Total Mass
Radioisotope Power System			**151.0**	**15%**	**22.6**	**173.6**
RPS System			**151.0**	**15%**	**22.6**	**173.6**
6 GPHS, Brayton Rotating Unit Assembly	1	135.6	135.6	15%	20.3	155.9
controller	1	14.0	14.0	15%	2.1	16.1
shunt	1	1.4	1.4	15%	0.2	1.6

TABLE 5.7.—EPS MEL CASE 1

Description Case 1_DRPS_DRM_Rover CD-2021-182	QTY	Unit Mass	Basic Mass	Growth	Growth	Total Mass
Electrical Power Subsystem			**13.4**	**35%**	**4.6**	**18.0**
Power Management & Distribution			**6.5**	**50%**	**3.2**	**9.7**
28 VDC Power Electronics Box	1	3.8	3.8	15%	0.6	4.4
Harness	1	2.7	2.7	100%	2.7	5.4
Energy Storage			**6.9**	**20%**	**1.4**	**8.3**
Lithium Ion Battery	1	6.9	6.9	20%	1.4	8.3

TABLE 5.8.—EPS MEL CASE 2

Description Case 2_Brayton_DRPS_DRM_Rover CD-2021-182	QTY	Unit Mass	Basic Mass	Growth	Growth	Total Mass
Electrical Power Subsystem			**17.0**	**35%**	**5.9**	**22.9**
Power Management & Distribution			**7.2**	**55%**	**4.0**	**11.2**
28 VDC Power Electronics Box	1	3.8	3.8	15%	0.6	4.4
Harness	1	3.4	3.4	100%	3.4	6.8
Energy Storage			**9.8**	**20%**	**2.0**	**11.8**
Lithium Ion Battery	1	9.8	9.8	20%	2.0	11.8

5.2 Thermal Subsystem

The DRPS rover will collect science data around and within a permanently shadowed crater on the lunar south pole. The rovers' systems require components to operate in both a PSR as well as in the sunlit ridge outside of the crater. An additional constraint on the system is the need to maintain pristine surface conditions prior to sampling by the science instruments. This requires the area in the front of the rover to be shielded from the heat generated by the RPS.

5.2.1 System Design

The design approach for the thermal system utilizes the worst-case hot and worst-case cold environmental conditions to size various components of the system. Solar intensity and view angle as well as the view to warm bodies such as the sunlit lunar surface along with the internal heat generation are used to determine the worst-case hot and cold conditions. The worst-case warm conditions occur while sunlit at lunar pole when all internal components are operating generating maximize waste heat. Whereas the worst-case cold operating conditions occur while operating within the PSR. The main thermal system components used in the system are listed below along with an operational summary given in Table 5.9. The thermal system layout on the rover is illustrated in Figure 5.5.

- Radiator panel with louvers for removing the waste heat from the electronics
- Heat pipes and cold plates for moving the heat from the electronics packages to the radiator
- Multi-Layer Insulation (MLI) to insulate the electronics as well as provide a barrier from the waste heat of the isotope power system to the surface in front of the rover
- Heaters
- Temperature Sensors, Controllers, Switches, Data Acquisition

TABLE 5.9.—THERMAL SYSTEM OPERATIONAL SPECIFICATIONS

Specifications	Value/Description
Dimensions: Rover Insulation	Estimated Electronics Enclosure Plus Heat Shielding: Length (l_e): 1.0 m, Width (w_e): 1.5 m, Height (h_e): 1.5 m Insulation surface area: 10.5 m^2
Waste heat:	Electronics Systems: 221.5 W
Operating Temperature	Electronics: 300 K
Insulation (MLI)	25 layers of MLI are used to cover all external surfaces for the electronics boxes and tank.
Environment	Lunar Polar (154 to 50 K) surface temperature range
Radiators	Surface mount radiator for rejecting heat from the electronics. Louvers are utilized on the radiator to adjust the heat flow to the surroundings between operation outside the crater under sunlit conditions and operation within the permanently shadowed crater.
Cooling	Water heat pipes with cold plates are used to move the heat from the electronics to the radiator.
Heating	Electric heaters are used to provide heating to the internal components as needed.

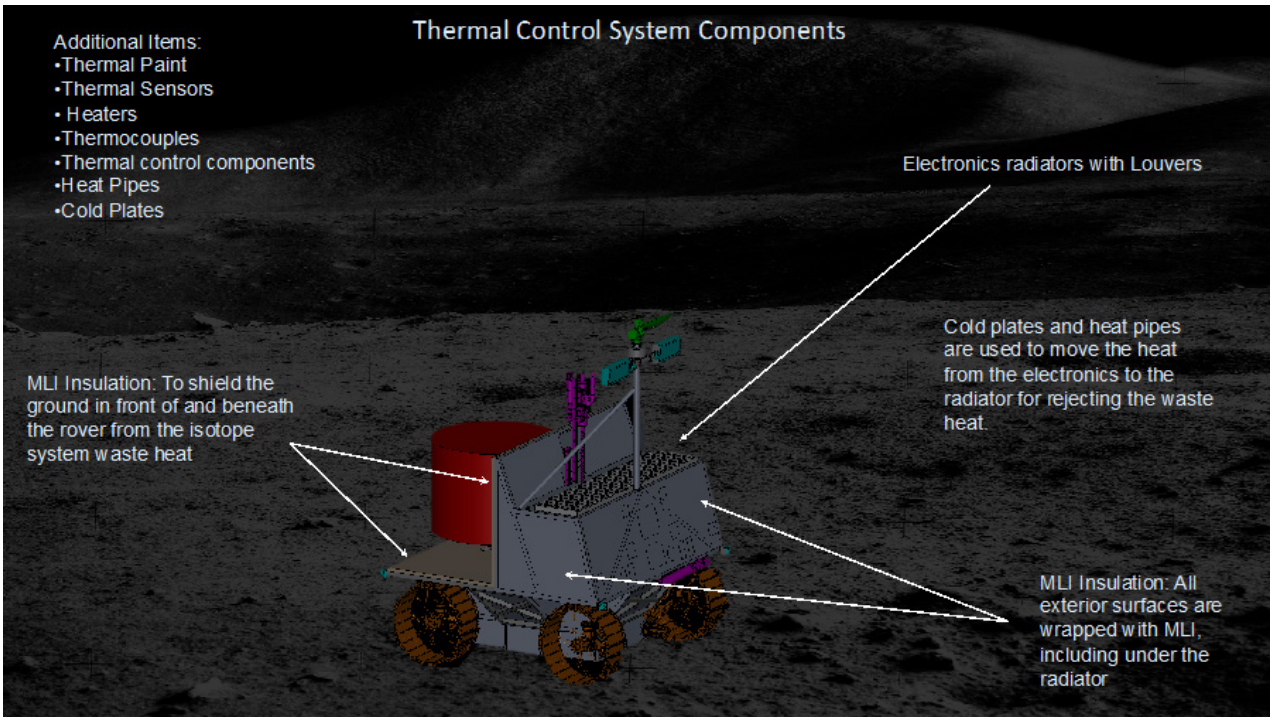

Figure 5.5.—Rover Power System Thermal Components.

5.2.1.1 Lunar Environment

The operational environment is a critical aspect to the thermal system design. To determine the operating conditions on the lunar surface, temperatures from Lunar Reconnaissance Orbiter (LRO) and other sources was utilized. The day and nighttime temperature swings on the lunar surface are severe and can fluctuate over 300 °C. During daytime operation near the equator, the surface regolith will reach a temperature of ~385 K. Nighttime temperatures at the equator are similar to those at other latitudes including the poles dropping below 100 K at nighttime. Due to the large temperature swings the equator has the worst operational thermal environment. At higher latitudes the temperature variation between day and night lessens and becomes colder for both the day and nighttime periods. This temperature variation as a function of latitude is shown in Figure 5.6.

The DRPS powered rover mission was designated to operate at the lunar south pole both in sunlight as well as in a PSR. In Figure 5.6 the temperature curve for 89° N Latitude shows a maximum temperature of ~150 K and a minimum temperature of ~50 K. There is also a long period of time where at this latitude there is continual darkness (from day 95 to day 230). This can be seen by the flat, slowly descending temperature curve over this range. Operation within a crater or PSR in the polar region provides extremes in temperature. These range from the PSR estimated to be maintained at 30 to 50 K to the sunlit portion which, depending on the latitude can achieve temperatures of approximately 240 K.

The temperature curves shown in Figure 5.6 represent average surface temperature at the latitudes shown. However, the actual surface temperature will vary significantly, particularly at the poles, depending on surface elevation and slope. This variation is shown in Figure 5.7 for the lunar south pole.

As shown in Figure 5.7, surface temperatures outside of the craters at the South pole under sunlit conditions will achieve temperatures in the range of 130 to 275 K depending on their elevation and angle to the Sun. Whereas temperature variation within a crater during daytime can range from less than 50 to 275 K. Based on the average surface temperatures and an assumed view factor to the surroundings of 0.5 the effective sink temperature at the pole for an object in sunlight is approximately 235 K.

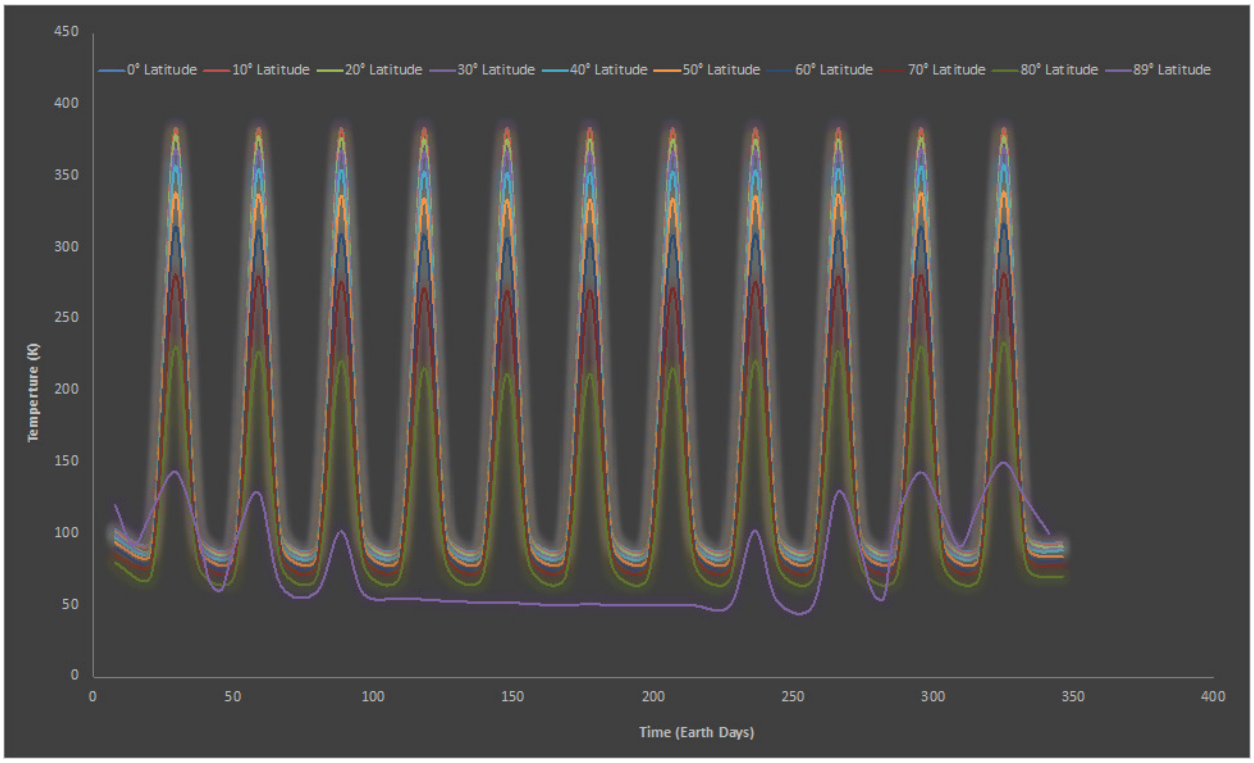

Figure 5.6.—Lunar Surface Temperature for Latitudes from the Equator to the Pole over 1 Earth Year.

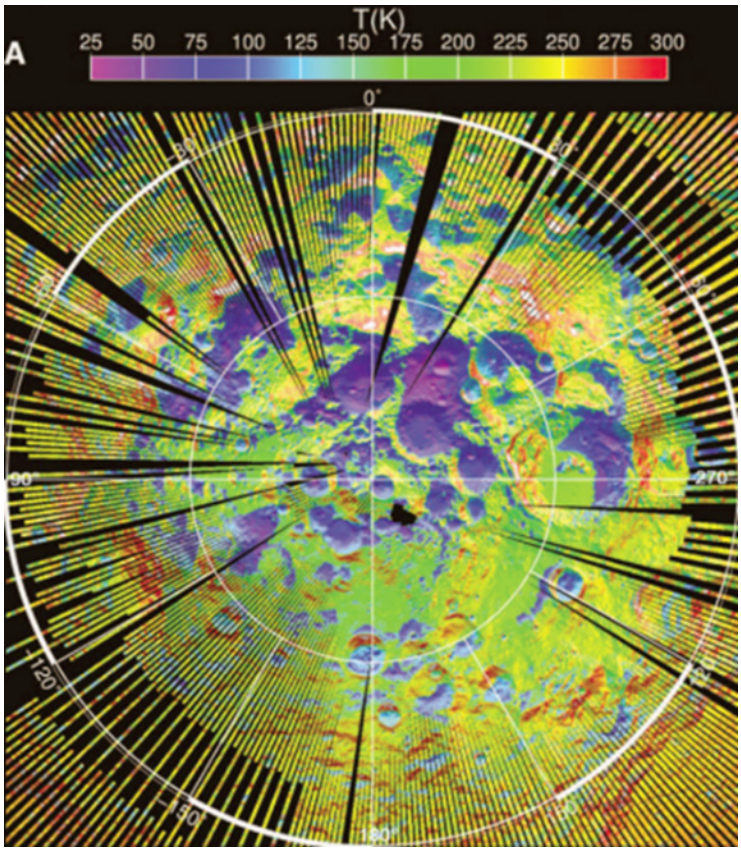

Figure 5.7.—LRO Surface Temperature Distribution for the Lunar South Pole.

Even though the lunar declination angle is small at 1.5°, there still are seasonal effects for the craters at or near the polar location. These effects are shown in Figure 5.8. Quadrants A and C show the maximum temperature variation between the summer and winter. This variation is on the order of 30-to-40 K where the permanently shadowed region of the crater would vary between 70 K in the summer and 40 K in the winter. The amplitude of the temperature, shown in quadrants B and D represent the day and night temperature variation for the summer and winter, respectively. This shows that the day and night temperature fluctuations are low and are comparable to or less than the variation between the maximum summer and winter temperatures.

The environmental conditions at the lunar pole are summarized in Table 5.10.

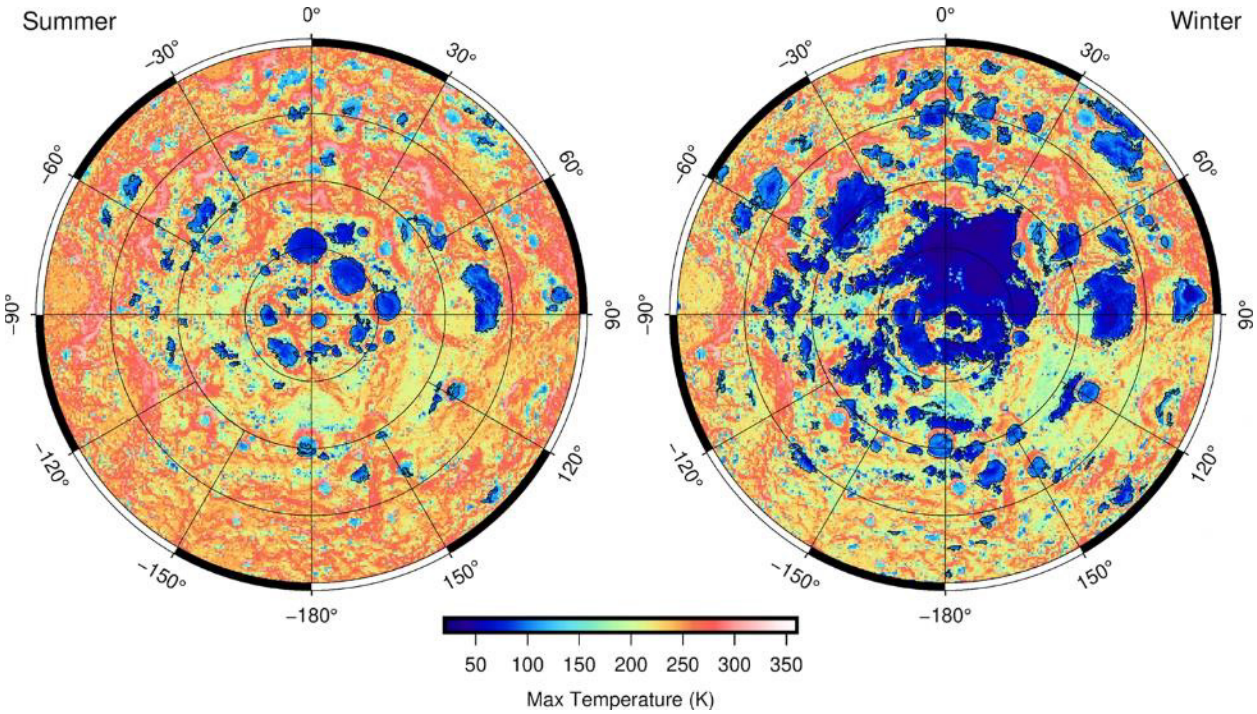

Figure 5.8.—Maximum Surface Temperature and Amplitude for PSRs at the Lunar South Pole (Ref. 9, Creative Commons CC BY-SA 4.0 license, https://creativecommons.org/licenses/by/4.0/).

TABLE 5.10.—ENVIRONMENTAL CONDITIONS

	Surface	PSR
Sky Temperature	4 K (–269 °C)	4 K (–269 °C)
Surface Temperature Sunlit	254 K (–19 °C)	NA
Surface Temperature Shadow	60 K (–213 °C)	60 K (–213 °C)
Average Sink Temperature Sunlit (horizontal Surface)	133 K (–140 °C)	NA
Average Sink temperature sunlit (6-sided cube)	235 K (–38 °C)	NA
Average Sink Temperature in Shadow	50.5 K (–222.5 °C)	50.5 K (–222.5 °C)
Solar Heat Input	1370 W/m^2	NA

5.2.1.2 Surface Heating

To effectively evaluate the surface composition, it is necessary that the surface remain in its initial pristine state during evaluation with the scientific instruments. The main reason for this is the heat rejected from the DRPS can heat the surrounding surface raising its temperature and potentially releasing volatiles which would affect the science data being collected, as illustrated in Figure 5.9. To determine the effect of the DRPS on the surrounding surface temperature an analysis was performed to determine the steady state temperature rise of the regolith surrounding the DRPS as a function of distance from the power source. The view factor of the DRPS to the surface ($f_{1\text{-}2}$) was determined as a function of the distance from the rover. This view factor is estimated based on the height (h) and diameter (d) of the DRPS system and the distance on the surface from it (d) and is given by Equation (3).

$$a = d\tan^{-1}\left(\frac{1}{d}\right) + h\tan^{-1}\left(\frac{1}{h}\right) - \sqrt{(h^2+d^2)}\,\tan^{-1}\left(\frac{1}{\sqrt{h^2+d^2}}\right) \tag{1}$$

$$b = \frac{1}{4}\ln\left[\left(\frac{(1+d^2)(1+h^2)}{1+h^2+d^2}\right)\left(\frac{d^2(1+h^2+d^2)}{(1+d^2)(h^2+d^2)}\right)^{d^2}\left(\frac{h^2(1+h^2+d^2)}{(1+h^2)(h^2+d^2)}\right)^{h^2}\right] \tag{2}$$

$$f_{1\to2} = \frac{a+b}{\pi d} \tag{3}$$

The equilibrium temperature of the regolith is given by Equation (4). This equation is solved iteratively for the surface temperature based on the view factor to the DRPS, the temperature of the DRPS (T_{dips} = 400 K) and the view factor the sky and corresponding sky temperature (T_{sky} = 4 K).

$$\frac{Q_r}{A_s} = 0 = \varepsilon\sigma\left[f_{sky}\left(T_{sur}^4 - T_{sky}^4\right) + f_{1\to2}\left(T_{sur}^4 - T_{dips}^4\right)\right] \tag{4}$$

$$f_{sky} = 1 - f_{1\to2} \tag{5}$$

The resulting surface temperature at a distance from the DRPS is shown in Figure 5.10. This figure shows the surface equilibrium temperature with exposure to the isotope power system. The equilibrium surface temperature is plotted as a function of the distance from the unshielded isotope power system. To keep the regolith in front of the rover in its pristine state remaining at the 50 K ambient environmental temperature during PSR science operations an MLI shield was placed underneath and, on the side, facing the front of the rover. This shielding will block the view of the surface to the DRPS for the terrain in front of the rover.

5.2.1.3 Electronics Coolant System

A single fixed radiator was utilized to provide cooling for the electronic components of the rover. Heat pipes and cold plates were used to move the heat from the electronics to the radiator.

The radiator orientation on the rover was above the electronics. This arrangement provides the best operating conditions for the heat pipe system by having the condenser section, located at the radiator, above the evaporator section, located at the cold plates, thereby returning the fluid in the direction of the gravity field. Two heat pipes are run from each cold plate to the radiator. The heat pipes share the load from each electronics box. Each heat pipe can move the total heat generated from its corresponding electronics box to the radiator. This provides a redundant heat transfer path for each heat source. The arrangement of the heat pipe coolant system is illustrated in Figure 5.11.

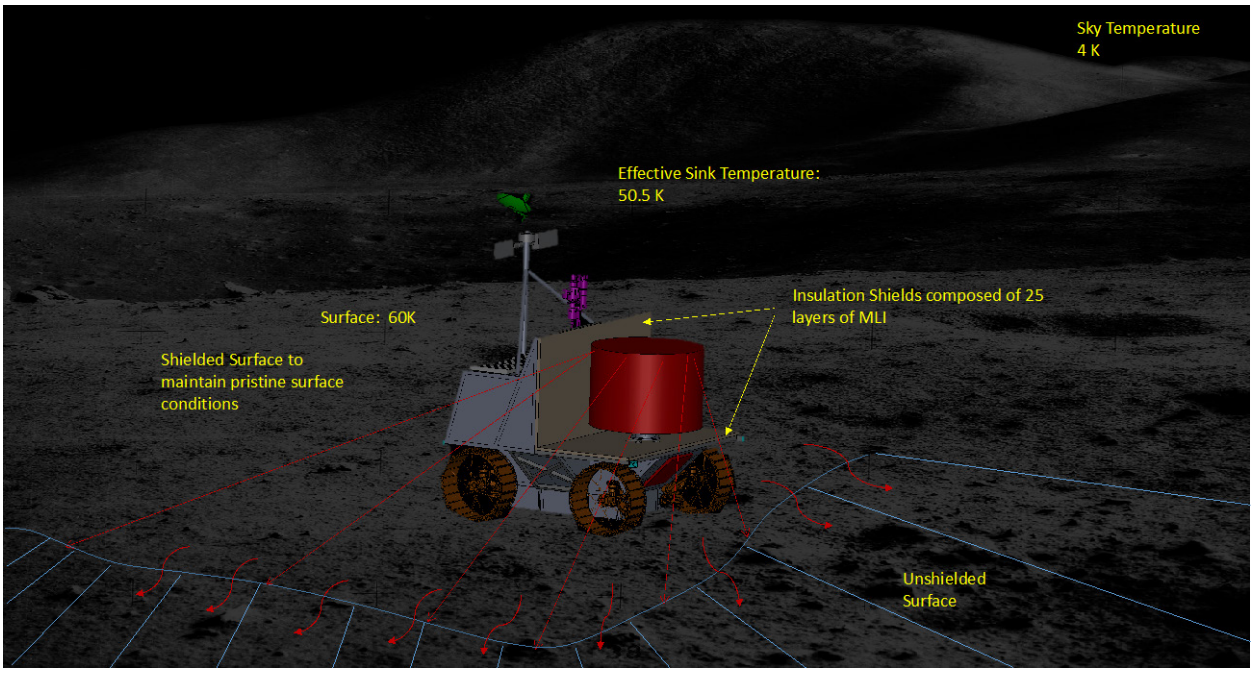

Figure 5.9.—View and Heat Transfer to the Surroundings form the DRPS.

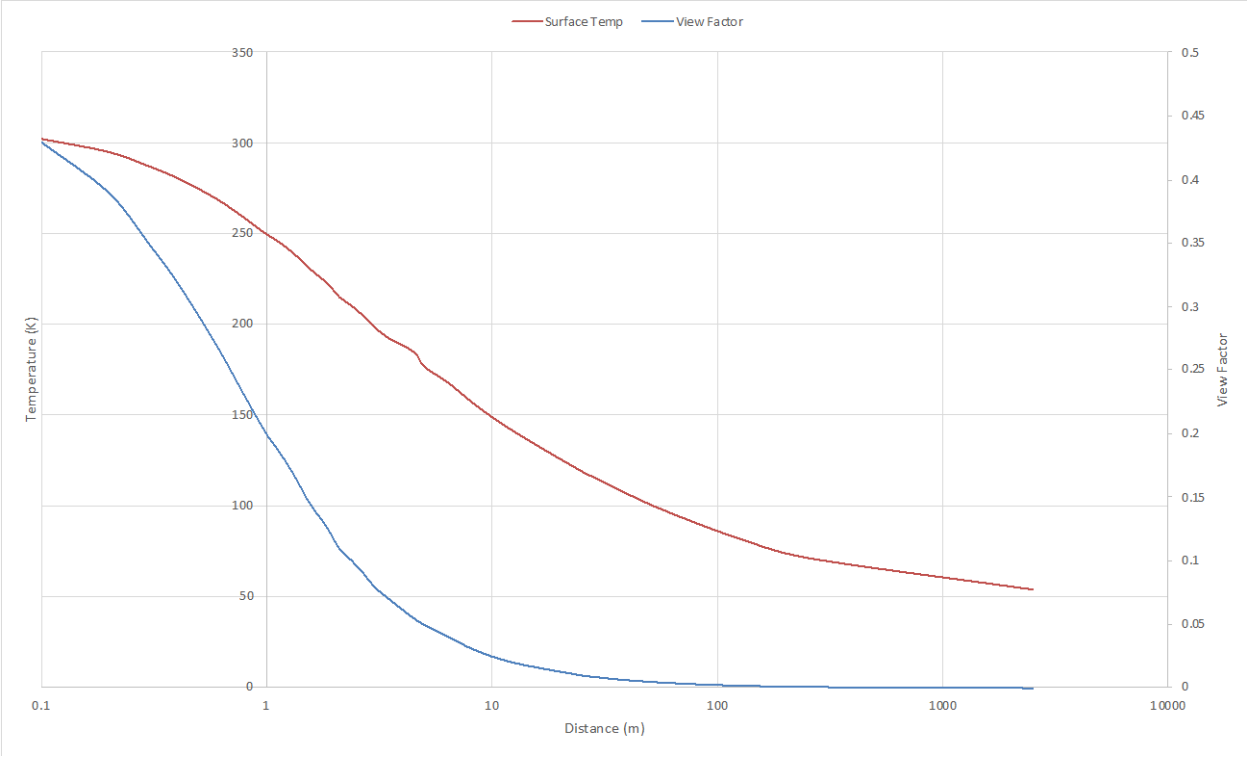

Figure 5.10.—Steady-State Surface Temperature and Surface View Factor to the DRPS.

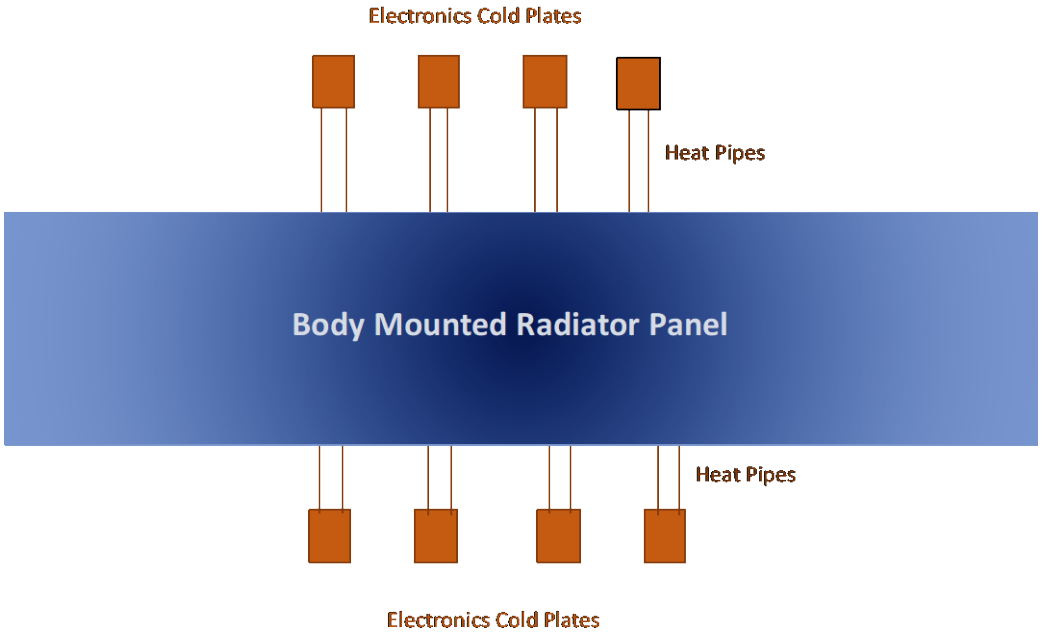

Figure 5.11.—Electronics System Cooling System Layout.

The electronics are mounted to the cold plates where the heat generated is collected. Variable conductance heat pipes move the heat from the cold plates to the radiator. The number of heat pipe runs are dependent on the amount of heat to be moved, their capacity and the amount of redundancy needed in the system. The heat pipe condenser sections are distributed throughout the back side of the radiator. The radiator is coated to reflect the majority of the incoming visible solar radiation. This reduces the heat load on the radiator.

5.2.1.3.1 Radiator

The radiator sizing was based on an energy balance analysis of the area needed to reject the electronics heat load to the surroundings. From the calculated radiator area, a series of scaling equations were used to determine the mass of the radiator. The radiator was sized to remove the waste heat from the electronics during worst case warm operational conditions which occur while sunlit outside of the PSR. The heat rejection for the RPS is integral to the power system design and is included in the power section of this report. The operational environment for the radiator is illustrated in Figure 5.12.

The radiator is located on the top deck of the DRPS rover. It is a body mounted single panel horizontally mounted radiator. This provides a good view to deep space and minimizes the Sun angle to the radiator. There is insulation between the radiator and rover body providing a single surface for radiating. The radiator is connected to the cold plates with heat pipes to move heat from the rover interior to the radiator. The radiator sizing was based on an energy balance analysis of the area needed to reject the identified heat load to space. From the calculated radiator area, a series of scaling equations were used to determine the mass of the radiator. Louvers were used on the radiator to help minimize heat loss during times when the rover will be operating in the PSR.

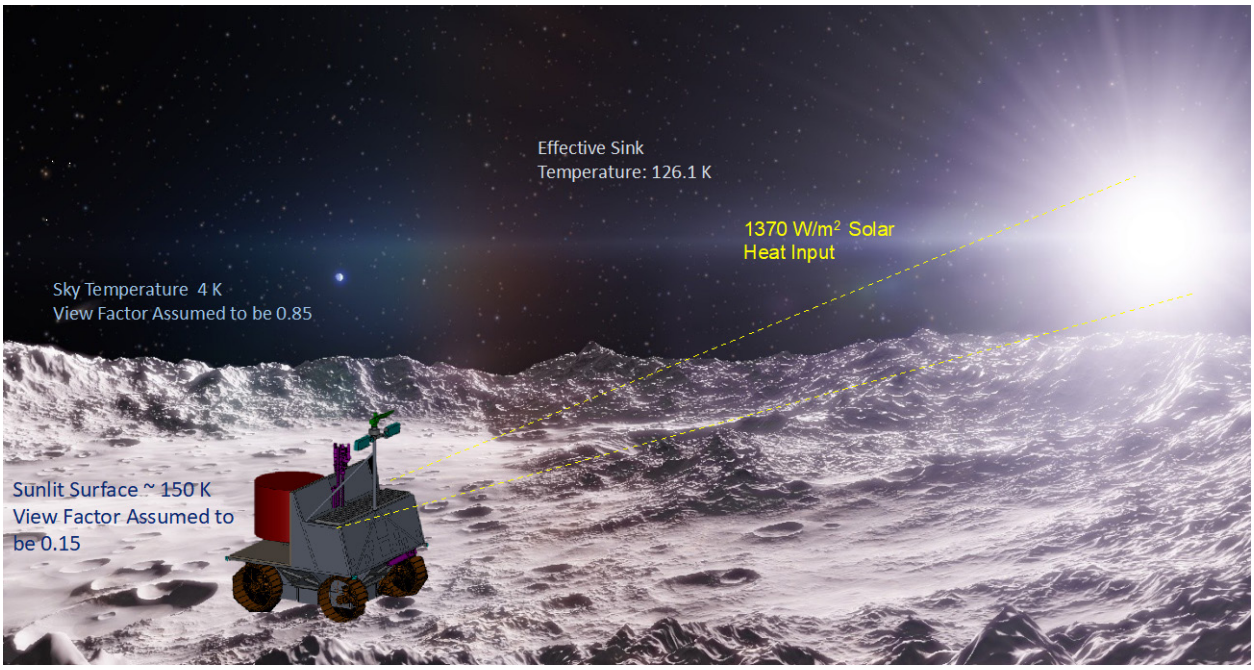

Figure 5.12.—Radiator Energy Balance and Environment Illustration.

The sizing of the system is based on the heat load that must be rejected and the heat transfer from the radiator by radiation to the surroundings. The radiation heat transfer (Q_r) on the lunar surface is based on the view the radiator has to both the surface (F_{sur}) and the sky (F_{sky}) as well as the input heat flux from the Sun. These two views compose the total view of the radiator to the surroundings as given by Equation (6).

$$1 = F_{sur} + F_{sky} \tag{6}$$

The total radiative heat transfer from the radiator to the surface and sky is dependent on the emissivity of the radiator (ε) as given by Equation (7).

$$Q_r = A_r \varepsilon \sigma \left[F_{sky} \left(T_r^4 - T_{sky}^4 \right) + F_{sur} \left(T_r^4 - T_{sur}^4 \right) \right] - \alpha \phi_s [\cos(\beta) + a \cos(\gamma)] \tag{7}$$

Where the Stefan-Boltzmann constant (σ) is:

$$\sigma = 5.670367 \times 10^{-8} \ [\mathrm{W/m^2K^4}] \tag{8}$$

An estimate of the mass of the radiator panel (m_r) can be made based on its required area. The radiator structure can be separated into the following components with a scaling coefficient for each component to linearly scale the mass based on the required radiator area: panels (C_p), coating (C_c), tubing (C_t), header (C_h), adhesives (C_a), stringers (C_s), and attachment (C_{at}). These coefficients were derived from satellite and spacecraft radiator mass data and are listed in Table 5.11. Equation (9) shows the total radiator mass.

$$m_r = C_p A_r + C_c A_r + C_t A_r + C_h A_r + C_a A_r + C_s A_r + C_{at} A_r \tag{9}$$

The specifications used to size the radiator are shown in Table 5.12.

To minimize heat loss at night or while in shadow, the electronics radiator on the rover utilizes louvers. Louvers are active or passive devices that regulate the amount of heat rejected by the radiator by opening and closing to change the view to the surroundings of the radiator radiating surface.

Active controlled louvers use temperature sensors and actuators to control the louver position whereas passive controlled louvers commonly use a bimetallic spring that opens and closes the louver based on temperature. The addition of louvers increases the required radiator area by approximately 30 percent over a radiator without louvers. This is due to the reduced view to the surroundings even when the louvers are fully opened. The louver specific mass is 4.5 kg/m^2.

TABLE 5.11.— RADIATOR MASS SCALING COEFFICIENTS

Coefficient	Value, kg/m^2
C_p	3.3
C_c	0.42
C_t	1.31
C_h	0.23
C_a	0.29
C_s	1.50
C_{at}	0.75

TABLE 5.12.—RADIATOR SIZING VARIABLES

Radiator Item	Value
View Factor to the sky (F_{sky})	0.85
View Factor to the surroundings (F_{sur})	0.15
Sun angle onto Radiator (β)	1.5°
Max angle of the Radiator to the Surface (γ, 0° normal, 90° Parallel)	88.5°
Radiator Heat Rejection (Q_r)	Total Power Dissipation is 221.5 W of this 89 W are lost as waste heat to the surroundings. Total Rejected Heat: 132.5 W
Radiator Emissivity (ε)	0.85
Radiator Solar Absorptivity (α)	0.14
Calculated Radiator Area (A_r)	0.43 m^2
Radiator Operating Temperature	300 K Crater Rim (sunlight operation) 300 K In PSR
Configuration	Horizontal Body Mounted

5.2.1.3.2 Heat Pipes

Heat pipes in general operate by boiling a liquid fluid when the heat pipe is subjected to heat at a design operating temperature. The fluid vapor then moves to the opposite end of the heat pipe (radiator) where the heat is rejected, and the fluid condenses back to a liquid. A wick structure in the absence of gravity is used to help move the fluid back to the heating section through capillary forces. Once back to the heat input section the fluid will boil again repeating the process.

Variable conductance heat pipes operate in a similar fashion but use a varying volume, non-condensable gas to adjust the amount of heat that the heat pipe can move while maintain a fixed operating temperature.

At high heat loads the temperature dependent saturation pressure of the working fluid increases. This increase in pressure compresses the non-condensable gas into a reservoir at the end of the heat pipe provide a larger active condenser are, thereby enabling more heat to be moved to the radiator by the heat pipe. As the heat load decreases the pressure decreases and the non-condensable gas fills up a greater volume of the heat pipe reducing the condenser area and thereby reducing the heat flow. Thus, a variable conductance heat pipe is a passive device that adjusts automatically to varying heat load inputs maintaining a constant operating temperature.

The working fluid for the heat pipe is chosen based on the desired operating temperature of the heat pipe and the heat removal requirement. To size the heat pipe and select the best working fluid a factor termed the Merit Number is utilized. The Merit number (N) is based on the properties of the working fluid as given by Equation (10). These properties include the latent heat of vaporization (H_v), the density (ρ_{wf}), surface tension (σ_{wf}) and the dynamic viscosity (μ_{wf}).

$$N = \frac{H_v \rho_{wf} \sigma_{wf}}{\mu_{wf}} \tag{10}$$

This number is plotted for various fluids in Figure 5.13. The higher the N the greater the performance of the heat pipe. From this figure it can be seen for the desired operating temperature of 300 K water provides the best choice.

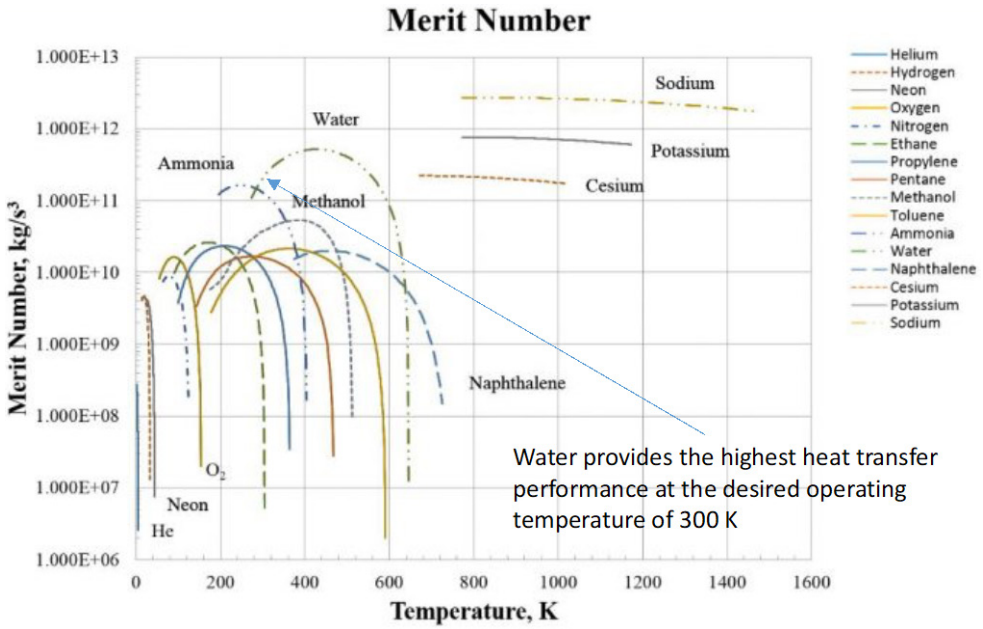

Figure 5.13.—Heat Pipe Merit Number Comparison for Various Working Fluids.

Using the Merit number, the heat pipe thermal power (P_{hp}) transfer capacity can be calculated as given by Equation (11) which is based on the heat pipe wick cross sectional area (A_w), the wick material permeability (K_w), the wick pore radius (r_{wp}) and the heat pipe length (L_{hp}).

$$P_{hp} = \frac{2NA_wK_w}{r_{wp}L_{hp}} \tag{11}$$

Using Equation (11) the heat pipes were sized for the heat produced by each of the loads. The required heat pipe size and specific mass are given in Table 5.13.

5.2.1.3.3 Cold Plates

Cold plates are used to interface the heat pipes to the loads. These plates come in a number of shapes and sizes depending on the heat source configuration. They are used to provide a good thermal connection between the heat source and the heat pipe evaporator section. The heat source is mounted to the cold plate which in turn has the heat pipe either mounted to it or incorporated into it. This provides a good thermal contact between the cold plate and the heat pipe.

The number of cold plates and heat pipe runs that are used is dependent on the distribution of the loads and the desired redundancy for the thermal system. The electronics cold plates have two heat pipe runs per plate. The heat pipes share the load from each cold plate, although each heat pipe can carry the full heat load from the cold plate. The two heat pipe runs are used to provide a redundant heat flow path in case of a failure of one of the heat pipes. The cold plate specifications are summarized in Table 5.14.

5.2.1.3.4 Heaters

Electric heaters are incorporated onto the cold plates as well as on critical components as needed. These heaters are used to maintain the temperature of these components above their minimum operating temperature throughout the mission. Waste heat from the internal components as well as electric heaters are used to provide heat to the spacecraft electronic components if needed. The flexible strip and plate heaters are used to provide heat to the electronic and mechanical components within the spacecraft. Flat plate heaters are used on each of the cold plates to provide heat to the mounted electronics and or packaging if necessary.

TABLE 5.13.—HEAT PIPE SIZING SPECIFICATIONS

Characteristic	Value
Heat Pipe Radius	0.5 cm
Heat Pipe Length	1.5 m
Heat Transfer Capability	20 W per heat pipe
Heat Pipe Mass	0.22 kg (0.15 kg/m) per heat pipe
Number of Heat Pipes	16 (2 per cold plate)

TABLE 5.14.—COLD PLATE SPECIFICATIONS

Variable	Value
Cooling Plate and Line Material	Al
Cooling Plate and Line Material Density	2,770 kg/m^3
Number of Cooling Plates	8 electronics
Cooling Plate Length	0.1 m electronics
Cooling Plate Width	0.1 m electronics
Cooling Plate Thickness	5 mm

Thermal control within the electronics enclosure is accomplished using a network of thermocouples whose output is used to control the power to the various heaters and a data acquisition and control computer is used to operate the thermal system. During normal operation it is estimated that the waste heat from the electronics components will be sufficient to maintain the temperature of the components within the rover within their desired operating temperature range. Therefore, the heater power will be zero or minimal during normal operations. If the waste heat of the system electronics is at least 89 W, the heater power will be zero. In an extenuating circumstance where waste heat is insufficient, heaters will make up the difference.

5.2.2 Insulation

There is no appreciable atmosphere on the Moon. Therefore, in the vacuum of space radiation heat transfer is the main mechanism for heat leak. Multi-layer insulation (MLI) provides the best method for reducing heat leak to the surroundings. MLI is constructed of a number of layers of metalized material with a nonconductive spacer between the layers. The metalized material has a low absorptivity which resists radiative heat transfer between the layers. MLI can be conformed to fit over various shapes. It can be held in place with Velcro or glue.

MLI is used to insulate the electronics enclosure on the rover as well as provide a barrier for the waste heat emitted by the DRPS from heating the surrounding regolith in front of the rover as shown in Figure 5.14. MLI is also used to insulate the wheel motors and the drill motor as well as other components that have temperature requirements above the ambient conditions that are located outside of the electronics enclosure. A thermal analysis of the heat loss that would occur during the nighttime or shadow period was performed. This analysis was used to determine the required heater power that would be required during nighttime operation or if the waste heat from the operation of the electronics was sufficient to maintain the internal operating temperature of the electronics. The heat loss paths from the electronics enclosure that were considered in the analysis included:

- Heat loss through the MLI
- Heat loss from passthroughs and seams in the MLI
- Heat loss through the wheels and support structure
- Heat loss through the drill and sensor structure

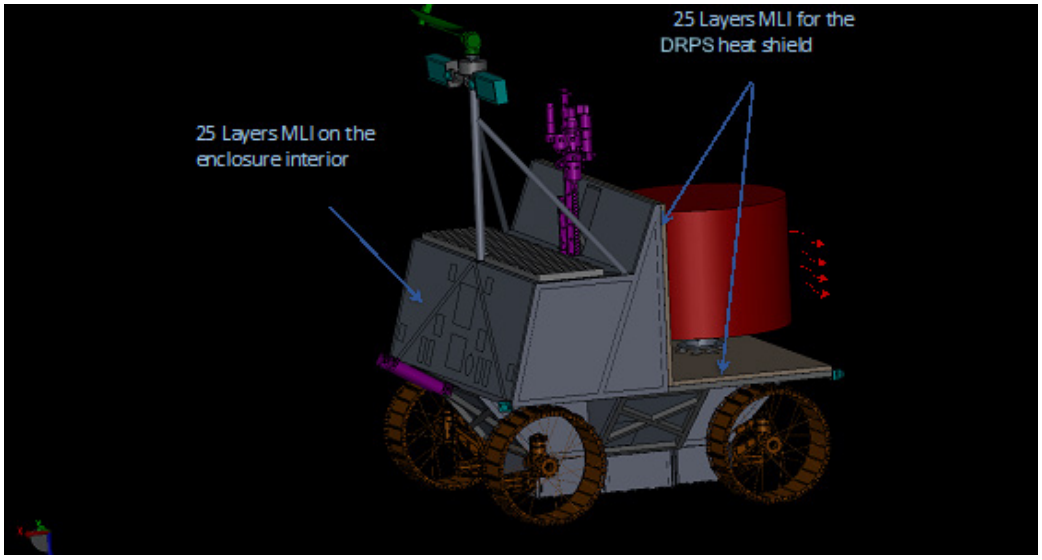

Figure 5.14.—Location of MLI used on the DRPS Rover.

The amount of heat lost through the insulation is dependent on the enclosure surface area, environmental temperatures (desired internal temperature T_{ei} and the nighttime sink temperature T_{sn}) and the type and number of layers of insulation (n). The heat loss from the enclosure through the insulation is given by Equation (12). The heat loss is based on the surface area of the enclosure (A_e) and the emissivity of both the enclosure wall surface (ε_{ew}) and MLI layers.

$$Q_{hi} = \frac{A_e \sigma (T_{ei}^4 - T_{sn}^4)}{\left(\frac{1}{\varepsilon_{ew}}\right) + \left(\frac{2n_l}{\varepsilon_i}\right) - (n_l + 1)} \tag{12}$$

The surface area for the enclosure is dependent on the dimensions given in Table 5.15 as given by Equation (13).

$$A_h = h_e l_e w_e \tag{13}$$

The MLI is very good at resisting heat flow. However, the majority of heat leak through the insulation occurs from passthroughs and seams (Q_{ps}) in the insulation covering. This heat leak is approximated by Equation (14) which is based on the mean insulation temperature (T_m) given by Equation (15) and constants f_p and f_n, given by Equations (16) and (17), respectively.

$$Q_{ps} = 0.664 \left(\frac{0.000136}{4\sigma T_m^2} + 0.000121 T_m^2\right) f_p f_n A_h \sigma \left(T_{hi}^4 - T_{sn}^4\right) \tag{14}$$

$$T_m = \left(\frac{(T_{hi}^2 + T_{sn}^2)(T_{hi} + T_{sn})}{4}\right)^{\frac{1}{3}} \tag{15}$$

The passthrough constant (f_p) is based on the presence of passthrough area (A_{pt}) of items such as wires or tubes that pass through the insulation. This area is given in percent value, for example if the estimated passthrough area is ½ percent, 0.5 is used as the percent passthrough area.

$$f_p = 0.73 + 0.27 A_{pt} \tag{16}$$

$$f_n = 4.547 - 0.501 n_l \tag{17}$$

The MLI specifications used for the variables in determining the heat loss through the passthroughs and seams are given in Table 5.15.

Since the radiator utilizes louvers to adjust its heat rejection to the surroundings, there is no appreciable heat leak from the radiator that has to be accounted for in the overall heat loss from the enclosure.

There will be heat leak through conduction from items that pass through the enclosure and are exposed to the surroundings such as the drill and sensor structure. Also, items such as the wheels that are in direct contact with the surface will conduct heat to the surface. The heat leak (Q_{cp}) through conduction from these sources is given by Equation (18) which is dependent on the number of conductive paths (n_{cp}), the thermal conductivity of the material (k), the cross-sectional area of the material normal to the direction of the heat flow (A_{cp}), and the length of the conductive path (L_{cp}).

$$Q_{cp} = \frac{n_{cp} k A_{cp} (T_{hi} - T_{sn})}{L_{cp}} \tag{18}$$

The cross-sectional area for the conductive paths is given by Equation (19). It was assumed that all the paths considered could be represented by a hollow cylinder shape with a specified inner diameter (d_{icp})

and wall thickness (t_{cp}) where the cross-sectional area of that shape is normal to the flow of heat from the interior of the habitat to the surroundings.

$$A_{cp} = \pi\left(\left(\frac{d_{icp}}{2} + t_{cp}\right)^2 - \left(\frac{d_{icp}}{2}\right)^2\right) \tag{19}$$

Table 5.16 summarizes the variables used to determine the heat leak for each of the identified conductive paths.

TABLE 5.15.—ENCLOSURE PASSTHROUGH AND SEAMS HEAT LEAK VARIABLES

Variable	Value
Insulation Emissivity (e_i)	0.07
Enclosure Wall Emissivity (e_{hi})	0.07
Number of Layers of insulation (n_l)	25
Percent of passthrough Area (A_{pt})	5 percent
Rover MLI Material	Aluminumized Kevlar
Rover MLI Material Aerial Density	
Outer Covering	0.11 kg/m^2
Inner Covering	0.05 kg/m^2
Spacer	0.0063 kg/m^2
Reflective Layer	0.055 kg/m^2
Attachment and Seals Percentage	10 percent
MLI Thickness	1 cm Rover Bus and heat shield
MLI Layer Spacing	0.2 mm
MLI Density	20 kg/m^3
Effective Thermal Conductivity	0.00016 W/mK

TABLE 5.16.—ENCLOSURE CONDUCTIVE PATH HEAT LEAK VARIABLES

Variable	Drill Structure	Sensor and Light Structure	Sensor and Power Wires	Wheels/Enclosure Support Structure
Number of Conductive Paths (n_{cp})	1	1	20	4
Thermal Conductivity (k)	19 W/mK (Stainless Steel)	19 W/mK (Stainless Steel)	400 W/mK (Copper)	6.7 W/mK (Ti-6Al-4V)
Inner Diameter (d_{icp})	5.0 cm	5.0 cm	1 mm	5.0 cm
Thickness (t_{cp})	1.0 cm	0.5 cm	NA	0.5 cm
Length (L_{cp})	0.5 m	0.5 m	0.5 m	10 cm
Interior Temperature (T_{hi})	300 K	300 K	300 K	300 K
Surrounding Sink Temperature (T_{sn})	50.5 K Crater 126 K Rim	50.5 K Crater 126 K Rim	50.5 K Crater 126 K Rim	50.5 K Crater 126 K Rim

The total heat loss from the enclosure to the surroundings during nighttime operation (Q_e) is given by Equation (20) and summarized in Table 5.17 and illustrated in Figure 5.15.

$$Q_e = Q_i + Q_{ps} + Q_{ds} + Q_{sl} + Q_{ss} + Q_w \quad (20)$$

Under normal operation the heat loss is less than the power consumed by the electronics and systems within the enclosure. Therefore, the waste heat from these systems can be used to maintain the enclosure temperature during normal operations.

TABLE 5.17.—ENCLOSURE HEAT LOSS SUMMARY

Heat Loss Path	Heat Loss in PSR (W)	Heat Loss Crater Rim (W)
Insulation (Q_i)	4.5	4.3
Passthroughs and Seams (Q_{ps})	34.0	33.0
Drill Structure (Q_{ds})	11.9	8.3
Support Legs (Q_{sl})	47.3	32.9
Sensor and Light Structure (Q_{ss})	6.7	4.7
Wiring (Q_w)	3.1	2.2
Total (Q_h)	107.5	85.4

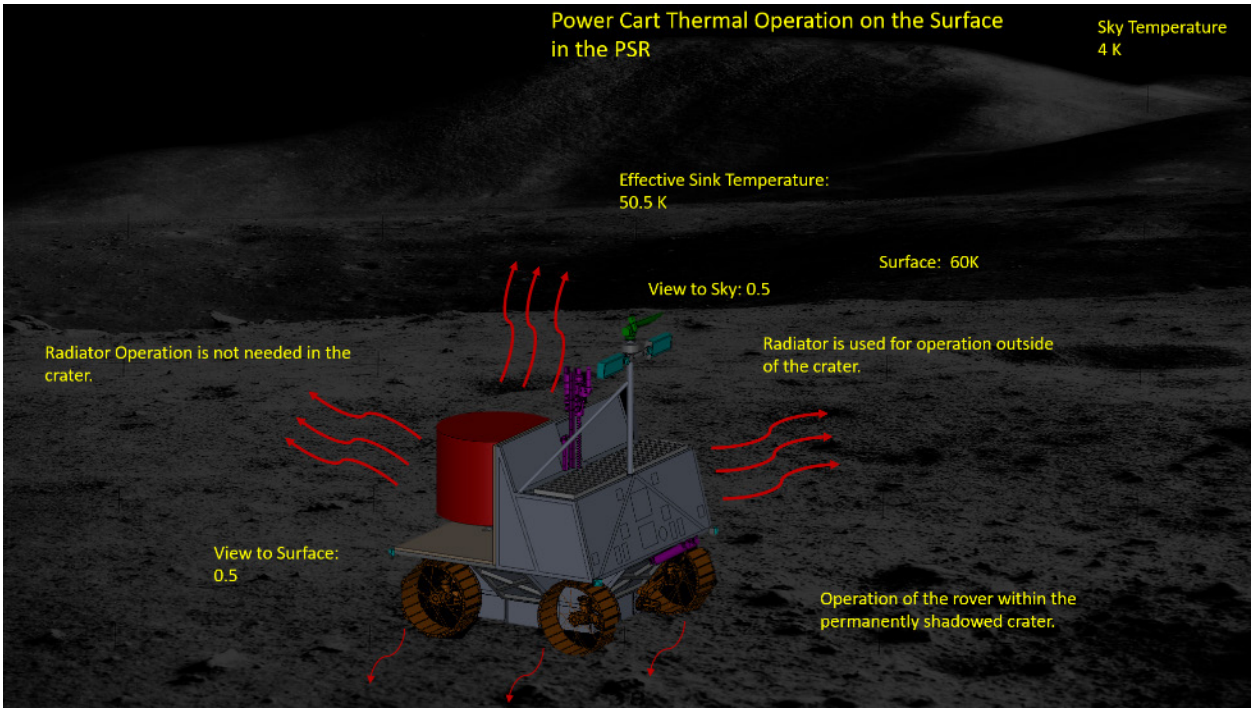

Figure 5.15.—Heat Loss from Electronics Enclosure within the PSR.

5.2.3 Master Equipment List

Table 5.18 and Table 5.19 show the thermal control MELs for the two cases.

TABLE 5.18.—THERMAL CONTROL CASE 1 MEL

Description Case 1_DRPS_DRM_Rover CD-2021-182	QTY	Unit Mass	Basic Mass	Growth	Growth	Total Mass
Thermal Control (Non-Propellant)			**34.8**	**18%**	**6.3**	**41.0**
Active Thermal Control			**2.5**	**18%**	**0.5**	**3.0**
Heaters	8	0.1	0.4	18%	0.1	0.5
Thermocouples	8	0.0	0.1	18%	0.0	0.1
Data Acquisition	5	0.3	1.3	18%	0.2	1.5
Switches	8	0.1	0.8	18%	0.1	0.9
Passive Thermal Control			**27.2**	**18%**	**4.9**	**32.1**
MLI Insulation	1	18.6	18.6	18%	3.4	22.0
Electronics Cold Plates	8	0.1	1.1	18%	0.2	1.3
Electronics Heat pipes	16	0.4	6.6	18%	1.2	7.7
thermal paint	1	0.9	0.9	18%	0.2	1.1
Semi-Passive Thermal Control			**5.0**	**18%**	**0.9**	**5.9**
Electronics Radiator	1	3.2	3.2	18%	0.6	3.8
Radiator Louvers	1	1.8	1.8	18%	0.3	2.2

TABLE 5.19.—THERMAL CONTROL CASE 2 MEL

Description Case 2_Brayton_DRPS_DRM_Rover CD-2021-182	QTY	Unit Mass	Basic Mass	Growth	Growth	Total Mass
Thermal Control (Non-Propellant)			**36.2**	**18%**	**6.5**	**42.7**
Active Thermal Control			**2.5**	**18%**	**0.5**	**3.0**
Heaters	8	0.1	0.4	18%	0.1	0.5
Thermocouples	8	0.0	0.1	18%	0.0	0.1
Data Acquisition	5	0.3	1.3	18%	0.2	1.5
Switches	8	0.1	0.8	18%	0.1	0.9
Passive Thermal Control			**28.6**	**18%**	**5.2**	**33.8**
MLI Insulation	1	20.0	20.0	18%	3.6	23.6
Electronics Cold Plates	8	0.1	1.1	18%	0.2	1.3
Electronics Heat pipes	16	0.4	6.6	18%	1.2	7.7
thermal paint	1	0.9	0.9	18%	0.2	1.1
Semi-Passive Thermal Control			**5.0**	**18%**	**0.9**	**5.9**
Electronics Radiator	1	3.2	3.2	18%	0.6	3.8
Radiator Louvers	1	1.8	1.8	18%	0.3	2.2

5.3 Structures

The DRPS DRM Lunar Rover structures must contain the necessary hardware for command and data handling, communication and tracking, electrical power, thermal control, science, and mobility. The structural components must be able to withstand applied mechanical and thermal loads. In addition, the structures must provide minimum mass and deflections, sufficient stiffness, and vibration damping. The operational loads include an approximate maximum axial acceleration of –5.5g along with a 0.5 g lateral acceleration from the launch vehicle. Also, a maximum lateral acceleration of 2.0 g along with a –4.0 g axial acceleration during the launch trajectory. There is a desire to have the payload cantilevered fundamental mode frequency to have a minimum of 8 Hz lateral and 15 Hz axial as is the case with NASA's Space Launch System (SLS) (Ref. 11), as well as other launch vehicles.

Mechanisms are used to setup the various systems into an operational condition. Mechanisms are used to deploy hardware. Also, mechanisms are use the orient instruments for operations.

5.3.1 System Requirements

The bus is to support the mounted hardware bearing launch and operational mechanical and thermal loads without failure. The structures shall not degrade for the extent of the mission in the Earth and lunar environments.

5.3.2 System Assumptions

The bus provides the backbone for the mounted hardware. The primary materials for the bus are Al, glass/epoxy composite, and Ti. The Al alloy is 7075-T6 as described in the Federal Aviation Administration's Metallic Materials Properties Development and Standardization (MMPDS-14) (Ref. 12). The glass/epoxy composite, S2-449 43.5k/SP 381 as described by Department of Defense (DOD) Military (MIL) Handbook (HDBK)-17(Ref. 13), is used in wound tubes of struts. Ti-6Al-4V is used for the strut tube ends. The materials are at a TRL6 as presented by Mankins (Ref. 14). Components are of shells and tubular members. Joining of components is by threaded fasteners, riveting, or bonding.

Secondary structures include the struts and adapters for the DRPS. Covers and brackets for the covers are part of the secondary structures also. Other secondary structures are the components for installation hardware.

Mechanisms include a Frangibolt® release for the mast mounted camera assembly. Also, the camera assembly uses a gimbal for turning and another gimbal for elevation adjustments.

5.3.3 Analytical Methods

The team structures lead used hand calculations and a spreadsheet to conduct preliminary stress analysis. In addition, a quick finite element analysis (FEA) was conducted on a simple model of the main structural components with smaller components being represented by concentrated masses. The FEA model utilized the study's computer aided design (CAD) model.

5.3.4 System Design

The main bus material is Al 7075-T6. Per the MMPDS (Ref. 12) the ultimate strength is 476 MPa (69 ksi) and the yield strength is 421 MPa (61 ksi). Applying safety factors of 1.4 on the ultimate strength and 1.25 on the yield strength and selecting the lower value, as per NASA Standard 5001B (Ref. 15), results in an allowable stress of 337 MPa (49 ksi) at room temperature. The Young's modulus (Ref. 16) is 71.7 GPa (10.4×10^6 psi), the density is 2.80 g/cm^3 (0.101 lb/in^3), and the Poisson's ratio (Ref. 17) is 0.33.

The DRPS supports consist of struts with tubes of a glass fiber reinforced epoxy, S2-449 43.5k/SP 381. Lamina properties are from the DOD-MIL-HDBK-17F (Ref. 13). Ply thickness is 89 μm (0.0035 in.). The ultimate strength is 1.70 GPa (246 ksi) and the Young's modulus is 47.6 GPa (6.91×10^6 psi) from the DOD-MIL-HDBK-17F (Ref. 13). The final laminated composite uses a layup of $[0/60/30/–30/–60/0]_{2S}$ with resulting properties of 29.2 GPa (4.24×10^6 psi) for the Young's modulus in the axial direction and 18.8 GPa (2.72×10^6 psi) in the lateral direction and a failure stress of 193 MPa (28.0 ksi) with the Tsai-Hill failure theory, as described by Agarwal and Broutman (Ref. 18). Collier Research Corporation's HyperSizer® (Ref. 19) was utilized for determining the laminated composite properties. A safety factor of 2.0 is applied to the failure stress, per NASA-STD-5001B (Ref. 15), for a resulting allowable stress of 96.5 MPa (14.0 ksi). The density is 1.85 g/cm^3 (0.067 lb/in^3).

The DRPS support struts use Ti-6Al-4V for the ends. Per the MMPDS (Ref. 12) the ultimate strength is 647 MPa (93.8 ksi) and the yield strength is 539 MPa (78.1 ksi). The resulting allowable stress is 431 MPa (62.5 ksi). The Young's modulus is 114 GPa (16.5×10^6 psi). The density is 4.4 g/cm^3 (0.16 lb/in^3).

A preliminary stress calculation was performed on the struts. Only a vertical load from the DRPS of 100 kg (220 lb) was considered under a 6 g acceleration. It was assumed that the load was shared equally among the struts. The resulting stress in strut tubes is 5.36 MPa (778 psi).

The rover in a stowed configuration on the launch vehicle was evaluated with NASA Structure Analysis (NASTRAN) FEA. A model was compiled using beam and plate elements for the main bus. Major components are represented as concentrated masses. Rigid elements were used to connect various components. Constraints were applied at assumed locations on the base plate to represent stowed mounting points. Figure 5.16 illustrates the meshed model. The two launch vehicle acceleration cases were evaluated.

A modal analysis was conducted initially. The first modal frequency is at 1.7 Hz. It is primarily due to the flexing of the base plate. It should be noted that due to time constraints the base plate was modeled as a simple plate as opposed to an orthogrid architecture. Figure 5.17 illustrates the model at the first modal frequency.

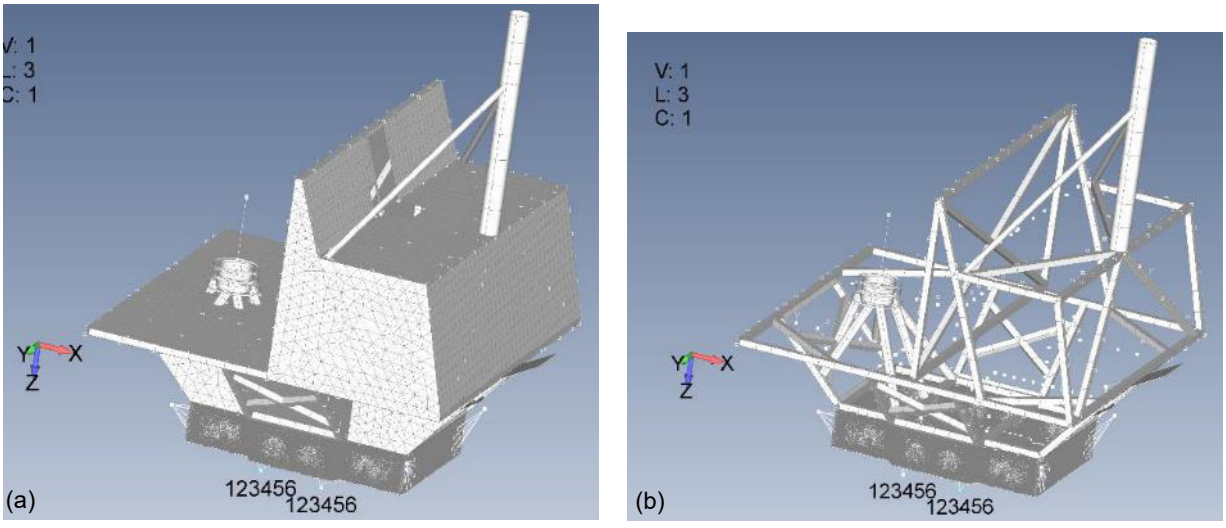

Figure 5.16.—The meshed model of the rover: (a) Full mesh, with plate elements for the covers. (b) Plate elements were hidden to expose the space frame architecture.

Figure 5.18 and Figure 5.19 illustrate the stress state in the RPS support struts under launch loads. Figure 5.18 shows the stress state under the maximum axial acceleration of 5.5 g with a 0.5 g lateral acceleration. The resulting stress in the glass/epoxy composite tube is 21 MPa (3.0 ksi) which provides a positive margin of 3.7 relative to the allowable stress of 119 MPa (14.0 ksi).

Figure 5.19 shows the stress state in the RPS support struts under the maximum lateral acceleration of 2.0 g along with an axial acceleration of 4.0 g. The maximum stress in the strut glass/epoxy tube is 38 MPa (5.5 ksi). The margin is positive at 1.5 relative to the allowable stress of 119 MPa (14.0 ksi).

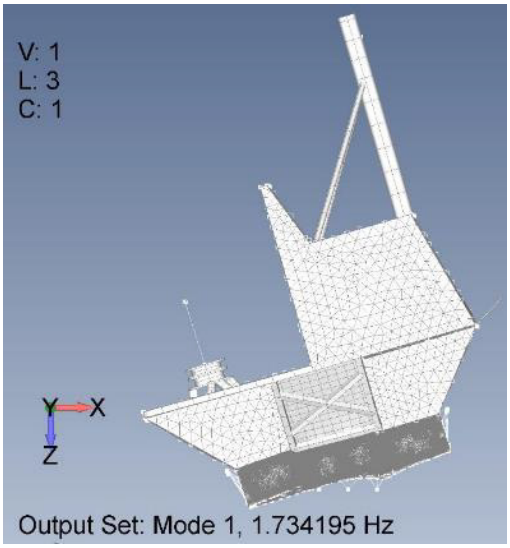

Figure 5.17.—Mode 1 frequency at 1.7 Hz for the stowed rover.

Figure 5.18.—Stress state of the struts supporting the RPS under a 5.5 g axial acceleration and 0.5 g lateral acceleration.

Figure 5.19.—Stress state of the struts supporting the RPS under a 4.0 g axial acceleration and 2.0 g lateral acceleration.

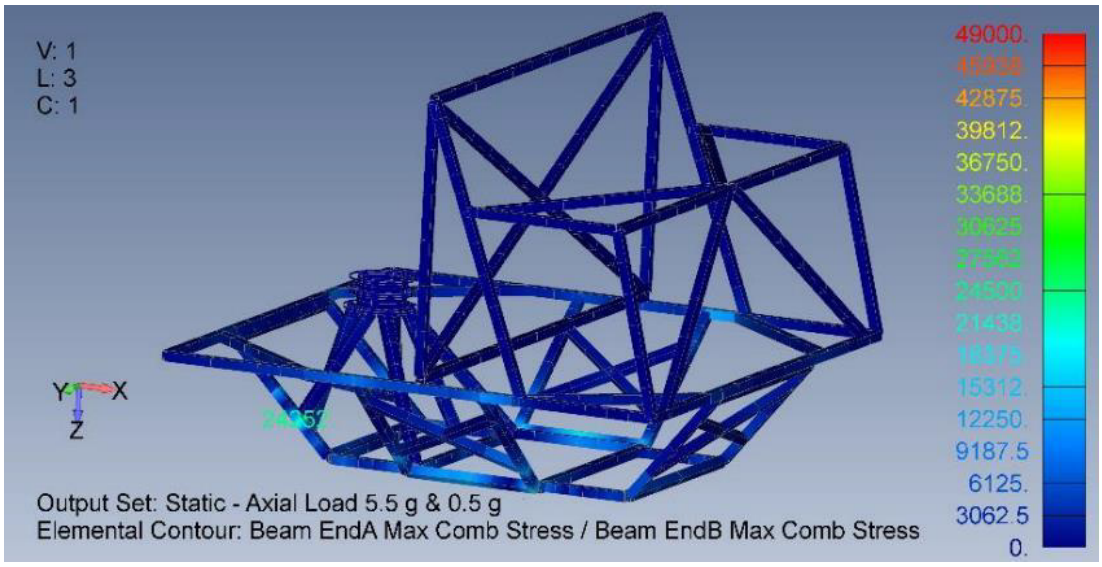

Figure 5.20.—Stress state of the Al tubular members of the space frame under a 5.5 g axial acceleration and 0.5 g lateral acceleration.

Figure 5.20 and Figure 5.21 illustrate the stress state in the tubular space frame of the bus under launch loads. Figure 5.20 shows the stress state under the maximum axial acceleration of 5.5 g with a 0.5 g lateral acceleration. The resulting peak stress in the Al tube is 167 MPa (24.3 ksi) which provides a positive margin of 1.0 relative to the allowable stress of 337 MPa (49.0 ksi).

Figure 5.21 shows the stress state in the tubular space frame under the maximum lateral acceleration of 2.0 g along with an axial acceleration of 4.0 g. The maximum stress in the Al tubes is 247 MPa (35.8 ksi). The margin is positive at 0.37 relative to the allowable stress of 337 MPa (49.0 ksi).

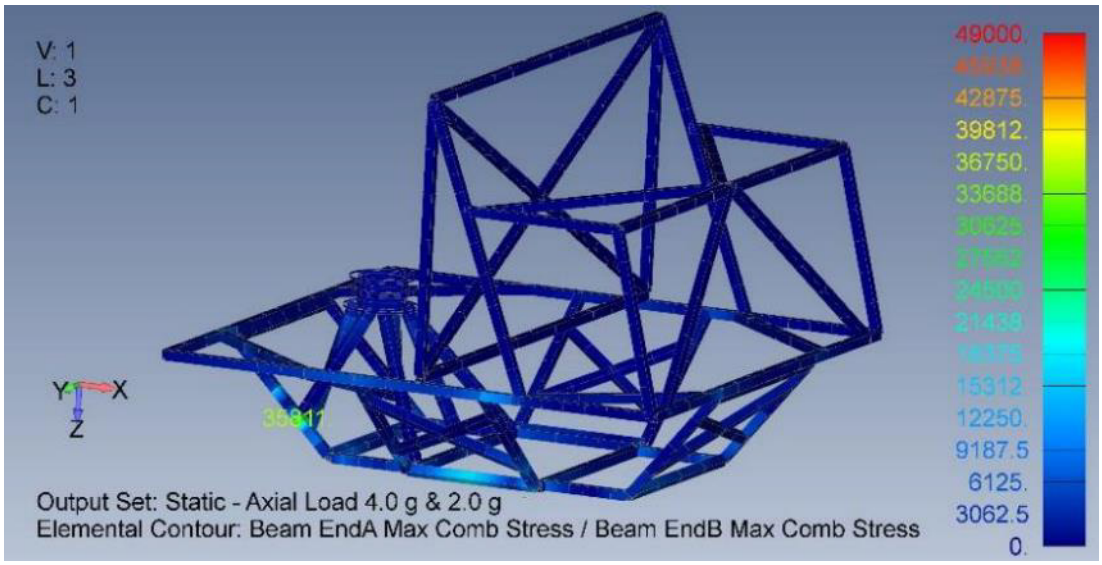

Figure 5.21.—Stress state of the Al tubular members of the space frame under a 4.0 g axial acceleration and 2.0 g lateral acceleration.

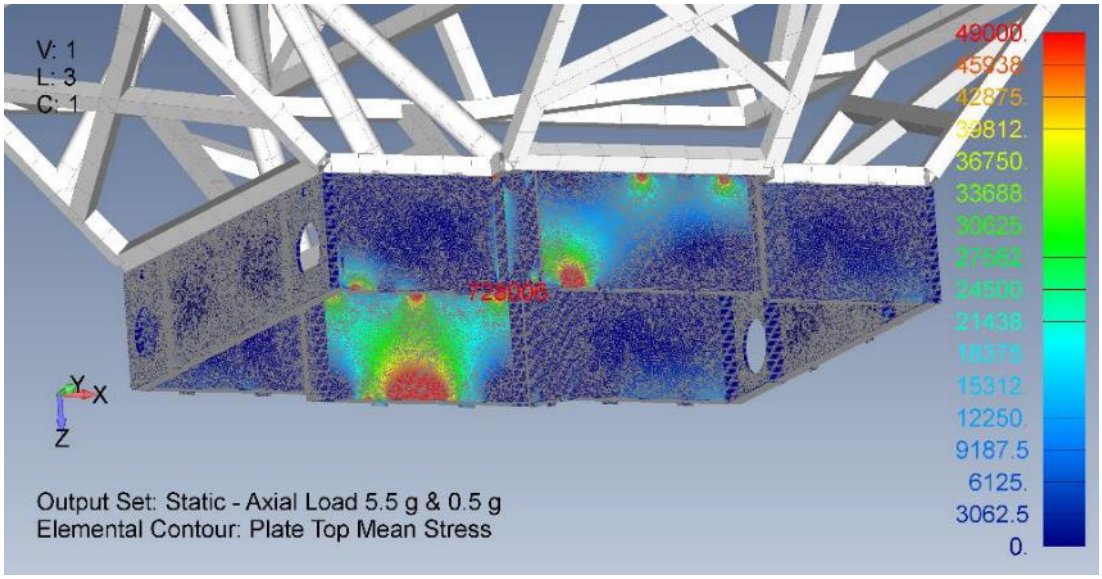

Figure 5.22.—Stress state of the Al base plates of the rover bus under a 5.5 g axial acceleration and 0.5 g lateral acceleration.

Figure 5.22 and Figure 5.23 illustrate the stress state in the base plates of the bus under launch loads. Figure 5.22 shows the stress state under the maximum axial acceleration of 5.5 g with a 0.5 g lateral acceleration and Figure 5.23 shows the stress state under 4.0 g axial acceleration and 2.0 g lateral acceleration. The resulting peak stresses exceed the allowable stress of 337 MPa (49.0 ksi) in large areas. The plate thickness needs to be increased but the model component interconnections may have to be reevaluated also. The low fidelity modeling of the base plate may be another source for the high resulting stresses.

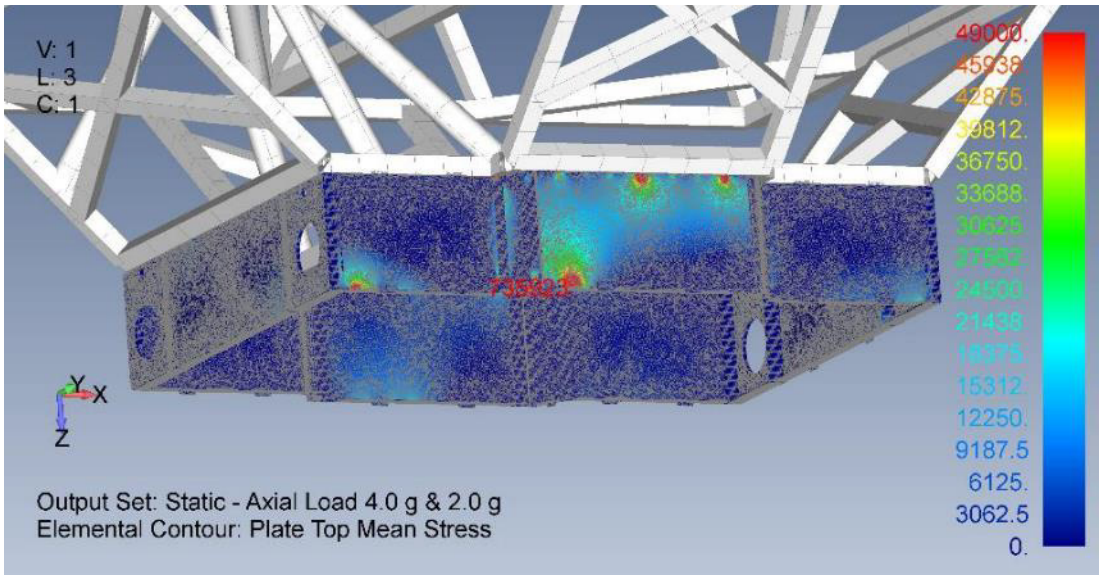

Figure 5.23.—Stress state of the Al base plates of the rover bus under a 4.0 g axial acceleration and 2.0 g lateral acceleration.

Installation hardware is calculated as 4 percent of the installed hardware mass. Heineman (Ref. 20) has shown that past spacecraft indicate that the 4 percent is a good approximation for the mass. The 4 percent installation hardware mass was applied to the command and data handling; communication and tracking; electrical power; thermal control; science; and mobility systems.

Mechanisms are used for the rover. A Frangibolt is used to release the mast mounted camera assembly from a stowed condition. Also, a gimbal is used to turn the cameral assembly on the mast and a gimbal is used to adjust elevation.

5.3.5 Recommendation(s)

The fidelity of the FEA model needs to be increased. The base plate needs the details of an orthogrid to be incorporated for additional stiffness. A higher fidelity model would provide more accurate modal frequencies and responses to various launching and operational loads. Greater use of orthogrid or isogrid panels or advanced fiber reinforced polymer matrix composites may help increase stiffness and reduce bus mass.

5.3.6 Master Equipment List

Table 5.20 and Table 5.21 show the structures and mechanisms MELs for the two cases.

TABLE 5.20.—STRUCTURES AND MECHANISMS CASE 1 MEL

Description Case 1_DRPS_DRM_Rover CD-2021-182	QTY	Unit Mass	Basic Mass	Growth	Growth	Total Mass
Structures and Mechanisms			**42.1**	**18%**	**7.6**	**49.6**
Structures			**30.1**	**18%**	**5.4**	**35.5**
Primary Structures			14.9	18%	2.7	17.6
Base Plate Assy.	1	6.4	6.4	18%	1.2	7.6
Space Frame	1	8.0	8.0	18%	1.4	9.4
Mast	1	0.2	0.2	18%	0.0	0.2
Mast Braces	2	0.2	0.3	18%	0.1	0.4
Secondary Structures			15.2	18%	2.7	17.9
RTG Support Strut Assy.	1	3.9	3.9	18%	0.7	4.6
RTG Adapter Set	1	1.2	1.2	18%	0.2	1.5
Cover Set	1	9.7	9.7	18%	1.8	11.5
Cover Bracket Set	1	0.3	0.3	18%	0.0	0.3
Mechanisms			**12.0**	**18%**	**2.1**	**14.1**
Power System Mechanisms			0.5	18%	0.1	0.5
Camera/Light Elevation Gimbal	1	0.2	0.2	18%	0.0	0.3
Camera/Light Turning Gimbal	1	0.2	0.2	18%	0.0	0.3
Adaptors and Separation			0.1	2%	0.0	0.1
Frangibolt Camera Release	2	0.0	0.1	2%	0.0	0.1
Installations			11.5	18%	2.1	13.5
C&DH Installation	1	0.6	0.6	18%	0.1	0.7
Comm. & Tracking Installation	1	0.4	0.4	18%	0.1	0.5
Electrical Power Installation	1	0.5	0.5	18%	0.1	0.6
Thermal Control Installation	1	1.4	1.4	18%	0.3	1.6
Science Installation	1	3.9	3.9	18%	0.7	4.5
Mobility Installation	1	3.0	3.0	18%	0.5	3.6
Chemical Propulsion Installation	1	1.6	1.6	18%	0.3	1.9

TABLE 5.21.—STRUCTURES AND MECHANISMS CASE 2 MEL

Description Case 2_Brayton_DRPS_DRM_Rover CD-2021-182	QTY	Unit Mass	Basic Mass	Growth	Growth	Total Mass
Structures and Mechanisms			**45.6**	**18%**	**8.2**	**53.8**
Structures			**31.5**	**18%**	**5.7**	**37.1**
Primary Structures			15.5	18%	2.8	18.3
Base Plate Assy.	1	6.4	6.4	18%	1.2	7.6
Space Frame	1	8.6	8.6	18%	1.5	10.1
Mast	1	0.2	0.2	18%	0.0	0.2
Mast Braces	2	0.2	0.3	18%	0.1	0.4
Secondary Structures			16.0	18%	2.9	18.8
RTG Support Strut Assy.	1	3.9	3.9	18%	0.7	4.6
RTG Adapter Set	1	1.2	1.2	18%	0.2	1.5
Cover Set	1	10.5	10.5	18%	1.9	12.4
Cover Bracket Set	1	0.3	0.3	18%	0.0	0.3
Mechanisms			**14.1**	**18%**	**2.5**	**16.6**
Power System Mechanisms			0.5	18%	0.1	0.5
Camera/Light Elevation Gimbal	1	0.2	0.2	18%	0.0	0.3
Camera/Light Turning Gimbal	1	0.2	0.2	18%	0.0	0.3
Adaptors and Separation			0.1	2%	0.0	0.1
Frangibolt Camera Release	2	0.0	0.1	2%	0.0	0.1
Installations			13.6	18%	2.4	16.1
C&DH Installation	1	0.7	0.7	18%	0.1	0.9
Comm. & Tracking Installation	1	0.4	0.4	18%	0.1	0.5
Electrical Power Installation	1	0.7	0.7	18%	0.1	0.8
Thermal Control Installation	1	1.4	1.4	18%	0.3	1.7
Science Installation	1	6.0	6.0	18%	1.1	7.1
Mobility Installation	1	2.7	2.7	18%	0.5	3.2
Chemical Propulsion Installation	1	1.6	1.6	18%	0.3	1.9

5.4 Science Subsystem

The Science Subsystem must encompass instruments capable of completing exceptional science on the lunar surface. For the purposes of this design, the science subsystem was almost entirely copied directly from available information on the VIPER science subsystem. This design hopes to build on the science accomplished by VIPER by extending its range and duration (Ref. 21).

5.4.1 Science System Assumptions

The science subsystem is assumed to use the same science instruments as VIPER. These instruments include:

- Neutron Spectrometer System (NSS): used to find potential water present on the lunar surface, and up to 3 ft below the surface, to be further investigated by the balance of the instrument suite.
- Near-Infrared Volatiles Spectrometer System (NIRVSS): used to determine the nature of the H_2 in the lunar regolith, namely whether it is contained in water molecules, hydroxyl, or simply H_2

atoms. The instrument also includes a context imager and a calibration sensor which measures temperature. Both lend context to the data collected.

- Mass Spectrometer Observing Lunar Operations (MSolo): A mass spectrometer primarily focused on identifying water ice and other volatiles by assessing gases in the environment.
- The Regolith and Ice Drill for Exploring New Terrains (TRIDENT): A 1-m rotary percussive drill capable of sweeping drill cuttings into a pile for further investigation by NIRVSS and MSolo.

Additionally, the team carried a 10.5 kg unnamed science instrument with 2 W of standby power and 10 W of operating power to account either for unforeseen instrument growth on VIPER or the ability to add another science instrument, such as a gravimeter.

5.4.2 Master Equipment List

Table 5.22 shows the science MEL.

5.5 Mobility System

The VIPER mobility system is based on the Resource Prospector architecture RP1A with numerous design updates. These updates include increased loads requirements (300 to 450 kg rover), lunar shadow survival, better design adherence to NASA Standard (STD) 8070 (NASA-STD-8070) (Ref. 22), slight kinematic changes to the design, and component optimization based on lessons learned during both ground testing and numerous Mars rover campaigns.

5.5.1 System Requirements

The mobility system is required to provide a prospecting speed of 10 cm/s, a top speed on level terrain of 20 cm/s, and the ability to transverse a slope of ± 15° with no more than 40 percent slip. The suspension system should provide the rover with the capability to clear a 20 cm obstacle while still being compact enough for launch. To provide maximum directional control of the rover, the mobility system is required to provide a zero radius turn capability, thus requiring a steering range *greater than* ±45°. To navigate potentially rugged terrain, the mobility system should be fully functional in both forward and reverse, as well as provide for independent control of each wheel in steering, suspension actuation, and propulsion.

TABLE 5.22.—SCIENCE MEL

Description Case 1_DRPS_DRM_Rover CD-2021-182	QTY	Unit Mass	Basic Mass	Growth	Growth	Total Mass
Science			40.0	3%	1.2	41.2
Science Package			40.0	3%	1.2	41.2
Main Rover Science			40.0	3%	1.2	41.2
NSS Sensor Modules	1	1.0	1.0	3%	0.0	1.0
NSS Data Processing Modules	1	1.0	1.0	3%	0.0	1.0
NIRVSS Spectrometer Modules	1	1.8	1.8	3%	0.1	1.8
NIRVSS Observation Brackets	1	1.8	1.8	3%	0.1	1.8
Msolo	1	6.0	6.0	3%	0.2	6.2
TRIDENT	1	18.0	18.0	3%	0.5	18.5
TBD Instrument	1	10.5	10.5	3%	0.3	10.8

5.5.2 System Assumptions

It is assumed the rover has a nominal mobility power load of 60 W, with a peak mobility power requirement of 300 W. The rover wheelbase is assumed to be 1.5- by 1.5-m with a wheel assembly located nominally at each corner. Each wheel assembly is assumed to have independent steering, independent suspension actuation, and an independent drive motor. The system is also assumed to have high ratio gear trains, triple seal systems at rotation joints, be capable of surviving cryogenic hibernation without the use of radioisotope heating units (RHUs) while remaining fully functional at temperatures down to –50 °C.

5.5.3 Analytical Methods

The analytical methods used in analyzing the mobility system comprised of basic geometric relationships and various spreadsheet calculations to assess mobility limits and overall system capability.

5.5.4 Risk Inputs

There are two major risks for this design. First is the risk of excessive component wear due to lunar dust. Lunar dust can be invasive; therefore, the current rover design utilizes a triple seal design to protect the mobility system joints and bearings. This new design has shown promise in testing, but currently has no flight or lunar heritage.

Second, there are risks associated with operating in the extreme lunar thermal environment. Although the mobility system has been designed to withstand cold lunar temperatures, and the appropriate lubricants have been identified for the gear trains, there is a risk of unknown issues due to the current lack of operational experience in the cold lunar environment.

5.5.5 System Design

The rover mobility system consists of an actuated wheel assembly located nominally at each corner of the chassis. Each wheel assembly has independent steering, independent suspension actuation, and an independent drive motor. Each actuation assembly has a high ratio gear train and a triple seal system at all rotational joints. This system consists of an outer labyrinth seal, a felt wiper seal, and an inner spring energized seal to protect the bearing and inner actuator components from the lunar dust. All the mobility system motors are a frameless DC design, operate on 24 Vdc bus voltage, have a continuous current draw of less than 10 A, and a peak current draw between 10 to 20 A for under 10 s.

A prototype of this system has been tested in simulated lunar regolith to assess wheel, steering, mobility, and suspension system performance, as well as overall chassis dynamics. Pictures of this testing are shown in Figure 5.24 and show both 45°e steering actuation and the use of independent steering and drive motors (Ref. 23).

The wheels are 50 cm in diameter and 20 cm wide. They are constructed of individual sheet metal channels that are riveted together and attached to both the outer rims via tabs and the inner hub via tensioned spokes. These channels form the tread of the wheel and have crowned grousers with a depth of ~2.5 cm. The wheels are made of 7075 Al alloy and stainless-steel spokes and are designed to operate for greater than 40 km under nominal wear.

The inner hub attaches directly to the drive motor assembly which houses the drive motor, a three-stage planetary gearbox with a greater than 400:1 gear reduction ratio, and an integrated three stage seal system protecting the drive motor actuator assembly. This system can survive cryogenic hibernation without the use of RHUs while remaining fully functional at temperatures down to –50 °C. Figure 5.25 shows the VIPER chassis.

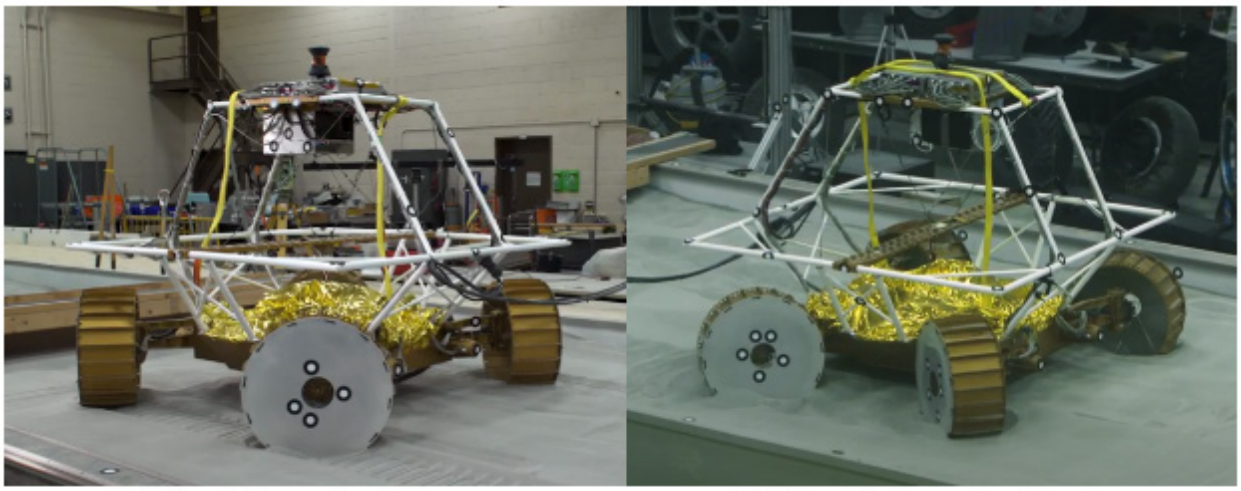

Figure 5.24.—Prototype Chassis Testing in Lunar Simulant.

Figure 5.25.—VIPER Chassis.

Steering is provided via an actuator assembly that is mounted to the steering knuckle inside the inner wheel rim. These actuators have greater than 120:1 gear reduction ratio, provide for more than ± 45° of independent steering, and have an integrated triple seal system at both the top and bottom of actuator assembly, where they attach to the steering knuckle brackets. Each steering knuckle bracket is attached to two suspension system arms that form a four-bar linkage with the rover chassis. This arrangement allows each wheel to travel vertically relative to the rover as the suspension system actuates. This system provides for ± 40° of suspension travel relative to horizontal and is actuated by actuator assemblies mounted on the rover chassis. Each actuator has greater than 600:1 gear reduction ratio, an integrated anti-back drive device, and a triple seal system.

As the suspension actuates through its ± 40° range of motion, it allows the rover chassis to rise from a minimum ground clearance of 5.8 cm to a fully raised 41.8 cm, with the nominal position yielding 23.8 cm. The lower position is used as the stowed position for launch, while the fully raised position gives the rover ample clearance to drive over objects of interest, thus allowing the instrument suite on the bottom of

rover access to them. By articulating the front and rear suspension to their extreme positions, the rover chassis is tilted to 14° from horizontal. This allows the rover to travel on a 14° slope with a horizontal chassis orientation, as long as 5.8 cm of ground clearance is adequate at the lowered end. The suspension systems range of articulation is shown in Figure 5.26.

5.5.6 Recommendation(s)

It is recommended to further evaluate the use of a protective sleeve that encases each suspension and mobility system. This sleeve consists of abrasion resistant inner and outer layers with layers of MLI in between to protect against dust, abrasion, and thermal deviation. The sleeve's design, however, must not appreciably increase any required motor power or limit the mobility systems range of motion in any plane.

5.5.7 Master Equipment List

The MEL for the mobility system is shown in Table 5.23

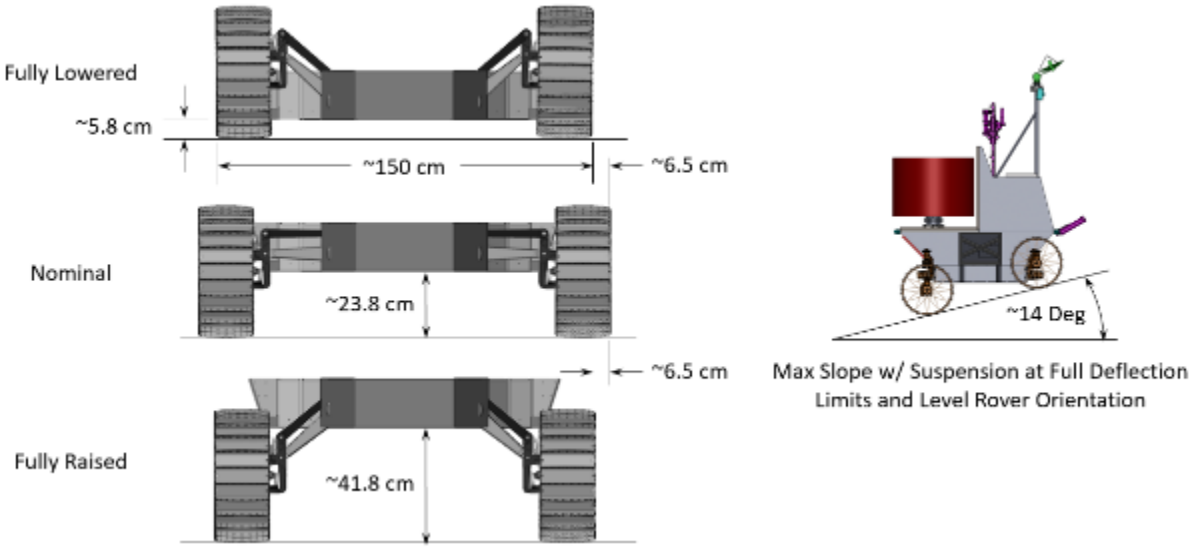

Figure 5.26.—Suspension System Articulation Range.

TABLE 5.23.—MOBILITY SYSTEM MEL

Description Case 1_DRPS_DRM_Rover CD-2021-182	QTY	Unit Mass	Basic Mass	Growth	Growth	Total Mass
Mobility			**67.0**	**15%**	**10.1**	**77.1**
Mobility System			**67.0**	**15%**	**10.1**	**77.1**
Mobility System Hardware			67.0	15%	10.1	77.1
Supension Actuators	4	4.5	18.0	15%	2.7	20.7
Steering Actuators	4	4.5	18.0	15%	2.7	20.7
Drive Actuators	4	4.5	18.0	15%	2.7	20.7
Supension Arm Assemblies	4	2.0	8.0	15%	1.2	9.2
Wheels	4	1.3	5.0	15%	0.8	5.8

5.6 Command and Data Handling

The C&DH system provides command, control, health management, and data processing to the subsystems of the DRPS DRM Lunar Rover. This design estimates the requirements to interface with drivers, analog systems, and digital systems. The dimensions and mass of the wiring harness and avionics enclosure are derived from the C&DH master equipment list. The C&DH system includes an AiTech SP0 single board computer (SBC) as the main processing unit. The SBC runs a Real Time Operating System (RTOS) to house the C&DH specific flight software and contains 8 GB storage. A mass flash memory card was added for science data storage. Software estimation is outside the scope of this design.

The C&DH system was designed using a variety of interface cards to connect to the peripherals of the rover. Custom software tools model the mass of the wiring required to connect to all peripherals and the makeup of a custom actuator driver system to operate the actuators and motors. The system is housed in an avionics enclosure with an integrated power converter to power each card. All components used within this analysis are based on military/space rated commercially available products from verified aerospace system vendors. Each component in this design has a high TRL. Included in this assessment are the preliminary study requirements, system assumptions, analytical methods used, design, recommendations, and the MEL.

5.6.1 System Requirements

The team determined the requirements for the C&DH system based on key system capabilities analyzed in the time allotted for this study. The team derived the C&DH component and design decisions from the following list of non-exhaustive requirements:

- All components shall be rated for 100k rad Total Ionized Dose (TID).
- All science supporting components shall be single fault tolerant with cold backups.
- The components used shall fit the 3U compact Peripheral Component Interconnect (cPCI) form factor standard.
- C&DH shall support data processing for guidance, navigation, and control (GN&C) tracking loop.
- C&DH shall support uplink and downlink data handling for the communication system.
- C&DH shall provide mass data storage for science data storage.
- C&DH shall provide drive control to all electric actuators and motors.

5.6.2 System Assumptions

To work within the timeline allotted for this study, the following assumptions were made to meet the requirements specified in Section 5.6.1:

- Software-based estimation is used to determine the mass of the wiring using a Monte Carlo mathematical distribution (Ref. 24).
- Software-based estimation is used to determine the size, mass, and power usage of the actuator driver system.
- Software-based estimation is used to determine the size and mass of the avionics enclosure.
- Based on science data requirements, 128 GB of hard state storage would be sufficient for science payload processing and storage for transmission.
- A single SP0 single board computer would be sufficient for processing of science payload and communication data.

- 100 percent wire mass growth and 30 percent equipment growth is used based on the AIAA guidelines.
- Wire lengths are based on distance to peripherals in the CAD model of the lunar rover.
- Command and control of the DRPS and GN&C systems are handled by their respective subsystems with interfaces to the C&DH system.
- Power requirements for motor drivers and actuators.
- Data budgets and software requirements.

5.6.3 Analytical Methods

A suite of avionics software is used to estimate the mass and power usage of the C&DH system. This suite contains a motor driver mass/power estimator, an avionics enclosure dimension/mass estimator, and a wire harnessing mass estimator. Each of these tools are described and results are given in the following sections.

5.6.3.1 Motor Driver Estimation

The motor drivers were estimated by separately calculating the waste heat and area of each form-factor printed circuit board (PCB). The waste heat is calculated from the equation:

$$Waste\ Heat = \frac{Motor\ Power}{Driver\ Power\ Supplied} * driver\ dissipation * motor\ count \tag{21}$$

The area required by the PCB is similar to the waste heat calculation:

$$Area = \frac{Motor\ Power}{Driver\ Power\ Supplied} * area\ per\ channel * \frac{motor\ count}{100} \tag{22}$$

The area required is then used to calculate the 3U cPCI card count. The results of this estimation are shown in Table 5.24.

Five 3U cPCI motor controller cards are sufficient to meet the required PCB area calculated from the tool. This totals to a mass of 2 kg.

TABLE 5.24.—MOTOR ESTIMATION

Actuator Name	Peak Power/Actuator	Number of Actuators	Waste Heat	PCB Area Required (cm^2)
Locomotion System	75	12	35.4	514.3
Science and Navigation System	66	1	2.6	37.7
TRIDENT Drill	175	1	6.9	100
Communication and Tracking Gimbal	5	4	0.8	11.4

5.6.3.2 Avionics Enclosure Estimation

The avionics enclosure size and mass were estimated from the C&DH system's 3U card count. The box mass includes the power conversion unit required to power the avionics cards and the backplane interface. Aluminum was chosen because of its weight and radiation attenuation.

The avionics box size is calculated using the number of cards and their volume. This is shown in Equations (23), (24), and (25).

$$Box\ Hight = 3UcPCI\ Card\ Hight + (2 * Material\ Thickness) + (2 * Clearance) \tag{23}$$

$$Box\ Depth = 3UcPCI\ Card\ Depth + (2 * Material\ Thickness) + (2 * Clearance) \tag{24}$$

$$Box\ Width = (Number\ of\ cards * 3UcPCI\ Card\ Pitch) + (2 * Material\ Thickness) + (2 * Clearance) \tag{25}$$

The mass of the avionics box is calculated using Equation (26).

$$Box\ Mass = (Density\ of\ Material * Thickness\ of\ Materal) * (Surface\ area\ of\ box) + (Power\ Conversion\ Unit\ Mass) + (Backplane\ Mass) \tag{26}$$

The inputs and results from these calculations are shown in Table 5.25 and Table 5.26.

5.6.3.3 Wiring Harness Estimation

A Monte Carlo method (Refs. 24 and 25)based software estimation tool is used to estimate the mass of the wiring required to interface between the peripherals of the lunar rover and the avionics box. The Monte Carlo method is used for drawing a sample at random from an empirical distribution. The method then performs an unbiased risk analysis by creating a model of possible solutions around a probability distribution. As applied to a wire mass simulation, the Monte Carlo method is used for drawing a random length of wire from a distribution between estimated minimum and maximum wire lengths. The mean-value Monte Carlo method is used in this analysis to determine wire mass and is represented in the equation below (Ref. 25)

$$\hat{\theta} = \frac{1}{B} * \sum_{b=1}^{B} f(u_b) \tag{27}$$

In this equation, $\hat{\theta}$ represents the solution for the mass of the wire harness, B is the number of samples, and the function $\sum_{b=1}^{B} f(u_b)$ represents the summation of the samples in the distribution.

Wire gauge was selected based on the current carrying required. Twinaxial 28 American wire gauge (AWG) is used to represent the communication busses. Table 5.27 lists the wiring harnessing mass estimator inputs and results for the lunar rover.

TABLE 5.25.—AVIONICS BOX INPUTS

Form Factor (cPCI)	Number of Cards	Material	Thickness (mm)
3U	18	Al	10

TABLE 5.26.—AVIONICS BOX OUTPUTS

Box Height (cm)	Box Depth (cm)	Box Width (cm)	Box Mass (kg)
16	22	40	6.9

Figure 5.27 shows the results of the Monte Carlo method simulation are distributed along a bell curve. The mean value is the solution to the wire mass used for the wiring to interface with the science systems.

Table 5.28 lists the wiring harness mass estimation for the analog devices.

TABLE 5.27.—MONTE CARLO DIGITAL WIRE MASS SIMULATION INPUTS

Cable	Wire Protocol	kg/m	Number Cables	Min Length (m)	Max Length (m)
NSS Sensor Modules	Twinax 28 AWG	0.058	5	0.5	0.8
NSS Data Processing Modules	Twinax 28 AWG	0.058	5	0.25	0.4
NIRVSS Spectrometer Modules	Twinax 28 AWG	0.058	5	0.6	0.8
Msolo	Twinax 28 AWG	0.058	5	0.8	1.2
TRIDENT	Twinax 28 AWG	0.058	5	1.5	2.1
TBD Instrument	Twinax 28 AWG	0.058	5	1	2.5
TRIDENT Drill Drive	20 AWG	0.035	2	1.5	2.1

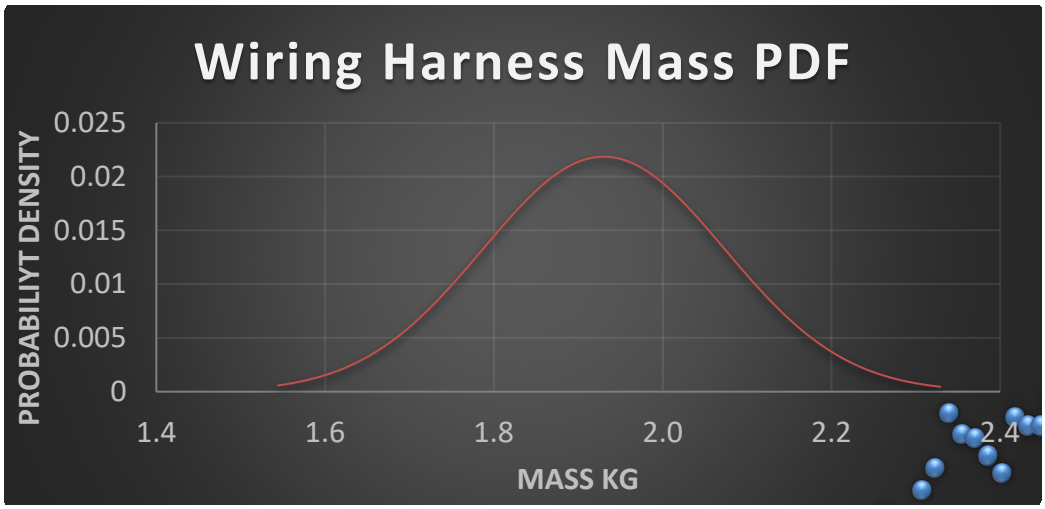

Figure 5.27.—Monte Carlo Science Wire Mass Simulation Distribution Output.

TABLE 5.28.—MONTE CARLO ANALOG WIRE MASS SIMULATION INPUTS

Cable	Wire Protocol	kg/m	Number Cables	Min Length (m)	Max Length (m)
Suspension Actuators	22 AWG	0.0035	8	0.85	1.2
Steering Actuators	22 AWG	0.0035	8	0.85	1.2
Drive Actuators	22 AWG	0.0035	8	0.85	1.2
Thermal Sensors	24 AWG	0.0022	10	0.5	3.5
NAV Cameras OpNav DVR	Twinax 28 AWG	0.058	5	1.4	1.7
HAZ Cameras	22 AWG	0.0035	4	1.2	1.6
RPS Controller	Twinax 28 AWG	0.058	5	0.65	1.1
SDR - TX/RX	Twinax 28 AWG	0.058	5	1.1	1.45
Antenna Gimbal	24 AWG	0.0022	6	2.4	3.9

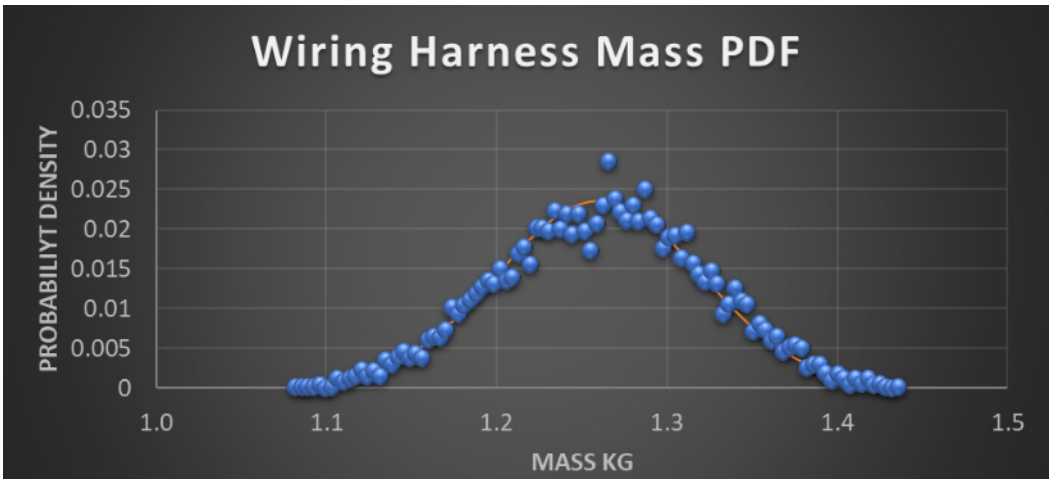

Figure 5.28.—Monte Carlo Locomotion, Guidance, Navigation, and Control interfacing Wire Mass Simulation Distribution Output.

Figure 5.28 shows the results of the Monte Carlo method simulation are distributed along a bell curve. The mean value is the solution to the wire mass used for the wiring to interface with the Locomotion and GN&C systems.

5.6.4 Risk Inputs

Each component is rated up to 100 K rad TID, but there always exists the risk of a single event upset due to the radiation environment. During an upset, the system may not have time to recover, such as during guidance, navigation, and control functions. When the time is not sufficient to recover, the system will switch to the backups immediately. This can be done by running the backup system hot. To mitigate long-term damage from ionizing doses parts were selected with a TID tolerance greater than 100 krad. To mitigate single event upsets, triple mode redundancy (TMR) with voting in code, error detection and correction (EDAC), hardened memory cells, and data scrubbing should all be considered in the final system design.

5.6.5 System Design

The C&DH avionics packages are designed around the AiTech SP0 SBC and adhere to single-fault tolerance requirements. Each computer is responsible for the C&DH of all subsystems including most actuator controllers, and each package contains a set of standard/analog IO interface cards and motor drivers. Each unit attached to the cPCI backplane adheres to the 3U avionics card size standard, and the cPCI handles all DC-to-DC power conversion required by the avionics package. Each SP0 SBC operates with 8 GB of storage, which will contain the RTOS, C&DH specific flight software (not modelled) and any emergency backup storage required. The system also maintains 128 GB of Southwest Research Institute (SWRI) mass memory for each system, allowing for data recording/storage. All components are radiation tolerant up to 100k TID.

The C&DH system was designed using a list of specific components. These components are listed below:

- AiTech SP0 SBC – Main Flight Computer (Ref. 26)
- Moog MOAB – Analog IO (Ref. 27)
- Moog CASI – Camera IO (Ref. 28)
- Southwest Research Institute Multi-Mission Mass Memory (M4) – Flash Storage (Ref. 29)
- Moog Actuator Drivers (Ref. 30)

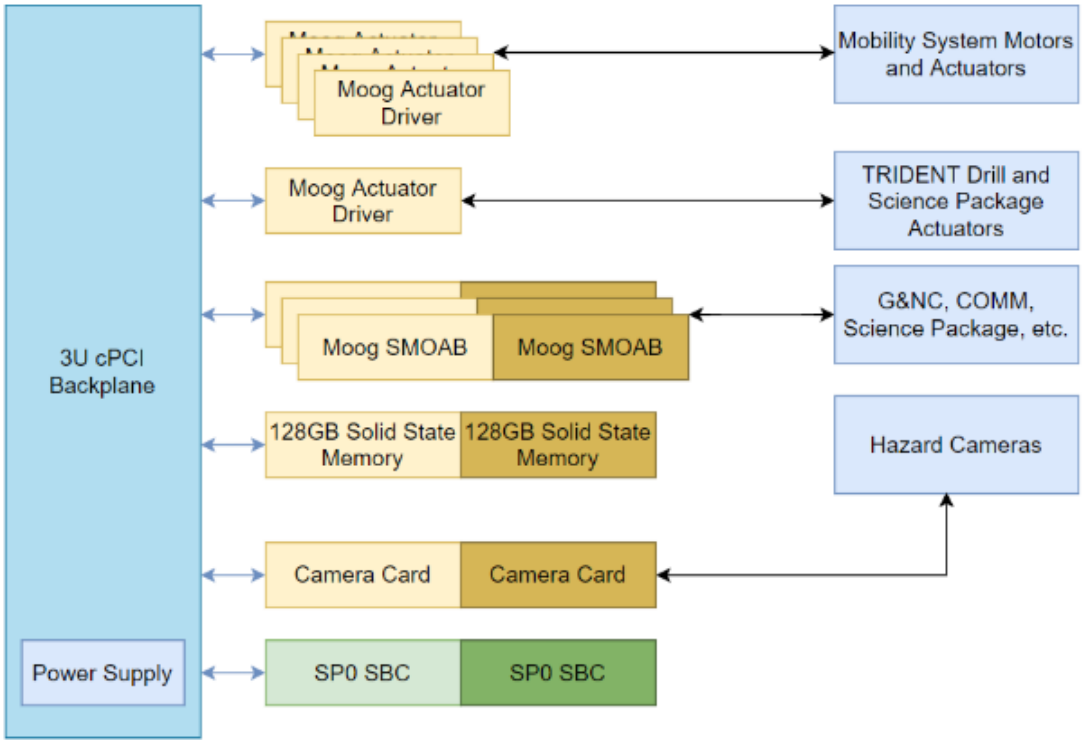

Figure 5.29.—C&DH System Block Diagram.

The block diagram of the system design is shown in Figure 5.29.

5.6.6 Recommendation(s)

The DRPS DRM Lunar Rover C&DH Compass team recommends the following improvements to the study:

1. 6U form-factor with flight computer trades for a more robust system.
   a. *Rationale*: Design was conducted using the 3U form-factor. A future system trade should be conducted to inspect the usage of 6U components with different COTS flight computers.
2. Estimate the software effort months/lines of code required for the mission.

5.6.7 Master Equipment List

The MEL for the C&DH system is shown in Table 5.29.

5.7 Navigation System

The navigation system for the rover allows it to safely and autonomously traverse the terrain between a starting location and a desired ending location. The rover is not provided a landmark or hazard map of the terrain. It must generate the map based on sensor measurements, using its internal map to locate itself relative to the landmarks present in the map while in transit to the desired ending location. The rover is equipped with various navigational hardware that allows it to accomplish this task.

TABLE 5.29.—C&DH MEL

Description Case 1_DRPS_DRM_Rover CD-2021-182	QTY	Unit Mass	Basic Mass	Growth	Growth	Total Mass
Command & Data Handling			18.4	42%	7.7	26.1
C&DH Hardware			15.2	30%	4.5	19.7
AiTech SP0 SBC	2	0.4	0.8	30%	0.2	1.0
Moog Actuator Driver	5	0.5	2.5	30%	0.8	3.3
Moog SMOAB	6	0.4	2.4	30%	0.7	3.1
Moog CASI	2	0.3	0.6	30%	0.2	0.7
M4 Memory	2	1.0	2.0	30%	0.6	2.6
Avionics Enclosure	1	6.9	6.9	30%	2.1	9.0
Instrumentation & Wiring			3.2	100%	3.2	6.4
Harness	1	3.2	3.2	100%	3.2	6.4

5.7.1 System Requirements

The following system requirements apply to the navigation system:

- The navigation system is zero-fault tolerant.
- The navigational hardware shall allow the rover to autonomously navigate between desired waypoints.
- The navigation system must provide means of detecting hazards that would impede or cause damage to the rover.

5.7.2 System Assumptions

Any desired waypoints are provided to the rover by an external source in the local reference frame of the rover.

5.7.3 Analytical Methods

A static tip-over analysis was conducted to assess the tip-over risk associated with events such as traversing sloped terrain or driving down the lander ramps. The analysis required a center of mass (CM) estimate which was obtained by applying the masses listed in the MEL to modeled components in a representative CAD model. Figure 5.30 depicts the approximate location of the CM as a green circle:

The dimensions shown along with the assumption that the rover can raise itself another 36 cm from the stowed position shown in Figure 5.30 means the CM is approximately 97 cm from the surface. The component of the CM not shown in Figure 5.30 is nearly aligned with the center of the rover. Therefore, the short wheelbase as compared to the wider track-width suggests the rover is most susceptible to tipping forward or backward.

Using the above dimensions and assuming the rover would first rotate about its front axle before tipping over leads to an approximate tip-over angle of 36°. The Brayton case effectively increases the vertical CM component to 111 cm, reducing the tip-over angle to 33°. It is important to note this analysis does not account for the independent suspension of the rover which can effectively increase its tolerance to tipping forward or backward by an additional ~14°. It is unclear if the rover is capable of scaling slopes this steep, so the most likely scenario where tip-over may occur is entering a crater and/or driving off the lander vehicle.

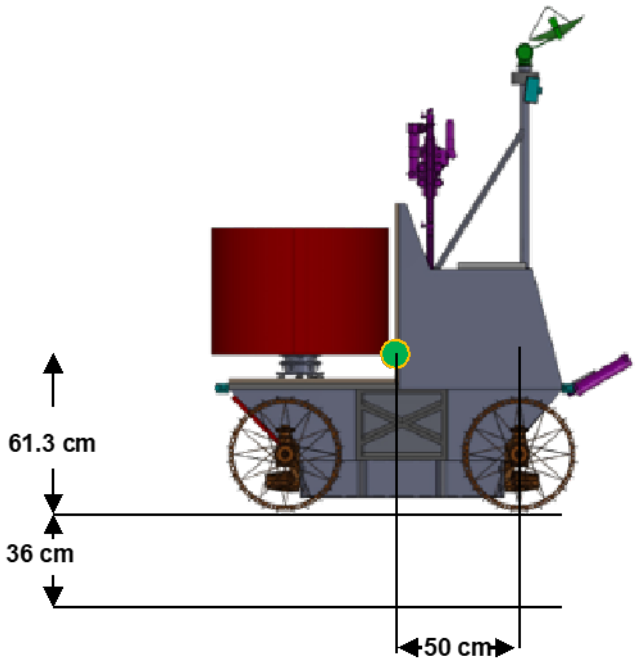

Figure 5.30.—Center of Mass Location.

5.7.4 System Design

The following hardware components are used to satisfy the navigation system requirements:

- Inertial measurement unit (IMU)
  - Three single-axis rate gyros to measure vehicle body rates
  - Three single-axis accelerometers to measure vehicle body accelerations and vehicle attitude
- Navigation camera (x2)
  - Based on Mars Science Laboratory (MSL) Curiosity Rover navcams
  - Stereo ranging out to ~100 m
  - 45° field of view (FOV) | 0.5 m degrees of freedom (DOF)
  - Mounted on articulating mast
- Hazard Detection Camera (x4)
  - Based on MSL Curiosity Rover navcams
  - Stereo ranging out to ~100 m
  - 45° FOV | 0.5 m DOF
  - Mounted on articulating mast
- Navigation Lights
  - Based on MSL Curiosity Rover navcams
  - Stereo ranging out to ~100 m
  - 45° FOV | 0.5 m DOF
  - Mounted on articulating mast

These components are used to enact a Simultaneous Localization and Mapping (SLAM) navigation strategy. In short, the rover processes stereo images taken by the navcams in the direction of travel to establish landmarks that can be used to estimate its position with respect to the mapped landmarks. If the surrounding terrain is not illuminated, the rover can pulse its navigation lights to illuminate ~8 m out in

front of the forward direction once every 30 s (6 m of travel at 20 cm/s). The lights require ~300 to 400 W of power to sufficiently illuminate the nearfield landscape for enough time to acquire navigation images. After being discharged, the energy storage device is charged back up to prepare for another pulse.

The rover can remain stationary and image the surrounding terrain to obtain map information and reduce its local position uncertainty. Hazcams provide high resolution stereo images of areas just in front of and behind the rover. Hazard detection and avoidance algorithms are employed to make adjustments if necessary.

Points of interest are selected by remote operators who command the rover to waypoints. These commands are presented in the local frame of rover. The rover monitors its progress and attitude with the IMU while in transit.

5.7.5 Recommendation(s)

The navigation strategy relies heavily on the rover imaging the surrounding terrain to estimate a map and its position within that map. Further work regarding how frequent "panoramic" images must be taken to generate the map estimate must be conducted and may lead to a significant reduction in the theoretical maximum distance the rover can travel over the course of the mission.

5.7.6 Master Equipment List

The MEL for the navigation system is shown in Table 5.30.

5.8 Communications Subsystem

A DRPS lunar Rover mission designed to send scientific information from Spudis ridge, at the south lunar pole, to Earth via a near rectilinear halo orbit (NRHO) orbit relay satellite (Gateway, or DSG) and, if possible, direct to Earth (DTE) to a 20-m receive ground station antenna. This link to DSG was a major addition to the DRPS version of the VIPER rover and should allow almost continuous communications with the rover even when the earth is not in sight.

5.8.1 Communications System Requirements

The DRPS communications subsystem requirements are to provide (a) full-duplex high-data-rate K/Ka-band links to the NRHO Gateway Relay Satellite from the south pole region of the Moon, (b) full-duplex high-data-rate K/Ka-band links DTE given an available line of sight (LOS) 20-m diameter Earth station, and (c) emergency full-duplex K/Ka-band links to the Gateway ***or*** to 20-m antenna diameter commercial Earth Station.

TABLE 5.30.—NAVIGATION MEL

Description Case 1_DRPS_DRM_Rover CD-2021-182	QTY	Unit Mass	Basic Mass	Growth	Growth	Total Mass
Attitude Determination and Control			4.7	12%	0.6	5.3
Guidance, Navigation, & Control			4.7	12%	0.6	5.3
IMU	1	0.8	0.8	5%	0.0	0.8
NAV Camera	2	0.2	0.4	10%	0.0	0.5
HAZ Cameras	4	0.2	0.9	10%	0.1	1.0
OpNav DVR	1	1.1	1.1	10%	0.1	1.2
NAV Lights	2	0.8	1.5	18%	0.3	1.8

5.8.2 Communications System Assumptions

The communications subsystem design for DRPS will consist of the following components:

One *K/Ka-band Communications* (Comm) Subsystem with a single 0.254-m (10-in.) diameter steerable 3.6° Half-Power-Beamwidth Antenna for high-data-rate communications via the Lunar Orbiter Relay Satellite (Gateway), or DTE communications given an available Line of Sight (LOS) link; also carrying a separate K/Ka-band feed-horn 30° Half-Power-Beamwidth antenna, anchored to the same gimbal platform and pointed in the same direction as the 10-in. parabolic reflector, for emergency low-data-rate communications.

Further assumptions for the DRPS Comm are a minimum scientific data rate of 230 kbps, a minimum emergency data rate of 2 kbps, a separation distance of 70,000 km (Apolune), Single Fault Tolerant, i.e., redundant components for communications subsystem electronics, and a 3 dB link margin, which is included in the communications link for the link budget analysis. A 3 dB link margin is typical for space design applications due to the uncertainty of the components' performance and available end-of-life (EOL) effective isotropic radiated power (EIRP). DVB-S2 QPSK [1/4] at 10^{-7} bit error rate (BER) modulation/coding has been chosen with an implementation/coding loss of –3.5 dB. Rather than compute the information rates based on a certain-valued annual link availability (ALA) with the DTE and direct from Earth (DFE) link budget options, instead, given the specified information rates, any excess link margin (dB) will be presented as a 'Weather Margin.'

5.8.3 Communications System Trades

A Glenn Research Center Communication Analysis Suite (GCAS) study was conducted to establish access/contact windows *from* the Spudis ridge crater (lunar south pole: 89.66° S, 129.2° E) DRPS rover to the Lunar Gateway Satellite and three deep space network (DSN) 34-m Earth Stations. The Gateway satellite was pointed towards the Moon (Nadir) and the simulation time chosen was 31 days. The DRPS rover antenna minimum elevation angle was set to 10°. Depending on how far the Gateway 1.5-m antenna is allowed to move from boresight, the vector axis defined from the point of Apolune to the center of the Moon, the following were gained from GCAS simulations:

(a) when the Gateway antenna was allowed to swing a maximum of 0.6° off-boresight, the average available access/contact window was 16.6 min in duration, from five possible contact windows,

(b) when the Gateway antenna was allowed to swing a maximum of 12° off-boresight, the average available access/contact window was 7 h in duration, from five possible contact windows,

(c) when the Gateway antenna was allowed to swing a maximum of 60° off-boresight, the average available access/contact window was 64 h in duration, from five possible contact windows, and

(d) when the Gateway antenna was allowed to swing a maximum of 72° off-boresight, the average available access/contact window was 145 h in duration, from five possible contact windows. Moreover, all three DSN-34 m Earth stations were visible from the Lunar Gateway Satellite: Goldstone (U.S.), Madrid (Spain) and Canberra (Australia), as shown in Gantt chart (Figure 5.31).

Only when the minimum elevation angle of the DRPS rover antenna was allowed to be changed from 10° to 2° all three 34-m DSN stations were visible from the Lunar DRPS rover site as shown in the Gantt Chart (Figure 5.32). DSN-34m Stations are visible from both, Lunar Gateway Satellite and Lunar DRPS rover site. The annual link availability (atmospheric attenuation) was set to 99 percent. There is approximately a weeklong non-continuous window in the chosen 31 days of simulation with an average access time of 7 h for Canberra (AU), at least 9 h for Goldstone (U.S.) and at least 11 h for Madrid (Spain).

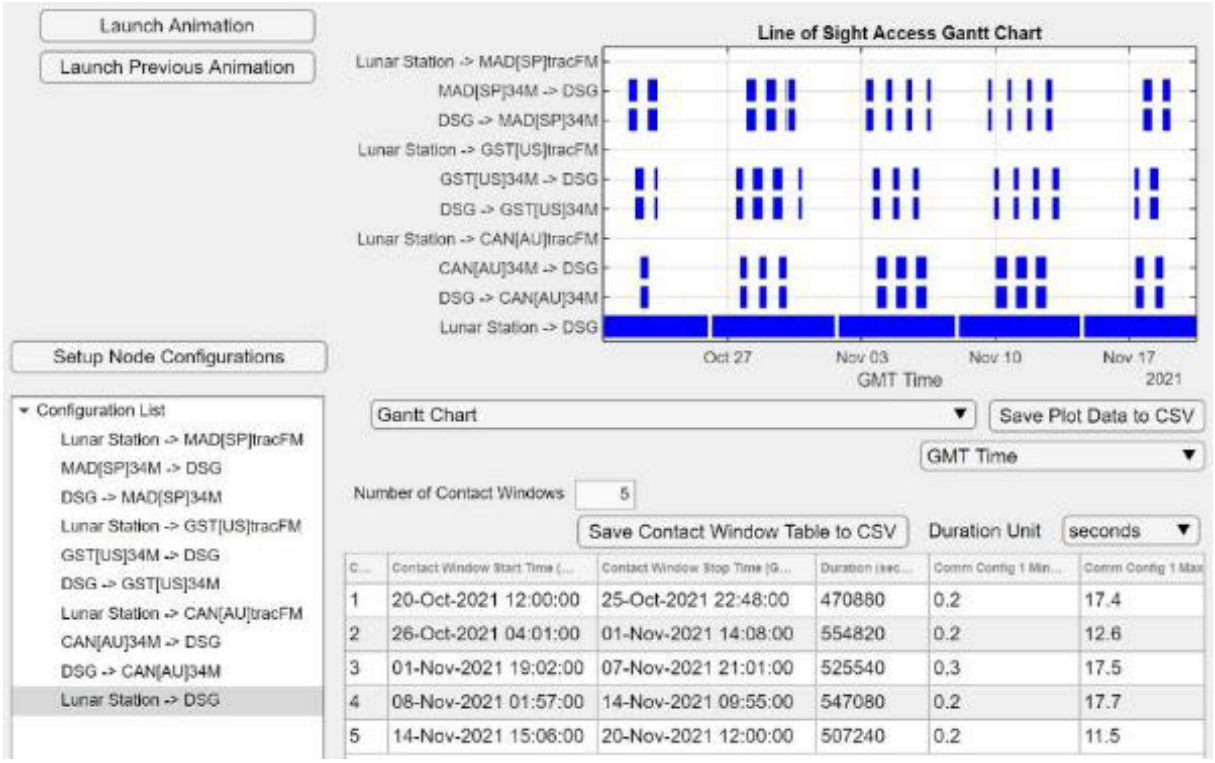

Figure 5.31.—GCAS Simulation Window (Lunar DRPS rover antenna minimum elevation angle 10°).

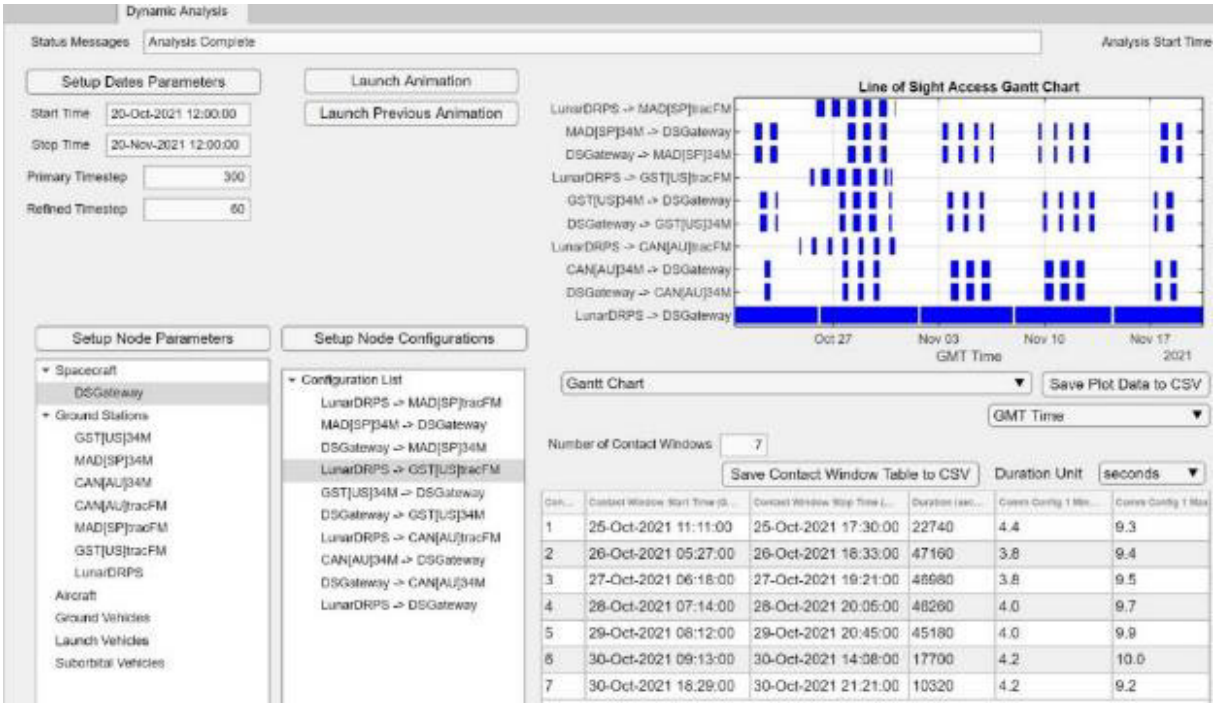

Figure 5.32.—GCAS Simulation Window (Lunar DRPS rover antenna minimum elevation angle 2°).

Some additional details were revealed from GCAS simulations with DRPS elevation angles varying between 5° and 7° as shown in Table 5.31.

TABLE 5.31.—GCAS DSN-34 m CONTACT WINDOWS (LUNAR DRPS ROVER ANTENNA ELEVATION ANGLE 5° TO 7°)

CONTACT WINDOWS BETWEEN DRPS Rover Elevation Angle & DSN-34m								
DRPS /El (°)	7	6			5			
CAN (AU) (hrs)	3.9	7.8	8.3	8.8	7.4	7.8	8.3	8.8
GST (US) (hrs)	—	—	4.9	—	9.4	12.6	4.9	2.9
MAD (SP) (hrs)	—	—	1.1	—	13.0	12.5	—	1.2

5.8.4 Analytical Methods

The communications subsystem design for higher information rates is a function of the transmitted power, carrier frequency, distance, atmospheric absorption (gas/cloud/rain fade), the modulation/coding scheme, antenna size and pointing accuracy.

Link budget analyses at the K/Ka-band were performed (a) going through a lunar relay satellite (Gateway) and (b) DTE and direct from Earth (DFE) by using a 20-m ground station. Figure 5.33 shows the High-Gain Antenna (HGA) and Low-Gain Antenna (LGA) options from the link budget analyses for the best information rates from the DRPS rover to the (a) Gateway and (b) Earth Station.

This Comm design is better than using a helical antenna for the emergency channel in that it requires only 1 W of RF power always pointed toward the Gateway (or a 20-m Earth Station in LOS), because both the 10-in. reflector and the feed-horn antennas are always pointed as an ensemble, with only one antenna energized at any one time. When going through an Earth Station, atmospheric attenuation is expected to rise as the Earth station's elevation angle is lowered and the signal frequency increases. The quantity 'Weather Margin (dB)' in Figure 5.33 indicates the amount of excess link margin for the chosen information rates.

5.8.5 Risk Inputs

5.8.5.1 Risk Statement

The main risk factor identified for the communications subsystem is based upon available RF power subject to mission duration, antenna pointing, antenna blocking, component aging, and the requirement for higher information rates. The impact of accumulated dust on the antenna shroud needs to be assessed.

5.8.5.2 Strategy

The current mitigation strategy is to increase K/Ka-band antenna diameter if a minimum information rate is to be maintained, to seal both feed-horns in a protective Ka-band frequency-friendly shroud such that no lunar dust can temporarily or permanently enter their internal volume, and if necessary to switch onto the emergency communications channel.

5.8.6 System Design

The subsystem design shown in Figure 5.34 consists of Ka-band Comm at 70,000 km away with the Lunar Gateway (or if visible at 385,000 km away with a 20-m Earth Station) via a gimballed 25.4-cm diameter HGA parabolic reflector, or a LGA feed-horn. The HGA channel information rates to the Gateway are 245 kbps, and from the corresponding LGA channel are 2 kbps. If a line of sight is available from the Moon's South Pole crater to any of the NASA (DSN) or any commercial 20-m (or larger) sites then the achievable information rates through HGA are 230 kbps, whereas through the LGA they would only be 2 kbps, while each channel has 12.7 dB of excess link margin for weather phenomena or higher information rates on a clear day.

Information Direction	DRPS HGA to Gateway	DRPS LGA* to Gateway	DRPS HGA to DTE	DRPS LGA to DTE	Gateway to HGA DRPS	Gateway to LGA DRPS	DFE to HGA DRPS	DFE to LGA DRPS
Carrier Frequency (*f*, *GHz*)	23.17		23.17		27.11		27.11	
Carrier Wavelength (λ, *mm*)	12.9		12.9		11.1		11.1	
Transmitter Power (W)	1		1		—		1	
Tx Losses (dB)	-1		-1		—		-1	
Tx Antenna Point Loss (dB)	-0.3		-0.3		—		-0.3	
Tx Antenna Diameter (cm)	25.4	—	25.4	—	150		2000	
Tx Antenna Beamwidth (°)	3.6	30	3.6	30	0.5		0.04	
Tx Antenna Gain (dBi)	33.2	12.6	33.2	12.6	—		72.5	
EIRP (dBW)	31.9	11.2	31.9	11.2	54.6		71.2	
Separation Distance (km)	70,000		385,000		70,000		385,000	
Rx Antenna Point Loss	0		0		0		0	
Rx Antenna Diameter (m)	1.5		20		0.254	—	0.254	—
Rx Antenna Beamwidth(°)	0.60		0.05		3	30	3	30
Rx Antenna Gain (dBi)	48.6		71.1		34.5	13.5	34.5	13.5
Waveguide Loss (dB)	0		0		-1.3		-1.3	
Receiver Noise Temp (K)	1550		512		1247		1247	
G/T (dBi/K)	16.7		44		4.9	-16.1	4.9	-16.1
Information Rate (kbps)	245	2	230	2	2,200	15	123	1
Bit Error Rate	10^{-7}				10^{-7}			
Modulation Scheme	DVB-S2 QPSK				DVB-S2 QPSK			
Implementation Loss (dB)	-3				-3			
Coding Scheme	DVB-S2 (1/4)				DVB-S2 (1/4)			
Coding Loss (dB)	-0.5				-0.5			
Link Power Margin (dB)	3				3			
Weather Margin (dB)	N/A	N/A	12.7	12.7	N/A	N/A	14.2	14.2

*Circular Waveguide Feedhorn (15dBi)
WC-10.06mm (or WC-0.396") Diameter
(Mid-K: 20.0 - 24.5 GHz)

Figure 5.33.—K/Ka-band Link Budgets.

5.8.7 Recommendation(s)

The Team recommends choosing a larger diameter Ka-band antenna system depending on higher information rates with the appropriate EOL available transmit power. Secondly, the Team recommends choosing a higher diameter Ka-band dish with deployable means. Finally, the Team recommends covering all external signal feeds with protective shrouds.

5.8.8 Master Equipment List

Table 5.32 lists the Communications Subsystem Master Equipment list for the Lunar DRPS DRM.

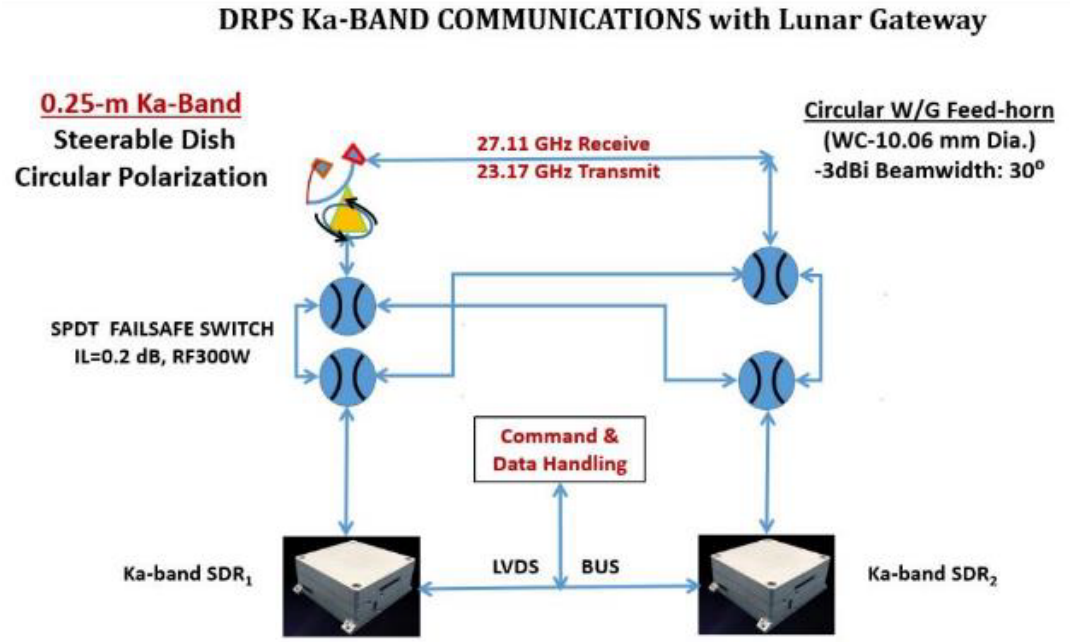

Figure 5.34.—Ka-band Communications Hardware Design.

TABLE 5.32.—COMMUNICATIONS MEL

Description Case 1_DRPS_DRM_Rover CD-2021-182	QTY	Unit Mass	Basic Mass	Growth	Growth	Total Mass
Communications and Tracking			10.7	10%	1.1	11.8
Ka Band System			10.7	10%	1.1	11.8
Parabolic Dish	1	2.0	2.0	10%	0.2	2.2
Feedhorn	1	0.04	0.0	10%	0.0	0.04
SPDT	4	0.5	2.0	10%	0.2	2.2
WR-42 to WC-10.06mm	1	0.03	0.0	10%	0.0	0.03
GIMBAL	1	5.0	5.0	10%	0.5	5.5
SDR-TX/RX	2	0.5	1.0	10%	0.1	1.1
CABLES	2	0.3	0.6	10%	0.1	0.7

6.0 Cost

The mission cost estimate includes the Phase A, B, C, and D costs for the DRPS Lunar Rover excluding the cost of the DRPS unit, launch vehicle, lander, and mission operations. The base estimate assumes some heritage from VIPER, and a secondary estimate that assumes new development is also included. The estimate was developed using a Microsoft® Excel-based parametric cost model created for this study; the costs reported are the mode of the Monte Carlo quantitative risk analysis that was performed based on probability density functions in the parametric cost model.

6.1 Ground Rules and Assumptions

The following ground rules and assumptions apply to the mission cost estimates:

- The scope of the estimates is Phase A, B, C and D costs for the DRPS Lunar Rover including NASA insight/oversight [program management (PM), systems engineering and integration (SE&I), and safety and mission assurance (S&MA)] and the RPS Cost to fuel, integrate, and launch. The phases are as defined in NASA Program Requirements (NPR) 7120.5.
- The DRPS Unit is assumed to be GFE and the DRPS Unit cost is not included in the estimate. The integration cost of the DRPS Unit with the Rover is included.
- Subsystem development costs are adjusted for commonality with the VIPER rover. In the base estimate, shown in Table 6.1 and Table 6.2, AD&C, C&DH, and mobility subsystems are assumed to be minor modifications of the VIPER rover. The Science instruments are assumed to be off the shelf (OTS) from the VIPER Suite of Science instruments. Traditional adjustment factors of 0.2 for OTS and 0.5 for minor modifications are used.
- Minimal test articles and flight spares are assumed in alignment with NPR 8705.4 Appendix C requirements for Class D missions.
- The costs of the launch vehicle, fuel, and lander are not included in this estimate. The cost of ground system and mission operations, a science team, and any tech development up to TRL 6 are also not included.
- Point estimates are presented as “most likely” (approximately 35th percentile) and lower level costs are adjusted pro rata ensuring that they sum to the total.
- Costs are presented in fiscal year (FY) 21 dollars.

6.2 Estimating Methodology

The estimate was developed using a Microsoft® Excel-based parametric cost model created for this study. The primary inputs to the cost model were taken from the MEL developed by the Compass team for this study. The cost estimating relationships (CERs) used in the model were derived in-house using data from NASA planetary and earth-orbiting missions with the exception of the science instruments, which were estimated using CERs from the NASA Instrument Cost Model (NICM). All elements of the mission were estimated using CERs. A Monte Carlo quantitative risk analysis was performed based on uncertainty of the mass inputs and the CER error terms.

6.3 Mission Cost Estimates

The estimated cost of the DRPS Lunar Rover is shown in Table 6.1 and Table 6.2. The detailed cost is separated into design, development, test, and evaluation (DDT&E) costs and flight hardware (HW) cost. The payload listed in Table 6.1 is the suite of science instruments detailed in Table 6.2.

TABLE 6.1.—MISSION POINT ESTIMATE (FY21, $M)

	FY21$M
Phase A	10
Phase B/C/D Costs	274
1.0 Program Management	19
2.0 Systems Engineering	24
3.0 Safety and Mission Assurance	9
5.0 Payload	30
6.0 Rover[a]	136
8.2 RPS Costs to Fuel, Integrate and Launch[b]	41
10.0 Systems Integration and Testing	16
11.0 Education and Public Outreach	1
Total Mission Cost	284
Total Mission Cost without RPS Cost	244

[a]DRPS is assumed GFE and not included

[b]Not Including Launch Vehicle

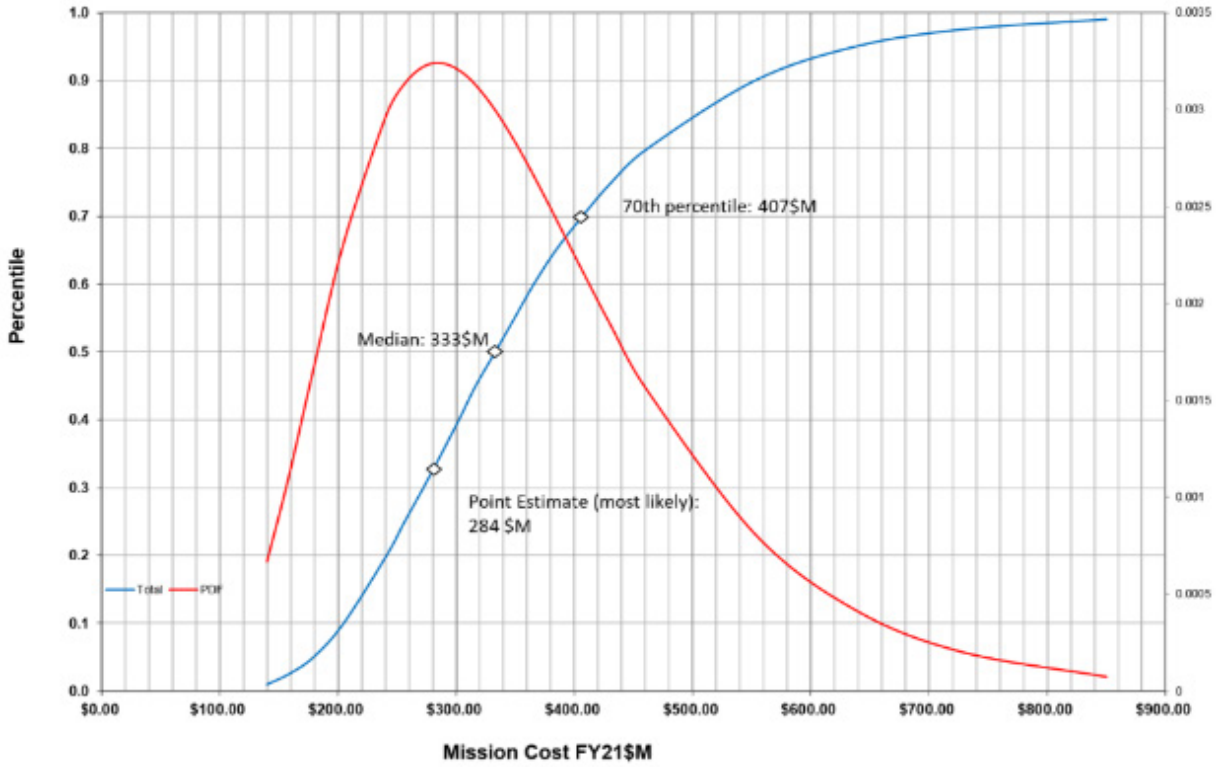

Figure 6.1.—Mission Cost Estimate Distribution (FY21, $M).

TABLE 6.2.—ROVER DETAILS (FY21, $M)

Description	DDT&E Total (FY21$M)	Flight HW Total (FY21$M)	Total (FY21$M)
Attitude Determination and Control	0.9	1.1	2.1
Command and Data Handling	8.3	28.0	36.3
Communications and Tracking	2.2	1.5	3.7
Electrical Power Subsystem	3.0	1.4	4.5
PMAD	1.8	0.7	2.5
Harness	0.1	0.2	0.4
Li Ion Battery	1.1	0.5	1.6
Thermal Control (Non-Propellant)	4.4	1.9	6.3
Science	9.1	21.1	30.2
NSS Instrument	0.4	1.2	1.6
NIRVSS Instrument	1.2	4.0	5.3
MSolo	1.6	5.5	7.1
TRIDENT	4.4	5.5	9.8
TBD Instrument	1.5	4.9	6.4
Structures, Mechanisms and Mobility	13.8	11.5	25.3
Subsystem Subtotal	41.7	66.5	108.2
Systems Integration			
Project Management	10.6	4.5	15.1
Systems Engineering	12.5	5.4	17.9
Mission Assurance	12.6	5.4	18.0
Integration, Assembly, and Test	3.6	1.5	5.1
Ground System Equipment	0.9	0.4	1.3
Rover Total	81.9	83.7	165.6

6.4 Mission Cost Estimate-New Development Assumption

An alternative set of assumptions with no rover heritage from VIPER were considered. The suite of science instruments was assumed OTS from VIPER and all other subsystems were assumed to be new development. All other assumptions are consistent with those of the base estimate detailed in Section 6.1, Ground Rules and Assumptions. The estimated cost of the DRPS Lunar Rover under these assumptions are shown in Table 6.3 and Table 6.4.

TABLE 6.3.—MISSION POINT ESTIMATE (FY21, $M)

	FY21$M
Phase A	10
Phase B/C/D Costs	295
1.0 Program Management	20
2.0 Systems Engineering	25
3.0 Safety and Mission Assurance	9
5.0 Payload	30
6.0 Rover[a]	151
8.2 RPS Costs to Fuel, Integrate and Launch[b]	41
10.0 Systems Integration and Testing	17
11.0 Education and Public Outreach	1
Total Mission Cost	305
Total Mission Cost without RPS Cost	265

[a]DRPS is assumed GFE and not included

[b]Not Including Launch Vehicle

TABLE 6.4.—ROVER DETAILS (FY21, $M)

Description	DDT&E Total (FY21$M)	Flight HW Total (FY21$M)	Total (FY21$M)
Attitude Determination and Control	1.9	1.1	3.0
Command and Data Handling	16.6	28.0	44.6
Communications and Tracking	3.0	1.5	3.7
Electrical Power Subsystem	3.0	1.4	4.5
PMAD	1.8	0.7	2.5
Harness	0.1	0.2	0.4
Li Ion Battery	1.1	0.5	1.6
Thermal Control (Non-Propellant)	4.4	1.9	6.3
Science	9.1	21.1	30.2
NSS Instrument	0.4	1.2	1.6
NIRVSS Instrument	1.2	4.0	5.3
MSolo	1.6	5.5	7.1
TRIDENT	4.4	5.5	9.8
TBD Instrument	1.5	4.9	6.4
Structures, Mechanisms and Mobility	17.2	11.5	28.7
Subsystem Subtotal	54.4	66.5	120.9
Systems Integration			
Project Management	11.1	4.8	15.8
Systems Engineering	13.1	5.6	18.8
Mission Assurance	13.3	5.7	19.0
Integration, Assembly, and Test	3.8	1.6	5.4
Ground System Equipment	0.9	0.4	1.3
Rover Total	96.6	84.6	181.2

Appendix A.—Acronyms and Abbreviations

ΔV	Delta-V, Change in Velocity
AD&C	Attitude, Determination and Control
AIAA	American Institute for Aeronautics and Astronautics
ALA	Annual Link Availability
AMSC	American Superconductor Corporation
ASRG	Advanced Stirling Radioisotope Generator
BER	Bit Error Rate
BOL	Beginning of Life
C&DH	Command and Data Handling
CAD	Computer Aided Design
CBE	Current Best Estimate
CER	Cost Estimating Relationship
CG	Center of Gravity
CM	Center of Mass
CONOPS	Concept of Operations
COTS	Commercial Off-the-Shelf
cPCI	compact Peripheral Component Interconnect
DDT&E	Design, Development, Test, and Evaluation
DFE	Direct from Earth
DOD	Depth of Discharge
DOE	Department of Energy
DOF	Degrees of Freedom
DRM	Design Reference Mission
DRPS	Dynamic Radioisotope Power System
DSN	Deep Space Network
DTE	Direct to Earth
DVR	Digital Video Recorder
ECLSS	Environmental Control and Life Support System
EDAC	Error Detection and Correction
EIRP	Effective Isotropic Radiated Power
EOL	End of Life
EOM	End of Mission
EPS	Electrical Power System
FEA	finite element analysis
FOM	figure of merit
FOV	Field of View
FY	Fiscal Year
GCAS	Glenn Research Center Communication Analysis Suite
GFE	Government Furnished Equipment
GN&C	Guidance, Navigation and Control
GPHS	General Purpose Heat Source
GRC	Glenn Research Center
Hazcam	Hazzard Camera
HGA	High-Gain Antenna
HW	Hardware
IMU	Inertial Measurement Unit
ISRU	In-Situ Resource Utilization
LGA	Low-Gain Antenna
LOS	Line of Sight
LRO	Lunar Reconnaissance Orbiter
LSP	Launch Services Program
MATLAB®	MATrix LABoratory
MEL	Master Equipment List
MGA	Mass Growth Allowance
MLI	Multi-Layer Insulation

MMPDS	Metallic Materials Properties Development and Standardization
MSL	Mars Science Laboratory
MSolo	Mass Spectrometer Observing Lunar Operations
NASTRAN	NASA STRucture ANalysis
Navcam	Navigation Camera
NEPA	National Environmental Policy Act
NICM	NASA Instrument Cost Model
NIRVSS	Near-Infrared Volatiles Spectrometer System
NRHO	Near Rectilinear Halo Orbit
NSS	Neutron Spectrometer System
OTS	Off-the-Shelf
PCB	Printed Circuit Board
PEL	Power Equipment List
PM	Program/Project Management
PMAD	Power Management and Distribution
PSR	Permanently Shadowed Region
RHU	Radioisotope Heating Units
RPO	Radioisotope Program Office
RPS	Radioisotope Power System
RTG	Radioisotope Thermoelectric Generator
RTOS	Real Time Operating System
S/C	Spacecraft
SBC	Single Board Computer
SE&I	Systems Engineering and Integration
SLAM	Simultaneous Localization and Mapping
SLS	Space Launch System
S&MA	Safety and Mission Assurance
STD	Standard
SWRI	Southwest Research Institute
TID	Total Ionized Dose
TMR	Triple Mode Redundancy
TRIDENT	The Regolith and Ice Drill for Exploring New Terrains
TRL	Technology Readiness Level
VIPER	Volatiles Investigating Polar Exploration Rover

Appendix B.—Study Participants

DRPS DRM Lunar Rover Design Session			
Subsystem	**Name**	**Affiliation**	**Contact Email**
Design Customer POC/PI	June Zakrasjek	GRC	
Compass Team			
Compass Team Lead	Steve Oleson	GRC	Steven.r.oleson@nasa.gov
System Integration, MEL	Betsy Turnbull	GRC	Elizabeth.r.turnbull@nasa.gov
Technical Editing	Lee Jackson	HX5, LLC	Lee.a.jackson@nasa.gov
Science	Ben Bussey	APL	
Science	Paul Ostdiek	APL	
Science	Kirby Runyon	APL	
Mobility	James Fittje	HX5, LLC	James.e.fittje@nasa.gov
Guidance, Navigation and Control, Mission	Brent Faller	GRC	Brent.f.faller@nasa.gov
Guidance, Navigation and Control, Mission	Christine Schmid	GRC	Christine.l.schmid@nasa.gov
Structures	John Gyekenyesi	HX5, LLC	John.z.gyekenyesi@nasa.gov
Environmental	Tony Colozza	HX5, LLC	Anthony.j.colozza@nasa.gov
Power	Paul Schmitz	GRC	Paul.c.schmitz@nasa.gov
Power	Brandon Klefman	GRC	Brandon.klefman@nasa.gov
C&DH, Software	Chris Heldman	GRC	Christopher.r.heldman@nasa.gov
Communications	Onoufrious Theofylaktos	GRC	Onoufrious.Theofylaktos-1@nasa.gov
Configuration	Tom Packard	HX5, LLC	Thomas.w.packard@nasa.gov
Cost	Tom Parkey	GRC	Thomas.j.parkey@nasa.gov
Cost	Natalie Weckesser	GRC	Natalie.j.weckesser@nasa.gov
Cost	Cassandra Chang	GRC	Cassandra.l.chang@nasa.gov

References

1. R. Vaughan, “VIPER – Volatiles Investigating Polar Exploration Rover: Mission Overview,” in *International Small Satellite Conference*, Virtual, 2020.
2. W. W. Mendell, “How Cold are the Floors of Lunar Polar Shadowed Craters?,” in *41st Lunar and Planetary Science Conference*, The Woodlands, TX, 2010.
3. “Gateway System Requirements, DSG-RQMT-001,” NASA, Washington, DC, 2019.
4. American Institute of Aeronautics and Astronautics (AIAA), “Standard: Mass Properties Control for Space Systems (ANSI/AIAA S-120A-2015 (2019)),” AIAA, Reston, VA, 2019.
5. Astrobotic, “Griffin Lander: Large Payload Delivery To Any Lunar Destination,” Astrobotic, 2021. [Online]. Available: https://www.astrobotic.com/griffin. [Accessed 7 April 2021].
6. Y.-H. Kim, “Product Specification Rechargeable Lithium Ion Battery Model: INR18650 M36T 12.50Wh,” LG Chem, 2017.
7. Terma, “Equipment Power Distribution Module,” 01 2012. [Online]. Available: https://www.terma.com/media/177695/equipment_power_distribution_module.pdf. [Accessed February 2021].
8. Terma, “Battery C/D Regulation Module,” 01 2012. [Online]. Available: https://www.terma.com/media/177689/battery_cd_regulation_module.pdf. [Accessed February 2021].
9. Schörghofer, N., Benna, M., Berezhnoy, A.A. et al. Water Group Exospheres and Surface Interactions on the Moon, Mercury, and Ceres. *Space Sci Rev* **217**, 74 (2021). https://doi.org/10.1007/s11214-021-00846-3
10. National Aeronautics and Space Administration (NASA), “Ideal Brayton Cycle,” NASA, 05 May 2015. [Online]. Available: https://www.grc.nasa.gov/www/k-12/airplane/brayton.html. [Accessed 12 April 2021].
11. National Aeronautics and Space Administration (NASA), Space Launch System (SLS): Mission Planner's Guide, Rev A ed., NASA, 2018.
12. Federal Aviation Administration, Metalic Materials Properties Development and Standardization (MMPDS) Handbook - 14, vol. MMPDS 14, Columbus, OH: Battelle Memorial Institute, 2019.
13. Department of Defense, Composit Materials Handbook, vol. 2, Department of Defense, 2002.
14. J. C. Mankins, “Technology Readiness Levels,” NASA, Washington, 1995.
15. National Aeronautics and Space Administration (NASA), “Structural Design and Test Factors of Safety for Spaceflight Hardware (NASA-STD-5001B),” NASA, Washington, 2016.
16. The Engineering Toolbox, “Young's Modulus - Tensile and Yield Strength for common Materials,” 2003. [Online]. Available: https://www.engineeringtoolbox.com/young-modulus-d_417.html. [Accessed 15 April 2021].
17. Engineering ToolBox, “Poisson's ratio,” 2008. [Online]. Available: https://www.engineeringtoolbox.com/poissons-ratio-d_1224.html. [Accessed 15 April 2021].
18. Agarwal, B. D. and Broutman, L. J., Analysis and Performance of Fiber Composites ISBN 0-471-05928-5, New York: John Wiley & Sons, Inc., 1980.
19. Collier Research Corporation, “HyperSizer,” 1995. [Online]. Available: http://hypersizer.com. [Accessed 13 October 2020].
20. Heinemann, Jr., W., “Design Mass Properties II: Mass Estimating and Forecasting for Aerospace Vehicles Based on Historical Data,” NASA Johnson Space Center, Houston, TX, 1994.
21. National Aeronautics and Space Administration (NASA), “VIPER: The Rover and Its Onboard Toolkit,” NASA, 2021. [Online]. Available: https://www.nasa.gov/viper/rover. [Accessed 08 April 2021].

22. National Aeronautics and Space Administration (NASA), “Space Launch System (SLS): Mission Planner's Guide,” NASA, Washington, D.C., 2018.
23. National Aeronautics and Space Administration (NASA) Glenn Research Center, “High Temperature Water Heat Pipes,” [Online]. Available: https://tec.grc.nasa.gov/microgravity-testing/high-temperature-water-heat-pipes/. [Accessed 30 October 2020].
24. Pease, Christopher, “An Overview of Monte Carlo Methods,” Towards Data Science, 2018. [Online]. Available: https://towardsdatascience.com/an-overview-of-monte-carlo-methods-675384eb1694. [Accessed 15 April 2021].
25. Holmes, Susan, “Monte Carlo,” 19 May 2004. [Online]. Available: http://statweb.stanford.edu/~susan/courses/s208/node14.html. [Accessed 07 21 2020].
26. AiTech, “AiTech SP0 3U cPCI Radiation Tolerant PowerPC SBC,” [Online]. Available: https://aitechsystems.com/product/sp0-s-rad-tolerant-3u-compactpci-sbc/. [Accessed 20 05 2020].
27. Moog, “Moog MOAB Series of Boards,” 2019. [Online]. Available: https://www.moog.com/content/dam/moog/literature/Space_Defense/spaceliterature/avionics/moog-moab-series-of-boards-datasheet.pdf. [Accessed 15 04 2021].
28. Moog Space and Defense Group, “Solar Array and Charge Control Interface (SACI) Payload and Power Interface (PAPI) McLasi(TM),” 2019. [Online]. Available: https://www.moog.com/content/dam/moog/literature/Space_Defense/spaceliterature/avionics/moog-saci-papi-mclasi-boards-datasheet.pdf. [Accessed 15 April 2021].
29. SWRI, “SWRI Flash Memory,” [Online]. Available: https://www.swri.org/industry/space-engineering/solid-state-recorders. [Accessed 01 03 2021].
30. Moog, “Moog Servo Motor Controller Electronics,” 2016. [Online]. Available: https://www.moog.com/content/dam/moog/literature/Space_Defense/Space_Access_Integrated_Systems/AVIONICS_Servo_Motor_Controller_Electronics_Datasheet_032416.pdf. [Accessed 20 05 2020].
31. Moog, “Moog MOAB Series of Boards,” [Online].